Estimating High-Pressure Hydrogen Storage Required to Refuel Heavy-Duty Vehicles

by

Nikolas Haave

A thesis presented to Lakehead University

In fulfilment of the

Thesis requirement for the degree of

Master of Science

In

Mechanical Engineering

Thunder Bay, Ontario, Canada, 2025

Abstract

One of the major challenges of the current generation, in Canada, is meeting the ambitious net-zero emission targets by 2050 to fend off the worst impacts of climate change. Heavy-duty (HD) hydrogen fuel cell electric vehicles (FCEV) present an opportunity to drastically cut greenhouse gas emissions produced in the transportation sector. A major hurdle in HD FCEV deployment is the design, development and implementation of hydrogen refueling stations (HRS), specifically estimating the high-pressure hydrogen storage required to refuel HD FCEVs. In this research, a numerical model was developed to estimate the high-pressure hydrogen storage required to refuel HD FCEVs with an on-board storage of 80 kg at a nominal working pressure (NWP) of 70 MPa achieving 100% state of charge (SOC). Equations of State (EoS) and Generalized Reduced Gradient (GRG) nonlinear programming are used throughout the numerical model to estimate the hydrogen storage pressure and the change of internal energy of various cascading strategies. The numerical model is validated against experimental testing performed at a specialized hydrogen test lab in Surrey, British Columbia. A parametric study focusing on the effect of storage and vehicle temperature on the numerical model is conducted. The numerical model is used to investigate the effects of increasing the storage pressure, storage volume and the number of cascades, based on energy consumption and volume ratio. Finally, a case study for refueling a 1,500L FCEV is performed, considering the available hydrogen storage at a hydrogen test facility located in Surrey, BC. A cascading strategy for HD fueling is suggested based on overall energy consumption.

Acknowledgments

I would like to extend a special thank you to all who have helped and supported me with the development of this thesis.

To Dr Ali. Tarokh, for providing guidance and supervision throughout the development of the thesis. The support through the early stages of research and shifting the research to a topic that better suited my interests was a key to this thesis coming to fruition. To the research committee, Dr Basel I. Ismail and Dr Baris Yilmaz, for providing support, suggestions and guidance, challenging me to improve the thesis. To Lakehead University for providing financial support.

To NSERC and OSAP for offering research scholarships and providing financial support throughout my education.

To Powertech Labs Inc. for providing a lab to carry out experimental testing and allowing the use of the data to validate the numerical model developed in this thesis. To the engineers and technologists who I have worked with for so many years, you have all made me into the engineer I am today. You have all played a significant role in my understanding of hydrogen technology and provided invaluable insights into the numerical model.

Finally, to my family and my friends, I am forever grateful to each, and every, one of you. You have all made a profound impact in my life. I will never be able to repay you, but I intend to use the time given to me to try.

To…

The spirit of radio

Echoes with the sound of the salesman…

Contents

List of Figures

List of Tables

List of Abbreviations & Symbols

Abbreviation	Definition
APRR	Average pressure ramp rate
BEV	Battery electric vehicle
CFD	Computational fluid dynamics
CHSS	Compressed hydrogen storage system
CNG	Compressed natural gas
CO2-eq	Carbon dioxide equivalent
EoS	Equation of state
FCEV	Fuel cell electric vehicle
GHG	Greenhouse gas
H70	Hydrogen cylinder rated to 70 MPa
HD	Heavy-duty
HP	High-pressure hydrogen storage
HRS	Hydrogen refueling station
LD	Light-duty
LP	Low-pressure hydrogen storage
MP	Medium- pressure hydrogen storage
NIST	National Institute of Standards & Technology
NREL	National Renewable Energy Laboratory
NWP	Nominal working pressure
OTV	On-tank valve
PSDV	Pressure switch difference value
PCV or FCV	Pressure control valve
SOC	State of charge

Symbol	Definition
a	Accuracy of instruments
mu	Measured uncertainty of instruments
mu_c	Combined measured uncertainty
mu_x	Expanded uncertainty
P_{atm}	Atmospheric pressure, 0.10132501 MPa
P_s	Storage pressure [MPa.g]
P_v	Vehicle pressure [MPa.g]
V_s	Storage volume [L]
V_v	Vehicle volume [L]
T_s	Storage temperature [°C]
T_v	Vehicle Temperature [°C]
n	Cascades
Z	Compressibility factor
ρ	Density (hydrogen) [g/L]
R	Universal gas constant, 8.314472 J/(mol.K)
M	Molar mass g/mol
m	Mass [kg]
Δ	Delta or change
u	Specific internal energy [kJ/kg]
U	Internal energy [kJ]
σ	Standard deviation

Chapter 1 - Introduction

1.1 - Introduction:

One of the major challenges of the current generation is meeting the ambitious net-zero emission targets by 2050 in order to fend off the worst impacts of climate change. A major contributor to global greenhouse gas emissions (GHG) is the transportation industry, which contributes 7.97 gigatonnes of CO_2 equivalent ($CO_{2\text{-eq}}$) emissions annually [1]. Fig. 1 shows the distribution of major $CO_{2\text{-eq}}$ emissions industries, revealing that transportation makes up 20.7% of global GHG. In British Columbia (BC), specifically, the transportation industry is responsible for more than 25 million tonnes of $CO_{2\text{-eq}}$ emissions annually, which is equivalent to approximately 41% of the total GHG in BC [2]. The staggering weight of emissions represents a major opportunity to implement renewable technologies to reduce the GHGs produced by the transportation sector, specifically for heavy-duty (HD) transportation, such as trucking, marine transport and aviation.

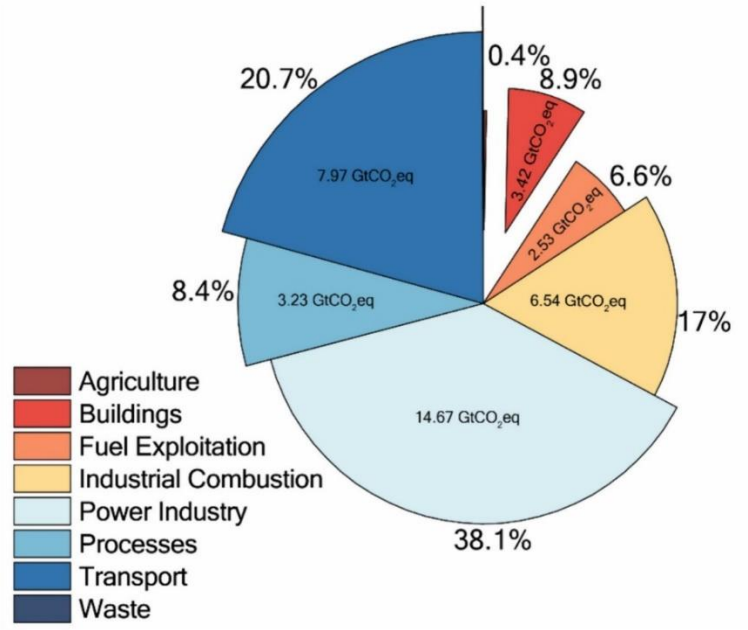

Fig. 1. Greenhouse gas emissions by sector in CO_2e gigatonnes [1].

To compete with traditional internal combustion engines, there are two major technologies that have been developed to reduce GHG emissions in the transportation sector, battery electric vehicles (BEVs) and hydrogen fuel cell vehicles (FCEVs). Although BEVs suffer long charging times, the range of BEVs are sufficient and are more economical for consumers [3]. Conversely, heavy-duty transportation, such as long-haul trucking, demands fast refueling and high on-board energy storage [4], [5].

In July 2021, the Government of British Columbia, released a hydrogen strategy which outlines the role of hydrogen technology for reducing BC's annual emissions [6]. The strategy outlines the need for advancement of hydrogen technology to support heavy-duty transportation, where direct electrification is not a viable solution. The strategy aims to support heavy-duty hydrogen vehicles for marine, aviation and other commercial transportation applications which benefit from short refueling times and a wider range of operability, when

compared to BEVs. Hydrogen has the potential to reduce BC's annual emissions by 7.2 megatonnes annually by 2050, accounting for 11% of BC's 2018 emissions [7].

The primary hydrogen storage method is in compressed gaseous form. However, there are a number of other storage methods that are being investigated. Such methods include liquid hydrogen, cryogenic compressed and material-based hydrogen storage. In this study, the storage method considered is gaseous hydrogen with a nominal working pressure (NWP) of 70 MPa. To store the compressed hydrogen gas, Type IV cylinders have been developed to reduce the weight of the hydrogen vehicles, when compared to Type I, Type II or Type III cylinders [8]. Type IV cylinders have a carbon fiber outer wrap to provide enough strength to withstand the high-hoop, axial and radial stresses experienced at high-pressure. To contain the gas, a thermoplastic liner is used as the inner layer of the Type IV cylinder. One of the major advantages of FCEVs is the fast-refueling time, 3 to 5 minutes for light-duty (LD) applications and 10 to 20 minutes for HD applications. One of the consequences of rapid pressurization of a compressible gas is that the temperature of the gas developed inside the container can increase quickly. If left unchecked, the temperature can approach the glass transition temperature of the thermoplastic liner, resulting in liner softening and potential failure. A solution for reducing the internal tank temperature while maintaining a fast-refueling rate is to cool the hydrogen gas before it flows into the cylinder. By pre-cooling the gas, a moderated internal tank temperature can be maintained, avoiding possible failure modes, as illustrated in Fig. 2 by Li et al. [9]. Li et al. used computational fluid dynamics (CFD) to show that pre-cooled gas entering a cylinder at -40°C can reduce the development temperature to less than 55°C at an average pressure ramp rate (APRR) of 13.4 MPa/min.

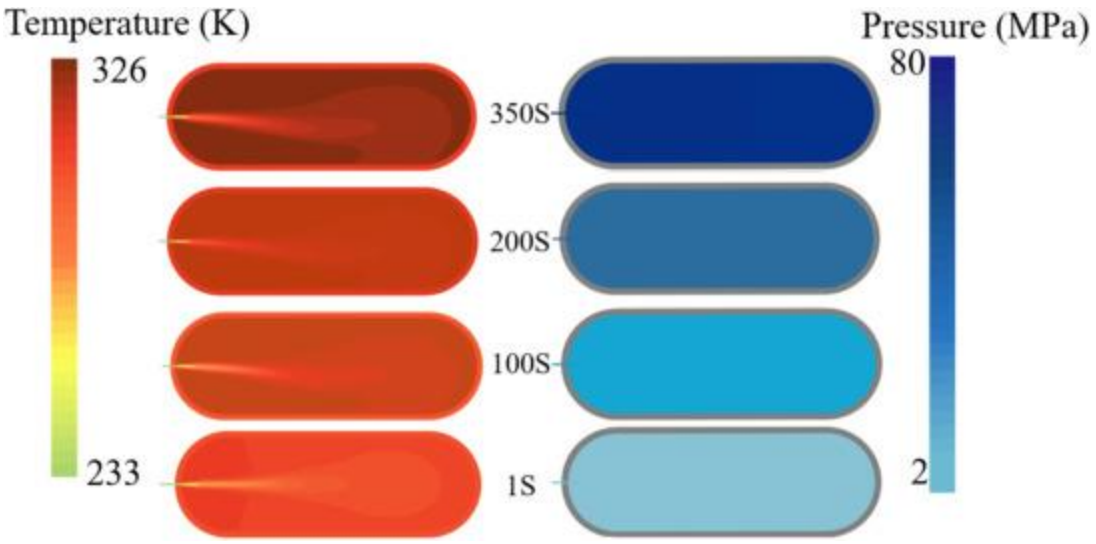

Fig. 2. CFD temperature and pressure distribution results [9].

To ensure that Type IV cylinders are safe for use in vehicles, technical regulations and standardized testing, such as the UN GTR No. 13 or CSA/ANSI HGV 2, were established [10], [11]. The rationale behind the UN GTR No. 13, in particular, describes critical tests that must be completed to ensure the cylinder design will be acceptable for long term use on the road in a hydrogen vehicle. Severe usage tests intended to simulate exposure to physical impacts, such as drop impact, surface damage and on road impacts are all performed before exposure to pressure. Additionally, the cylinder is exposed to chemicals that may be present in the on-road environment, such as battery acid, washer fluid and gasoline. Then the cylinder is exposed to a time-accelerated test where the cylinder is place in an environmental chamber heated to 85°C and pressurized to 1.25 times NWP. The test is performed as some composites exhibit temperature-dependent fatigue. 85°C was chosen as the maximum potential exposure because under-hood temperatures of more than 82°C have been measured in dark vehicles parked in direct sunlight with an outdoor temperature of 50°C. Ambient pressure cycling, using hydraulic

fluids such as water or mineral oils, is completed to demonstrate the cylinder's resistance to rupture. 22,000 ambient temperature hydraulic cycles from 2 MPa to more than 87.5 MPa must be completed, without rupture, for a design to be qualified for use with hydrogen gas. The number of cycles was determined by using vehicle data from the California Air Resource Board, Transport Canada and, Taxis operated in New York City, combined with risk calculations based on probability of a failure event and severity of the event [10]. Finaly, a burst test is required to ensure that the cylinder is able to maintain 80% of the original static pressure strength. The performance durability sequence tests are described in Fig. 3.

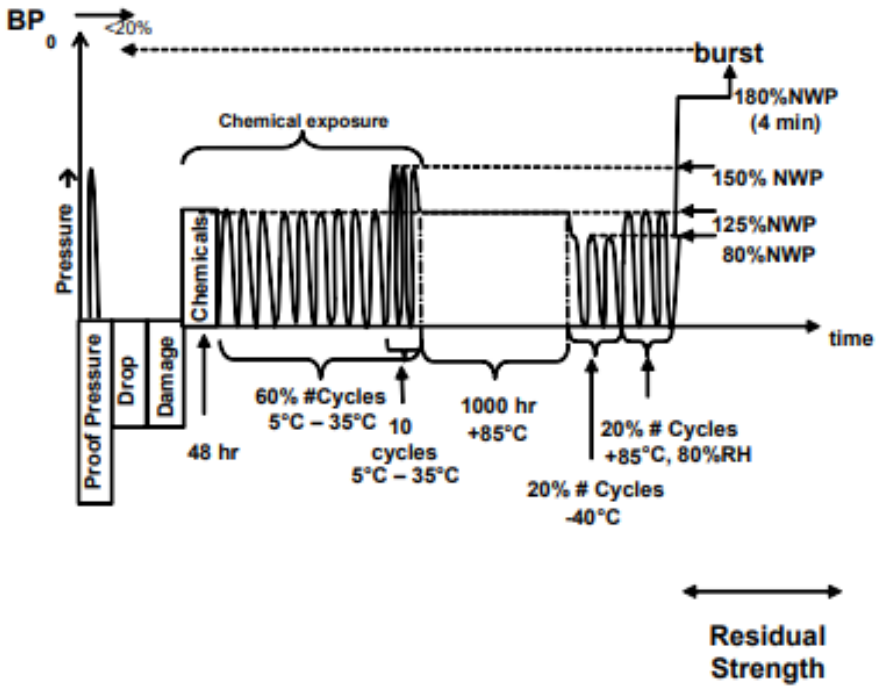

Fig. 3. Verification test for performance durability- hydraulic fluid [10].

Once all the above tests are completed, the cylinder design undergoes 500 pneumatic refueling cycles. The refueling cycles are carried out so that the cylinder is capable of performing essential safety functions under the expected worst-case driving conditions. Such exposures include hydrogen fuel, extreme environmental temperatures and normal usage conditions. Normal usage includes, expected lifetime range, driving range per fill, fueling conditions and frequency of fueling. Testing with hydrogen gas introduces stress factors associate with rapid and simultaneous in-tank temperature and pressure swings, and the infusion of gas into the thermoplastic liner. 500 pneumatic cycles are required to be completed at various environmental temperatures, to demonstrate the fuel system's capability to maintain leak free performance during the expected service of the vehicle. Based on the expected range per fill of FCEVs at the time of the introduction of the UN GTR No. 13, approximately 500 km, the expected lifetime range was taken to be ~250,000 km [10]. On-road data taken for CNG vehicles found that mechanical failures of CNG vehicle storage occurred due to gas intrusion into the thermoplastic liner and carbon fiber wrap after less than 50 fueling cycles [10]. Prototype H70 FCEVs showed that leaks at the o-ring sealing surfaces occurred after less than 50 fueling cycles. Additional failures were identified by McDougal et al. as described in the literature review of this report [12]. Therefore, the qualification requirement for completing 500 pneumatic pressure cycles was established as a conservative threshold based on failures observed during on-road performance of compressed natural gas (CNG), prototype FCEVs and during testing of both vehicle type storage systems. To ensure that the cylinders could operate as intended under any feasible temperature conditions, it was important to determine the average and extreme environment temperature conditions experienced in the most populated regions on Earth. Records from Environment Canada showed

that extreme cold temperatures as low as -40°C were experienced in regions above the 45th parallel, and temperatures as high as 50°C were experienced in desert regions closer to the equator [13]. Therefore, it was established that 50 of the 500 cycles would be performed at an ambient temperature of -40°C and 50 cycles would be performed at 50°C [13]. The remaining 400 cycles would be performed at 20°C ± 5°C. The fueling conditions for each of the pressure cycles were chosen to align with fueling protocols outlined in SAE J2601 [14]. The expected on-road performance sequence of tests is shown in Fig. 4.

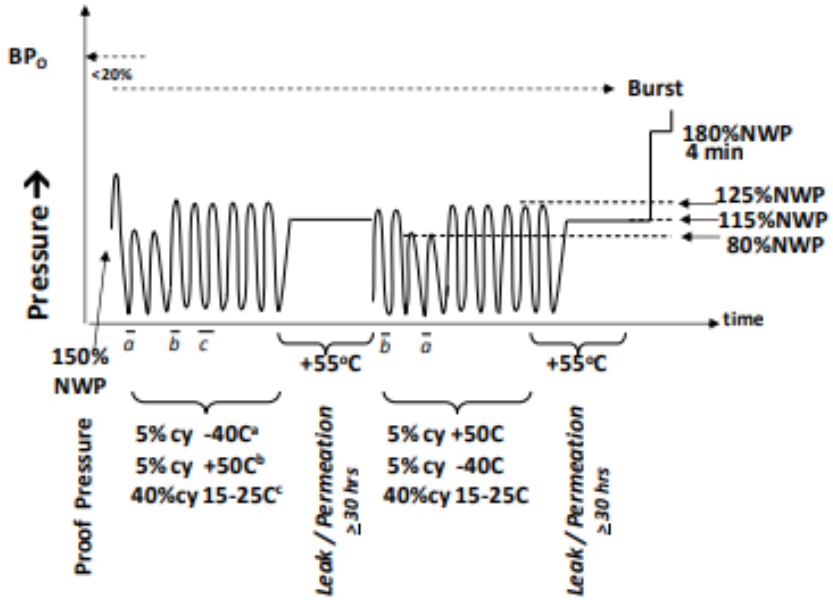

Fig. 4. Verification test for expected on-road performance - hydrogen gas [10].

SAE J2601 establishes the fueling protocol that would be experienced by a hydrogen vehicles at a hydrogen refueling station (HRS). The goal of the fueling protocol was to provide specific targets that an HRS should be capable of meeting to provide high density fueling as fast as possible to achieve a target SOC of 95% to 100%. To ensure a FCEV was capable of withstanding the extremes of the SAE refueling protocols the fuel delivery temperature, APRR and target

pressure were specified as the ambient parameters when performing refueling test cycles. At the time of the introduction of the UN GTR No. 13, there were no fueling protocols developed specifically for HD FCEVs. As the industry has matured, SAE J2601 was updated, as recently as February 2025, to include fueling protocols for HD refueling. In SAE J2601 there are two types of protocols than can be used, table-based refueling and MC method [14]. Table-based refueling uses the station delivery temperature, ambient temperature, compressed hydrogen storage system (CHSS) category and the initial pressure to choose the appropriate APRR and target pressure. Table-based refueling is most useful when there is no communication between the vehicle and the hydrogen refueling station (HRS). The fueling delivery temperature and APRR are selected in such a way to limit the development of high temperature inside the FCEV on-board storage, while achieving a SOC of 95% to 100%. Table-based refueling is the method used in testing outlined in UN GTR No.13. MC method, on the other hand, relies on real-time information from the station and the vehicle to update the pressure ramp rate dynamically in order to optimize the fueling performance. MC method is used most often at hydrogen refueling stations rather than under laboratory testing conditions.

Hydrogen vehicles are classified into different categories based on the mass of their on-board hydrogen storage. Light-duty (LD) vehicles which are typical passenger vehicles such as the Toyota Mirai or Hyundai Nexo, are defined by having less than 10 kg of on-board hydrogen storage [15]. An example of a hydrogen fuel cell passenger vehicle and the major components is shown in Fig. 5.

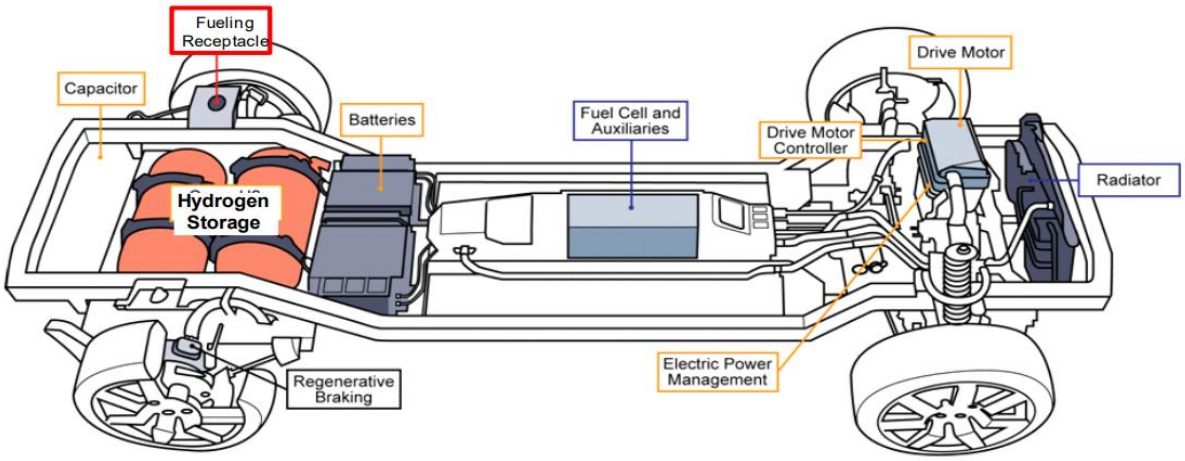

Fig. 5. Example of a Hydrogen fuel cell passenger vehicle – LD FCEV [16].

Medium-duty (MD) and heavy-duty (HD) vehicles are consolidated into one category and are defined as having more than 10kg of on-board hydrogen storage. MD and HD trucking vehicles are expected to be the first HD applications to be widely adopted by the transportation sector. Fig. 6 and Fig. 7 show examples of MD and HD hydrogen fuel cell vehicles.

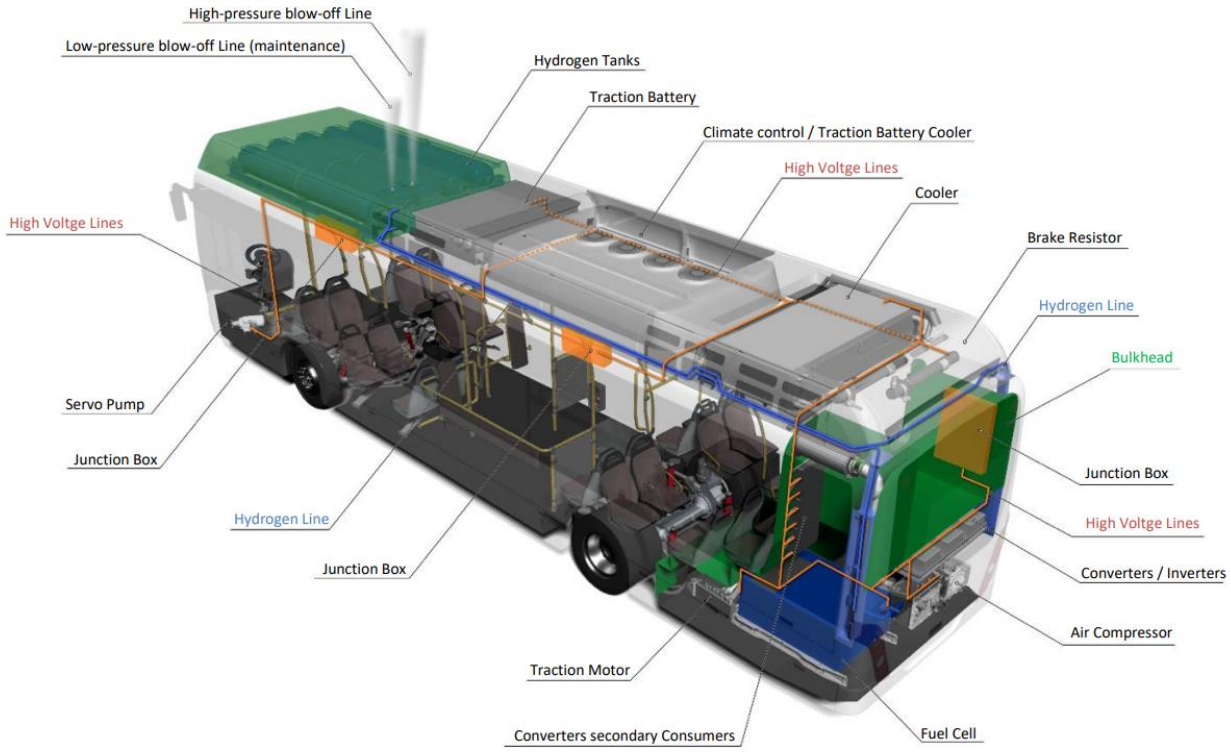

Fig. 6. Example of a hydrogen fuel cell bus – MD FCEV [16].

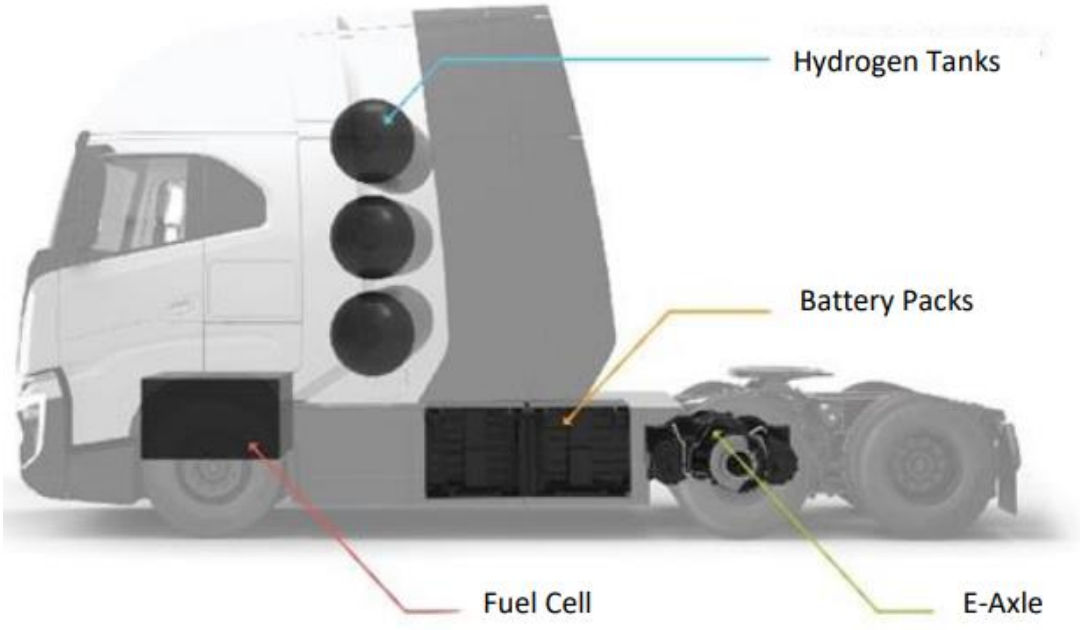

Fig. 7 Example of a hydrogen fuel cell truck – HD FCEV [16].

Research, development and testing of trucking applications are expected to enable other HD applications, such as: marine, port, freight and passenger rail, mining and industrial and potentially aviation. Each classification of FCEV has expected refueling times. For LD vehicles the expected refueling time is 3 to 5 minutes [14] and HD vehicles are expected to be filled in 10 to 20 minutes [15]. However, as vehicles increase their onboard hydrogen storage, the fueling times are expected to increase. As of right now the refueling times are established by refueling protocols, such as SAE J2601, which are based on experimental tests and surveys within the transportation industry.

Hydrogen refueling is a process driven by a pressure difference between the on-site hydrogen storage of an HRS and the on-board storage of an FCEV. A major hurdle in supporting a net-zero transportation sector is the development of HRSs. The development of hydrogen infrastructure is slow and holding back the widespread adoption of hydrogen technology [17]. One of the reasons for the lag in development of hydrogen refueling infrastructure is because of the supply and demand curve in the industry. The cost to develop a hydrogen refueling network to support FCEVs is high, and there are not enough vehicles to justify the cost. However, the adoption of FCEVs in transportation relies on a robust refueling network. [18] This indicates that there is value in studies focused on developing tools to facilitate the design, development and implementation of hydrogen refueling infrastructure.

The two most common refueling strategies are buffer refueling and cascade refueling. These two general strategies that have been studied and implemented in industry: buffer refueling and cascade refueling. The “3Emotion” project, which focused on refueling H35 fuel cell electric buses, included an HRS station in London, UK, which uses a single stage refueling strategy,

a simplified schematic shown in Fig. 8. [19], analyzed the operational data taken during refueling events and found that most refueling events dispensed 15 kg from the storage bank to the fuel cell bus. To complete a fill of the H35 bus, 350 kg of on-site hydrogen gas, pressurized to 50 MPa was required. An HRS commissioned in Aalborg, Denmark, employed a two-stage cascade refueling strategy, as shown in Fig. 9. In this case the on-site storage required to fill 15 kg to an H35 bus was 232 kg; 114 kg and 118 kg, pressurized to 30 MPa and 45 MPa, respectively. It has been established that, of the 2 strategies, cascade refueling is more energy efficient and scalable for larger vehicles [20].

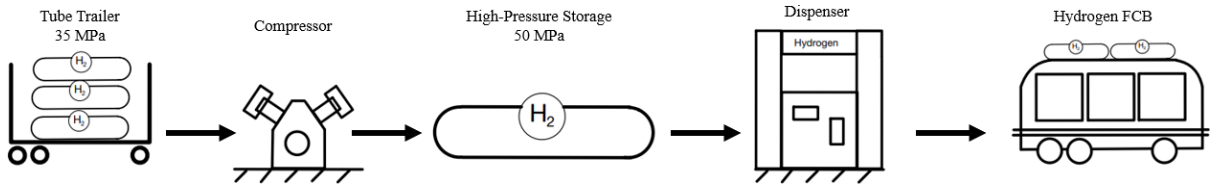

Fig. 8. Process diagram of hydrogen refueling station for fuel cell buses in London, buffer refueling [19].

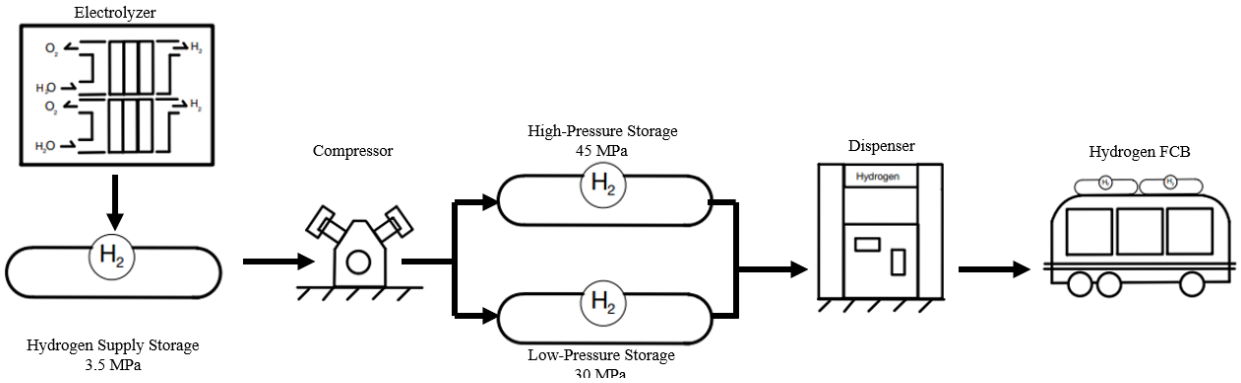

Fig. 9. Process diagram of hydrogen refueling station for fuel cell buses in Aalborg, cascade refueling [19].

To facilitate the design and development of HRSs, refueling protocols such as those defined by SAE J2601, which define the average pressure ramp rate and the gas conditioning

temperature during the fill of a vehicle, were developed through research or testing in specialized hydrogen test labs. As is the case with PRHYDE, a refueling protocol for HD hydrogen refueling, a consortium of industrial partners came together to provide guidance on standardized, cost-effective hydrogen station design, ultimately influencing the high-flow version of SAE J2601-5 [15]. In parallel, some groups have developed software, employing thermodynamic numerical methods to help design and develop hydrogen gas dispensers. These gas dispensers are analogous to the fuel pumps used at conventional gas stations. A rendering of a hydrogen gas dispenser is shown in Fig. 10.

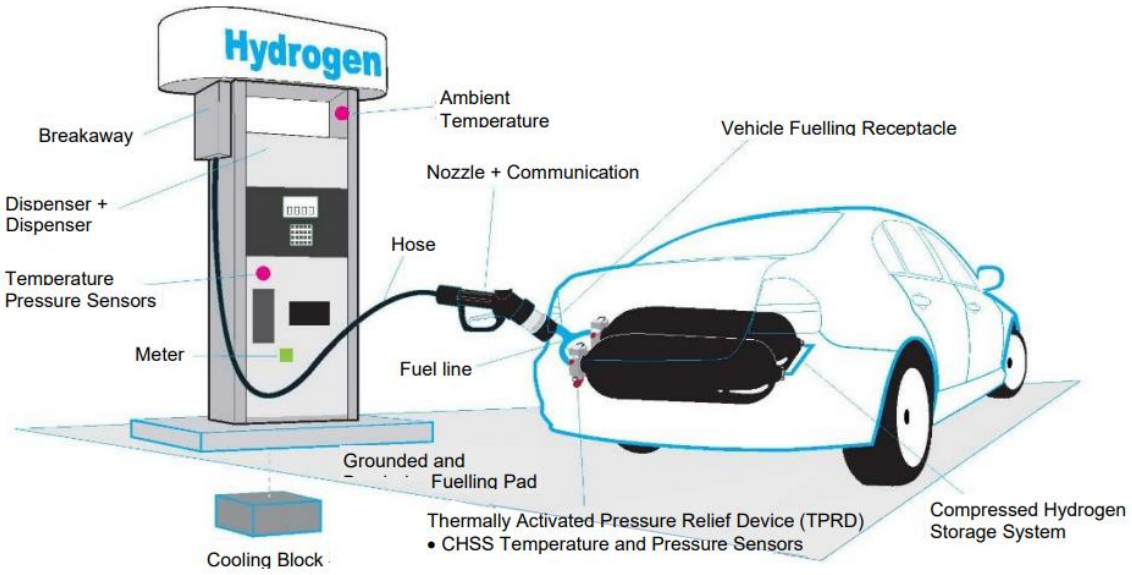

Fig. 10. Example of a hydrogen gas dispenser and the key components, including the vehicle CHSS [16].

Most thermodynamic numerical models solve for mass and energy balances and focus on simulating the actual refueling process. H2FillS [21], developed by National Renewable Energy Laboratory (NREL), solves the mass and energy balance equations for each component in a refueling station, from the high-pressure storage to the vehicle. H2FillS is a user-friendly software

that is free to use and is commonly used by hydrogen dispenser manufacturers to understand how the dispenser will perform during refueling. The user interface is shown in Fig. 11, and the output results are shown in Fig. 12. Note that the model provides data for vehicle pressure, vehicle temperature and fueling delivery temperature; however, the high-pressure hydrogen storage remains unchanged. As far as the author of this study is aware, the H2FillS model is not designed in such a way as to output a change in the high-pressure storage. Although this may not be an issue for dispenser manufacturers, this is a critical piece of information for HRS manufacturers, integrators and testing facilities. Note that the configuration shown in Fig. 11 and the data shown in Fig. 12, were generated by the author of this paper using the free H2FillS software [21].

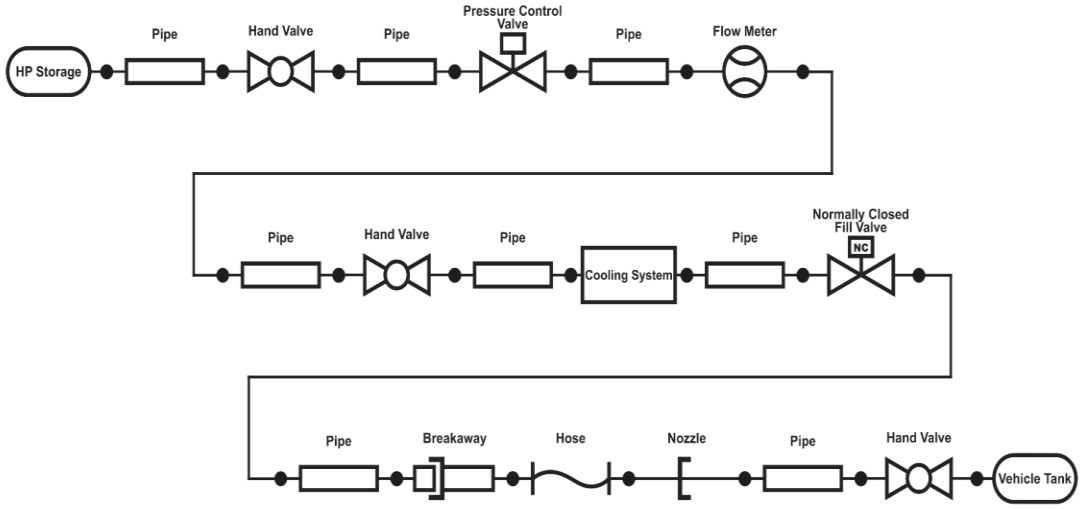

Fig. 11. H2FillS GUI for refueling a 40 L H70 FCEV, 92 MPa storage & -33°C pre-cooling [21].

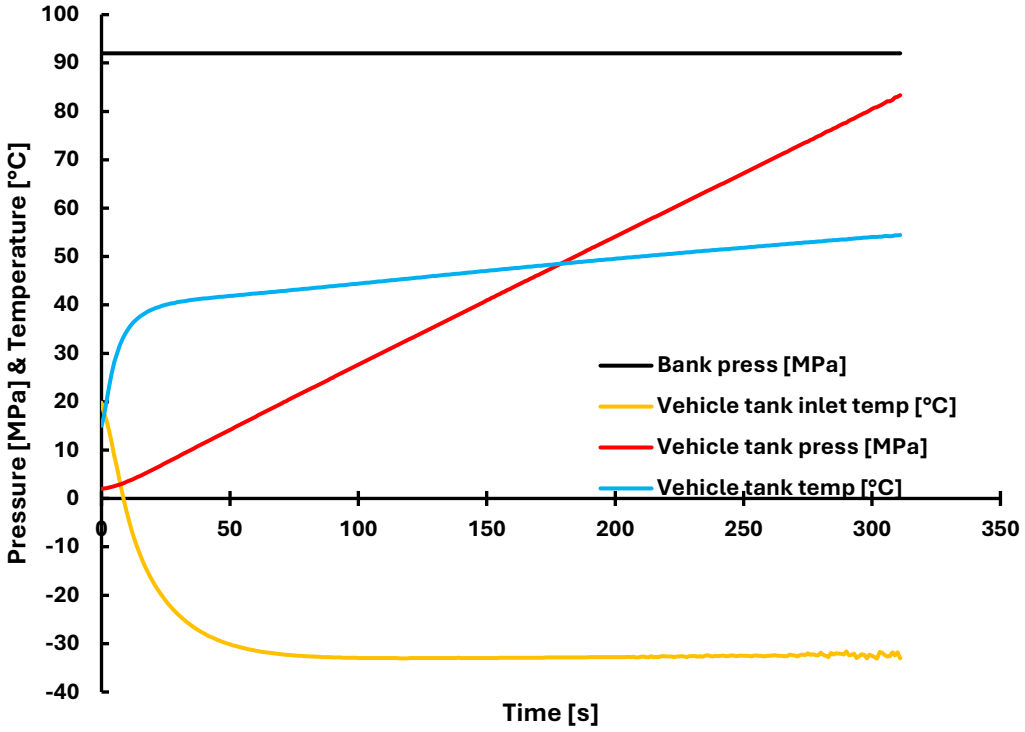

Fig. 12. H2FillS refueling simulation for 40 L H70 vehicle, 92 MPa storage & -33°C pre-cooling [21].

Research in light-duty refueling is extensive and many different cascading strategies have been suggested [12, 16, 20 - 24]. A three-cascade strategy, with a low-pressure (LP), medium-pressure (MP) and high-pressure (HP) storage banks is most commonly adopted by light-duty hydrogen refueling stations to balance the cost and complexity of hydrogen storage and the energy consumed during each refueling cycle [20].

It is important to note, briefly, that there are alternatives to compressed gaseous hydrogen storage solutions. Liquid hydrogen (LH2), commonly used in liquid oxygen and liquid hydrogen rockets [22], has been adapted for use as in transportation. The volumetric energy density of LH2 is nearly twice that of gaseous hydrogen compressed to 70 MPa [23]. One disadvantage to LH2 is the boil-off losses during periods of inactivity at refueling stations, which occur due to the phase

change from liquid to gaseous as the LH2 heats up. During that time, the pressure in the vessel increases until the safety pressure relief valve releases the excess pressure [24]. Despite some of the advantages to LH2, the focus of this study will remain on compressed gaseous hydrogen, as it is most commonly used in currently hydrogen vehicle applications.

As the hydrogen industry shifts from light-duty to heavy-duty vehicles, numerical tools like H2FillS will play an integral role in the development of infrastructure because they are significantly more cost-effective than performing experimentation and can investigate possible solutions in cases where the technology has yet to be developed. Hydrogen storage tanks, along with the valves and components used, control systems, refrigeration systems required to perform experimental testing, and measurement equipment can come at a very high cost. The cost of hydrogen gas alone comes at a significant cost as the hydrogen storage required to refuel heavy-duty vehicles is expected to be ten times greater, in terms of volume of the cylinders and the stored mass, than what is required to fill light-duty vehicles. Furthermore, fueling and defueling cycles incur significant time costs, as it may take multiple hours to defuel a hydrogen vehicle or compress hydrogen storage banks to full pressure. Finally, research lacks numerical models that focus on the hydrogen cascade refueling strategies valid for heavy-duty vehicles with on-board storage up to 60 kg.

In this thesis, a numerical model is developed to predict the high-pressure hydrogen storage required to refuel heavy-duty hydrogen vehicles, up to 60kg, to 100% state of charge (SOC). Rather than using standard thermodynamic mass and energy balance equations, the numerical model combines virial equations of state (EoS) and gradient descent techniques,

specifically the generalized reduced gradient (GRG) method, to describe the change in storage pressure and vehicle pressure after each cascade.

Experimental testing is performed to validate the numerical model for both light-duty vehicles and heavy-duty vehicles up to 14 kg on-board storage at 100% SOC. The numerical model is also validated against data from experiments presented by NREL, for HD vehicles up to 60 kg. The effects of increasing storage volume, storage pressure, and the number of cascades are investigated. Energy consumption and the volume ratio (VR) are used to compare different cascade refueling strategies. Using the developed model, a case study is performed to suggest refueling strategies for a heavy-duty FCEV with 1,500L (60kg) of on-board storage. The case study focuses the hydrogen infrastructure and on-site storage available at a testing facility in British Columbia, Canada.

1.2 – Objectives:

The objectives of this study are as follows:

- To perform refueling experiments and validate the numerical model for FCEVs up to 60kg
- To develop a numerical model to simulate heavy-duty hydrogen refueling using a combination of equations of state and a GRG non-linear solver.
- To perform parametric studies to investigate cascading refueling strategies for HD refueling, with a focus on the effects of storage pressure, storage volume and number of cascades, evaluating different strategies based on energy consumption and volume ratio.
- To use the numerical model to perform a case study focused on refueling a 1,500L H70 FCEV using the available hydrogen infrastructure at a test facility located in Surrey, BC, comparing possible strategies based on energy consumption and volume ratio.

In the chapters to follow, existing research relating to hydrogen refueling is explored through a literature review. Then, the experimental set-up and the data analysis of two refueling experiments are evaluated. The development of the numerical model is described and then validated against the results of the experiments. Using the numerical model, parametric studies are performed, and the effects of storage volume, pressure and the number of cascades are investigated and discussed. Finally, conclusions based on the findings of the numerical model are presented, and future work is discussed. Fig. 13 shows a flow chart outlining the approach taken throughout this study.

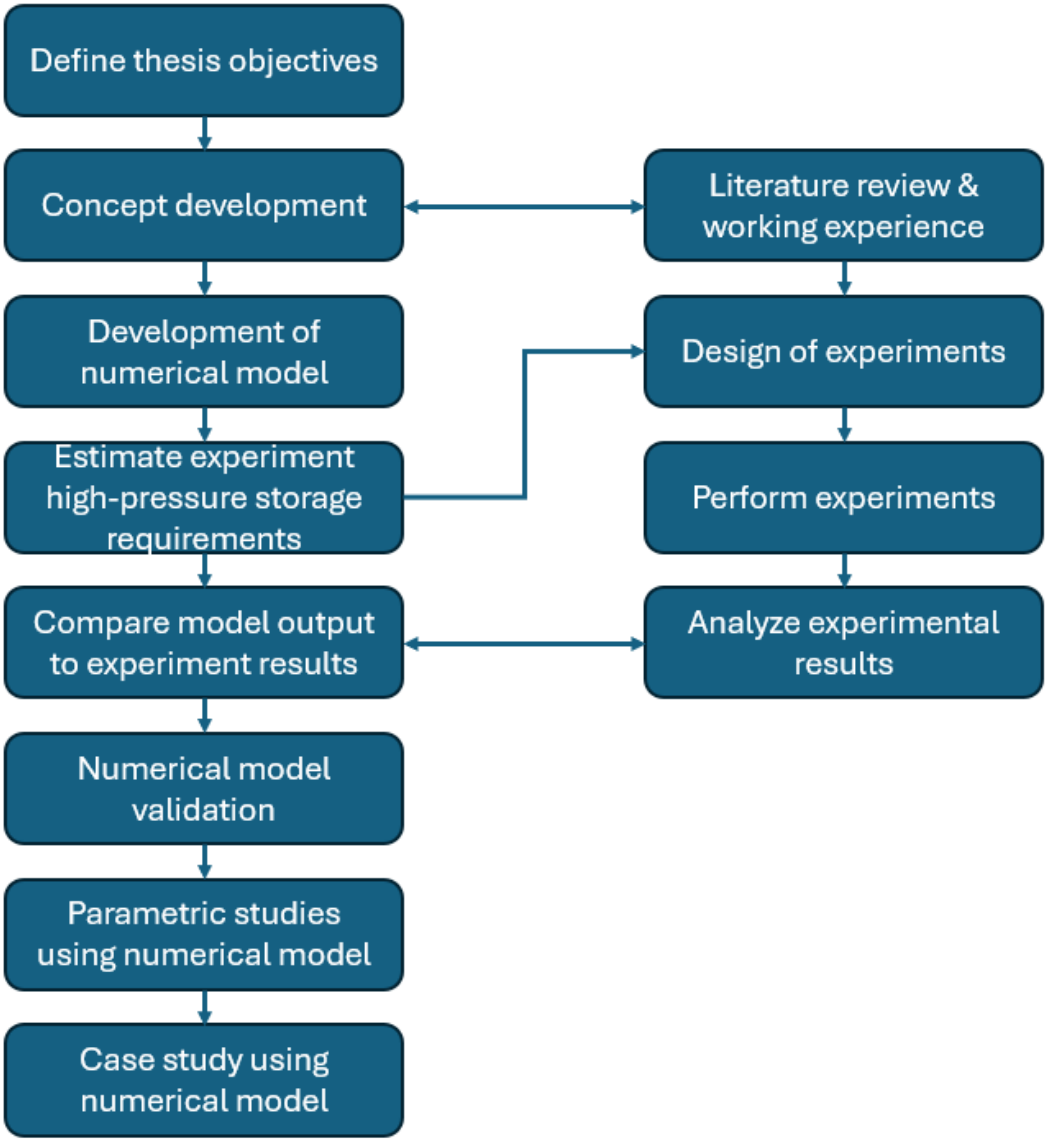

Fig. 13 Flow-chart outlining the approach taken in the development of a numerical model to estimate the high-pressure hydrogen required to refuel HD FCEVs.

Chapter 2 – Literature Review

The following section will expand on some of the topics introduced in the previous chapter of this report. There is limited research and experimental data available that focuses on simulating refueling for heavy-duty hydrogen vehicles with on-board hydrogen storage greater than 60 kg. Therefore, many of the studies presented in this section discuss the research performed for refueling light-duty vehicles.

In 2014, Rothuizen et al. studied the trade-offs between the number of cascades, the volume of each cascade and the pressure of each cascade, from the perspective of overall energy consumption, for a light-duty vehicle with a NWP of 70 MPa and 7 kg of on-board storage [20]. The study considered the total energy consumed by the major energy consumption components of an HRS: the compressors, refrigeration system, heat transfer from the vehicle cylinder, and plumbing pressure losses. The thermodynamic model used the first law equations in Dymola software. Rothuizen et al. showed that as the number of cascades increased less energy was consumed, noting that the largest energy consumption comes from the compressor, as illustrated in Fig. 14.

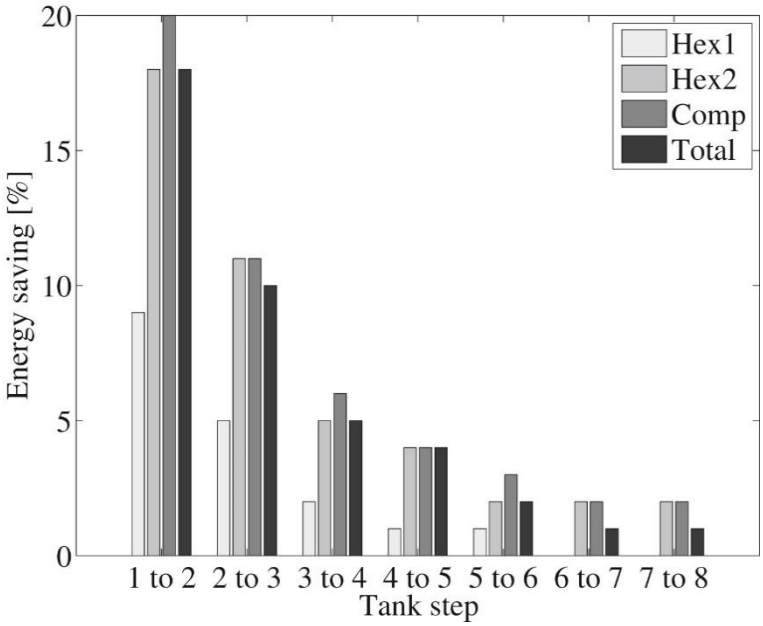

Fig. 14. Energy savings as a function of cascading refueling systems [20].

In another study from 2013, Rothuizen et al. showed that a three-stage cascading strategy yields a 12% energy savings related to cooling hydrogen and requires 17% less compression energy, when compared to the single-stage refueling of a similar light-duty vehicle [25]. Ultimately, it was determined that increasing the number of cascades can reduce the total energy consumption of the HRS, but they concluded that 3 or 4 cascades are optimal as the energy savings of 5 or more cascades is less than 3%. Rothuizen et al. determined that the total stored mass required to fuel a 7 kg vehicle from a single bank pressurized to 90 MPa was 138.85 kg. However, when considering a three-stage cascade system, pressurized to 45 MPa, 65 MPa and 91 MPa, respectively, the required stored mass was reduced to 112.3 kg [25]. Each bank was considered to have a volume of 1 m^3. Talpacci et al., 2018, used the conservation of mass and energy balance equations to determine the ideal cascading strategy from a cooling energy point of view [26]. Talpacci et al. found that cascading strategies with smaller low- and medium-

pressure storage banks compared to the high-pressure bank reduced the cooling energy consumption. Talpacci et al. determined that the optimal cascading strategy was 3:3:25. Finally, Blazquez-Diaz's 2019 study found that as the number of storage banks increased, the total volume required at a HRS decreased [27]. Their study built upon the studies performed by Rothuizen et al., focusing on reducing the total cost of a station, noting that the total hydrogen storage volume played the most significant role in the initial station cost. They suggested that an HRS should have a 4 to 5 cascade refueling strategy. They suggested that the storage should be configured so that the high-pressure storage had a volume up to 4 times that of the low-pressure storage bank.

The hydrogen research community benefited from research performed for CNG vehicles. Farzaneh-Gord et al., 2011, developed an optimization problem for refueling CNG cylinders, using the utilization ratio as the objective function [28]. The iterative optimization method considered the utilization ratio as the objective function to determine the optimal volume ratio. The utilization ratio is the ratio of mass that can be transferred from the storage cylinder to the vehicle compared to the initial mass in the storage cylinder. In 2012, Farzaneh-Gord et al. developed a thermodynamic model to compare buffer refueling and cascade refueling [29]. Farzaneh-Gord et al. developed a mathematical method using the continuity (conservation of mass) and first law of thermodynamics to find the specific internal energy and the specific volume of a CNG cylinder at any given time in the refueling process. Then, mass and energy balance equations were used to simulate the refueling process. The results of the study found that buffer refueling generated twice as much as the entropy as 3-stage cascading. However, filling times for buffer storage were nearly 66% less than cascading strategies. It was determined that the optimal volume ratio was 3:2:1, for 3-stage CNG applications with a NWP of 24 MPa. Then, in 2016, Farzaneh-Gord et al.

applied the model to refueling light-duty hydrogen vehicles with a nominal working pressure of 35 MPa and 150 L water volume (3.5 kg of on-board H_2) [30]. Cascade refueling generated about 55% of the entropy compared to buffer refueling but had longer refueling times. The cascading strategy suggested by Farzaneh-Gord et al. was a 3-stage cascade with the LP, MP and HP storage banks pressurized to 11 MPa, 21 MPa and 37 MPa, respectively. In 2012, Hosseini et al. performed a parametric study, varying the initial tank temperature, and evaluated exergy destruction using a similar numerical strategy [31]. Hosseini et al. found that cascading strategies had less exergy destruction compared to buffer refueling.

Yu et al. performed a study in 2022, focusing on the volume ratio, utilization ratio and specific energy consumption for three-cascade storage systems [32]. The thermodynamic model uses mass and energy balance equations to simulate refueling and employs a real gas equation of state to solve the mass balance equations. The real gas equation of state, shown in equation (2-1), where α was determined to be 1.9155×10^{-6} K/Pa, is based on curve-fitting of thermo-property tables and was developed by Chen et al. [33]. The study performed by Chen et al., in 2010, showed how the ideal gas assumption overestimates the density of hydrogen beyond 20 MPa, when compared to other real-gas equations and thermo-properties data from the National Institute of Science and Technology (NIST), shown in Fig. 15.

$$Z = \frac{PV}{RT} = (1 + \frac{\alpha P}{T}) \qquad (2-1)$$

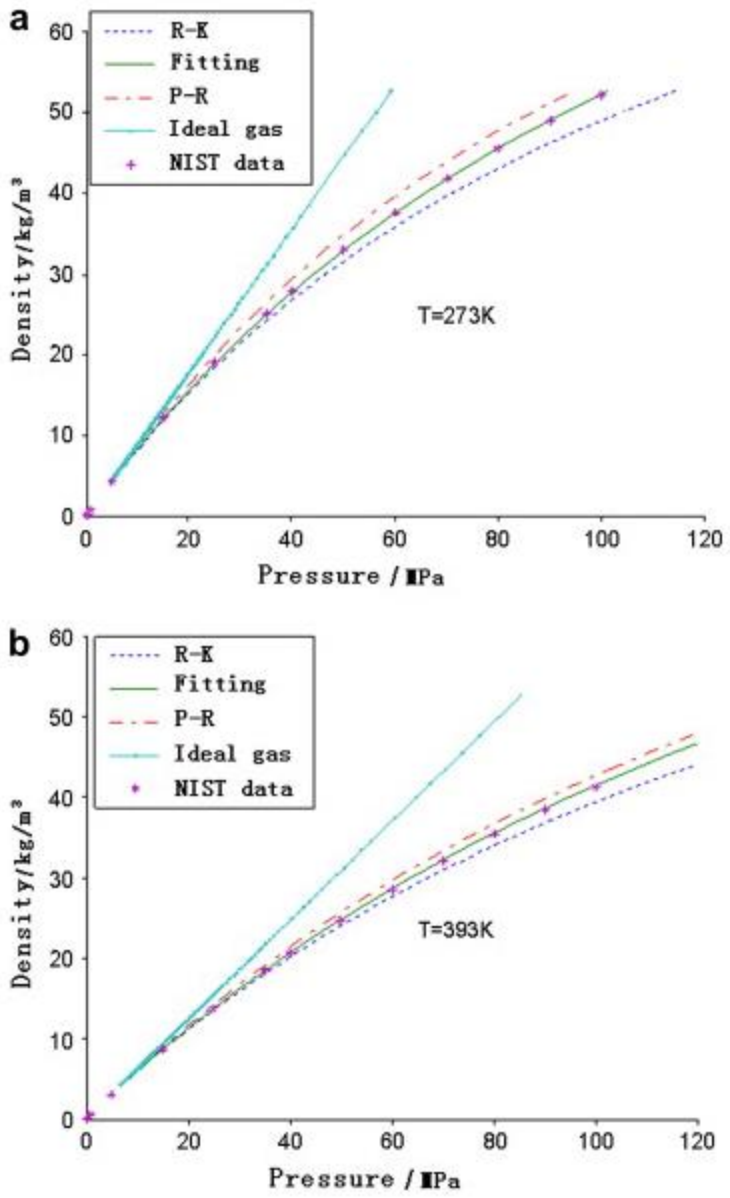

Fig. 15 Comparison of real-gas state equations a) T=273 K b) T=393 K [33].

When calculating the thermodynamic properties of gases, the pressure is often described as a function of temperature and density. However, as Lemmon et al. explain [34], this can be inconvenient for hydrogen refueling applications where an iterative process must be used to describe density as a function of temperature and pressure. It is known that at low pressure, less than 1 MPa, and high temperatures, above 27°C, hydrogen can be considered an ideal gas.

However, assuming hydrogen is an ideal gas at the pressures and temperatures experienced throughout refueling would result in significant errors when calculating the thermodynamic properties of hydrogen during refueling. In the vehicle, pressure varies from 2 MPa to 87.5 MPa, and temperature varies between -40°C to 85°C. This is because hydrogen gas deviates from ideal-gas behavior, and thus a correction factor, known as the compressibility factor Z, must be introduced.

In 2024, Bilgili et al. performed a CFD analysis, using ANSYS Fluent, on the effects that different real gas equations have on the fast-filling process of hydrogen storage tanks [35]. Bilgili et al. used the pressure-based solver in ANSYS Fluent for numerical computations, and the mass, energy and momentum equations were considered. The following four real-gas equations were studied: Redlich-Kwong (2-2), Soave Redlich-Kwong (2-3), Aungier Redlich-Kwong (2-4) and Peng-Robinson (2-5). Ultimately it was shown that out of the four equations used, the Redlich-Kwong equation provided results closest to the experimental results. Each of the equations are shown below, where a, b, c and α are constants found based on the critical pressure and temperature of the fluid considered.

$$P = \frac{RT}{V-b} - \frac{a}{\sqrt{T}V(V+b)} \qquad (2-2)$$

$$P = \frac{RT}{V-b} - \frac{a\alpha}{V(V+b)} \qquad (2-3)$$

$$P = \frac{RT}{V-b+c} - \frac{\alpha}{V(V+b)} \qquad (2-4)$$

$$P = \frac{RT}{V-b} - \frac{a}{V^2+2bV-b^2} \qquad (2-5)$$

Although the Peng-Robinson and Redlich-Kwong equations are much more accurate when compared to the ideal gas equation, the simplified real-gas equation developed by Chen et al. is even more accurate when compared to the data from the Reference Fluid Thermodynamic and Transport Properties Database, published by NIST [36]. The model proposed by Chen et al. uses curve-fitting combined with the NIST data to obtain the density of hydrogen in the pressure range of 0.1 MPa to 100 MPa with an accuracy of 1.1% between -20°C and 120°C, and 3.8%, between -100°C and 120°C, when compared to NIST data. Lemmon et al. provide a virial EoS for hydrogen gas to determine the compressibility factor and hydrogen density with an even higher accuracy, as shown in Table 1, and thus it is chosen as the EoS used in this study.

Table 1. Valid range for the Revised Standardized Equation for Hydrogen Gas Densities For Fuel Consumption Applications [33].

Pressure Range [MPa]	Temperature Range [°C]	Accuracy to NIST
0.1 to 70	-53 to 727	0.01%
0.1 to 120	-18 to 727	0.04%
0.1 to 200	-123 to 727	0.15%

It is clear, from the studies presented above, that research for LD refueling is extensive and there are many optimization techniques that have been used to improve refueling strategies. However, there have been limited experimental studies performed on HD hydrogen vehicles, with a nominal working pressure of 70 MPa and on-board storage greater than 60 kg, which makes validating numerical studies difficult. One of the major hurdles of performing experimental studies is having sufficient ground storage to be able to dispense hydrogen at high pressure, due to the significant cost.

One facility with the hydrogen capacity capable of refueling very large FCEVs is NREL. NREL was able to perform refueling tests for simulating FCEVs with 61.5 kg and 82.3 kg on-board hydrogen, achieving 94% and 100% SOC, respectively [37]. Additionally, NREL was able to complete the heavy-duty refueling tests, from 2 MPa to nearly 100% SOC in less than 10 minutes, specifically 4.7 minutes and 6.6 minutes, respectively. A simplified schematic provided in the NREL presentation is shown in Fig. 16. To accomplish this test, 1" and ¾" process tubing and air actuated air valves were required, to ensure a minimal pressure drop between storage and vehicle. The hydrogen storage required to complete the tests comprised of 81 kg stored in 6 cylinders pressurized to 41.4 MPa and 384 kg stored in 16 cylinders pressurized to 93 MPa [37]. The results of the tests performed by NREL can be used to understand the change of internal storage temperature for HD refueling applications and validate the numerical model for heavy-duty FCEVs.

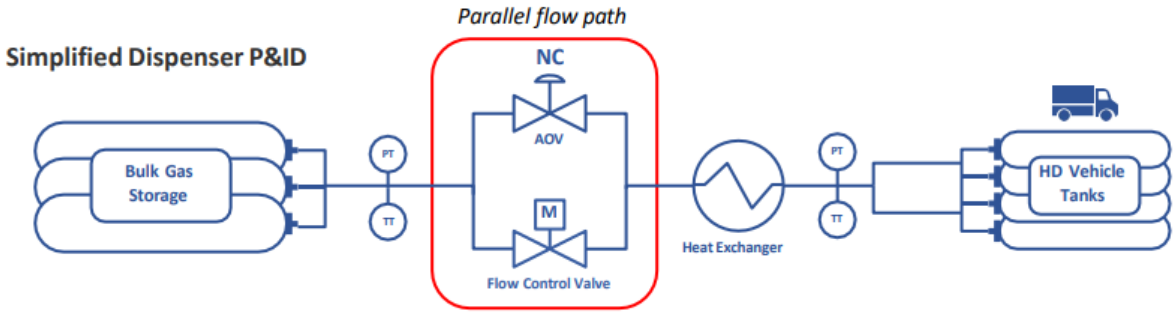

Fig. 16 Simplified P&ID of NREL H70 HD fueling experiment.

From the NREL data it can be observed that hydrogen was dispensed using a 14-stage cascade strategy, as shown in Fig. 17 below. The NREL data describes the pressure across the flow control valve (FCV), dispenser hose and the CHSS used for the experiment. Fig 18 shows the temperature inside each of the storage tanks during testing throughout the NREL experiment. It

can be seen that there is a significant change in temperature when large changes in pressure are experienced, and small changes in temperature when small changes in pressure are experienced. In the second and third cascade, it can be observed that the internal tank temperature approaches the low temperature limit. This is an important parameter for HRS manufacturers and operators to consider as HD FCEVs increase their on-board storage capacity. An additional consideration is the lower pressure limits identified in Fig. 17. For Type I and Type II storage cylinders there is a limit to the number of allowable deep cycles. In some cases, these tanks can be limited to as little as 100 cycles in order to limit the potential for failure from expansion and contraction cycles, therefore a minimum pressure may need to be considered as an additional constraint when developing a numerical model. The minimum pressure also reduces the amount of hydrogen that can be dispensed from these tanks, highlighting another important consideration for HRS manufacturers and operators, when designing and HRS. Fig. 19 shows the layout of the NREL hydrogen refueling facility.

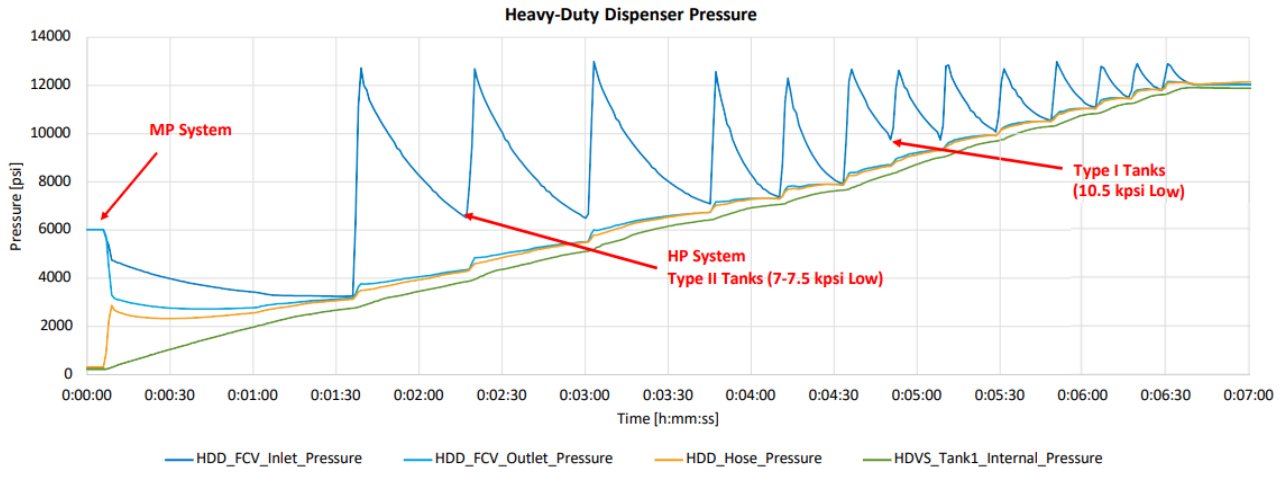

Fig. 17. Pressure profile of H70 HD fueling experiment performed by NREL - 82.3 kg [37].

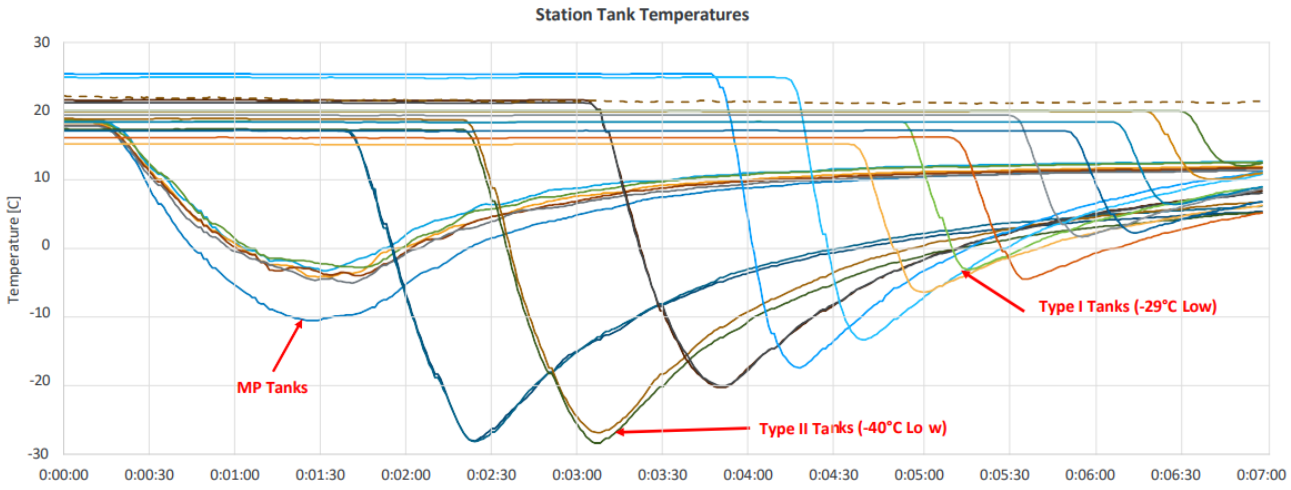

Fig. 18. Pressure profile of H70 HD fueling experiment performed by NREL - 82.3 kg [37].

Fig. 19. NREL HD Fast Flowing Test Facility [37].

Chapter 3 – Experimentation & Numerical Modelling

In the following chapter, the experimentation performed during this thesis is presented and is then followed by the development of the numerical model. This chapter is presented in this way to provide a practical understanding of hydrogen refueling before simplifying hydrogen refueling to develop the numerical model. However, throughout the development of this thesis, experimentation and numerical modeling were performed in parallel.

3.1 - Experimentation

The following section presents the experimental set-up used to obtain data from refueling two different hydrogen vehicle fuel systems. A fuel system is described as a hydrogen cylinder with an on-tank valve (OTV). OTVs are used to allow hydrogen gas to flow in and out of the cylinder and are equipped with a thermistor to monitor the internal tank temperature of the vehicle. Often a thermal pressure relief device is integrated into the fuel system to ensure that in the case of a fire the hydrogen gas can be vented off. The typical CHSS is shown in Fig. 20.

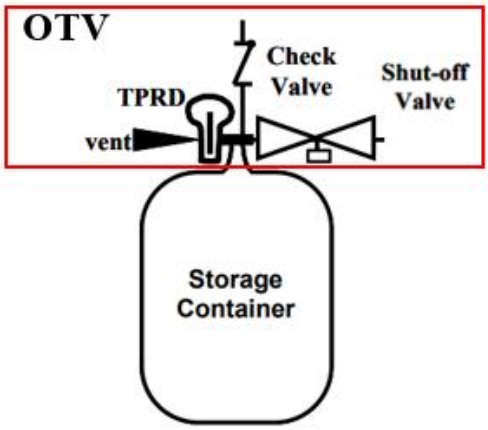

Fig. 20 Typical compressed hydrogen storage system

The first test was performed on an H70 fuel system with a water volume of 165 L. “Water volume” describes the volume of the cylinder when filled with water at atmospheric pressure. The water volume of the cylinder does not account for the expansion and contraction of the cylinder from thermal effects or due to pressurization of the cylinder. At 100% SOC the on-board hydrogen storage would be equal to approximately 6.6 kg, which would classify the fuel system as a LD hydrogen fuel cell vehicle. The second test was performed on an H70 fuel system with a water volume of 350 L, using the same test frame: however, it required additional hydrogen storage, as described in greater detail in section 3.1.1. At 100% SOC, the on-board hydrogen storage would be equal to approximately 14.0 kg, which would classify the fuel system as an HD vehicle.

3.1.1 – Experimental Overview

The 165 L experiment was conducted in accordance with ECE R134 (ECE/TRANS/WP.29/2014/ 78), Section 5.3: Verification test for Expected On-Road Performance (also known as the Pneumatic sequential tests) (Annex 3, Section 4) [10]. Specifically, 150 cycles were performed in accordance with the portion of the regulation commonly known as “Phase 3”. The test parameters of Phase 3 are described in Table 2, below.

Table 2. 165L Hydrogen Gas Cycle Test Parameters

Test Description	Ambient temp. [°C]	Fuel Delivery Temp. [°C]	Initial Pressure [MPa]	Target Pressure [MPa]	Fuel Ramp Rate [MPa/min]	Defuel Rate [g/s]
Ambient Cycles	20 ± 5	≤ -40	2 (+0 /-1)	87.5 (+2/-0)	21.9	~3

In June 2023, the Pneumatic Sequential test was updated and released, requiring some of the test parameters to be changed to realign with refueling protocols. Subsequently, the majority of performance testing carried out after June 2023 is to be performed in accordance with ECE R134 (ECE/TRANS/WP.29/2014/ 78) Phase 2 [16]. Therefore, to validate the model for larger volume FCEVs, a similar experiment using the same test frame as the 165L experiment, was carried out on a 350L cylinder using updated test parameters in accordance with ECE R134 (ECE/TRANS/WP.29/2014/ 78) Phase 2. 150 cycles were performed in accordance with the portion of the regulation commonly known as "Phase 3". The test parameters of Phase 3 are described in Table 3, below. The most notable differences for this phase of testing is the adjustment of the fuel delivery temperature and the target pressure. The fuel delivery temperature was changed from less than -40°C to a temperature corridor of -33°C to -40°C. The target pressure was changed to be a target SOC. Both were changed to align with the SAE J2601 refueling protocol [14].

Table 3. 350 L Hydrogen Gas Cycle Test Parameters.

Test Description	Ambient temp. [°C]	Fuel Delivery Temp. [°C]	Initial Pressure [MPa]	Target SOC [%]	Fuel Ramp Rate [MPa/min]	Defuel Rate [g/s]
Ambient Cycles	20 ± 5	-33°C to -40°C	2 (+0 /-1)	≥ 100	14.5	~5

3.1.2 – Equipment & Instrumentation

A simplified schematic of the gas cycle facility used to perform the hydrogen gas cycle testing is shown in Fig. 21. A heat exchanger, commonly known as a pre-cooler, was used to

control the fuel delivery temperature, which prevents the internal tank temperature from exceeding 85°C. An environmental chamber was used to control the ambient temperature.

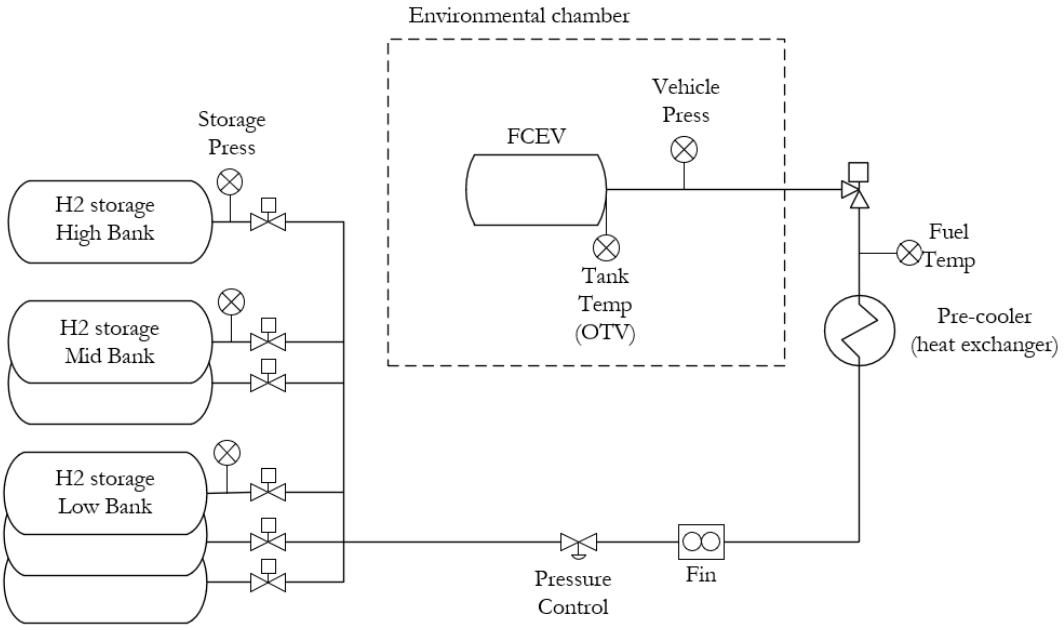

Fig. 21. Test Schematic for 165 L experiment.

Hydrogen gas is allowed to flow from the storage tanks, through the refueling panel consisting of a pressure control regulator, pre-cooler, and fill valve, to the FCEV. During refueling cycles, the pressure control regulator is responsible for applying the APRR. This is accomplished by programming the pressure control regulator to reach the target pressure over a specified time interval. A feedback loop using the vehicle pressure is used to adjust the APRR. The pre-cooler is responsible for maintaining the fuel delivery temperature. The fuel delivery temperature must be lower than -40°C within 30 seconds. A fill valve is used to isolate the vehicle from the test facility if undesirable conditions are met during testing. The vehicle temperature is measured using a thermistor provided by the manufacturer of the OTV. A temperature-resistance table is provided

by the manufacturer to determine the temperature. The equipment is described in more detail below:

3.1.2.1 - High-Pressure Ground Storage:

All the ground storage tanks used for testing are Type IV cylinders. The ground storage available for performing the experiments is outlined below:

- Storage bank 1: 16 x 100 L with an NWP of 70 MPa, divided into 3 cascades
    - Cascade 1: 8 x 100 L equal to 32 kg of H_2
    - Cascade 2: 5 x 100 L equal to 20 kg of H_2
    - Cascade 3: 3 x 100 L equal to 12 kg of H_2
- Storage bank 2: 5 x 175 L with an NWP of 70 MPa, one cascade
    - Cascade 1: 5 x 175 L equal to 35.2 kg of H_2
- Storage bank 3: 6 x 255 L with an NWP of 95 MPa, divided into 3 cascades
    - Cascade 1: 3 x 255 L equal to 37.5 kg of H_2
    - Cascade 2: 2 x 255 L equal to 25 kg of H_2
    - Cascade 3: 1 x 255 L equal to 12.4 kg of H_2

A 6-cascade fueling strategy was applied for both experiments. Like the HD testing performed by NREL [37], the cascading approach was to fill from low pressure storage to high pressure storage, from largest to smallest volume. The first 3 cascades had an initial pressure of approximately 70 MPa. Cascades 4, 5, and 6 were initially pressurized to approximately 94 MPa. For the 165 L experiment, storage banks 1 and 3 were used, whereas for the 350 L experiment, storage banks 1, 2, and 3 were used. The storage bank temperature was assumed to be equivalent to the outdoor ambient temperature, ranging from 15°C to 25°C, during the time of testing, as

there were no thermocouples installed inside the storage cylinders. The cascading strategy used for refueling the 165 L and the 350 L hydrogen fuel cell vehicles are shown in Table 4.

Table 4. Cascading strategies used for refueling 165 L & 350 L FCEVs

Experiment	Storage bank	Cascade	Pressure	Volume
165 L	1	1	70 MPa	800 L
	1	2	70 MPa	500 L
	1	3	70 MPa	300 L
	3	4	94 MPa	765 L
	3	5	94 MPa	510 L
	3	6	94 MPa	255L
350 L	1&2	1	70 MPa	1,675 L
	1	2	70 MPa	500 L
	1	3	70 MPa	300 L
	3	4	94 MPa	765 L
	3	5	94 MPa	510 L
	3	6	94 MPa	255L

3.1.2.2 - Dispensing Panel:

The dispensing panel considers the process tubing, control valves, and heat exchanger used during testing. The dispensing panel is used to emulate a dispenser found at a hydrogen refueling station.

- 3/8” outside diameter stainless steel tubing, used for all the process tubing
    - Rated pressure: 103.42 MPa
- Normally closed air-operated valves, used for all storage banks and shut-off valves
    - Rate pressure: 138 MPa
    - CV: 0.75

- Pressure control valve, used to control the APRR
    - Rated pressure: 138 MPa
    - CV: 0.3
- Heat exchanger, used for meeting the gas conditioning parameters
    - Rated pressure: 95 MPa
    - Design heat load absorption: 81.4 kW
    - Design flow rate: 60 g/s
- 165 L fuel system, Type IV cylinder & OTV
    - Rated pressure: 70 MPa
    - Temperature measurement: thermistor
    - Dimensions: N/A
- 350 L fuel system, Type IV cylinder & OTV
    - Rated pressure: 70 MPa
    - Temperature measurement: thermistor
    - Dimensions: N/A

The details of the instrumentation used are shown in Table 5. All the instrumentation for this test was recorded by a data acquisition system operating at a sampling rate of at least 20 Hz and a recording frequency of 2 Hz. All instrumentation was calibrated in accordance with ISO 17025 to ensure that the data collected were reliable and accurate. The measured uncertainty calculations are shown below and are applied to the results, presented in the discussion portion of this study. The instrumentation summary, shown in Table 5, is valid for both 165 L and 350 L experiments.

Table 5. Experimental instrumentation summary for 165 L & 350 L FCEVs

Instrument Type	Test Parameter	Make & Model	Range
Pressure Transducer	Vehicle Pressure, MPa	NoShok, 623-15000-1-1-6-6-20	15,000 psi
Thermocouple	Fuel Delivery Temperature, °C	Omega, TMQSS-125G-6	-200°C to +200°C
Thermocouple	Ambient Temperature, °C	Omega, TMQSS-125G-6	-200°C to +200°C
Pressure Transducer	*Storage Pressure, MPa	Stellar Technologies, GT1600-15000G-162	15,000 psi
DAQ Module	-	National Instruments, 9203	± 20 mA
DAQ Module	-	National Instruments, 9213	± 78.125 mV
DAQ Module	-	National Instruments, 9205	± 10 V

*Each cascade in a refueling strategy has a unique pressure transducer, Storage Pressure, in Table 4 above, represents the instrumentation used for all cascades at the test facility.

To obtain the total uncertainty of the measurement instrumentation, it is necessary to calculate the combined uncertainty of the DAQ module and the pressure transducers used during testing. The combined uncertainty calculation, shown below, reveals that there is a combined uncertainty of 0.153 MPa and 0.201 MPa for the storage pressure and vehicle pressure measurements, respectively. To ensure a high confidence level in the data collected during testing, an expanded uncertainty is applied. An expanded uncertainty with a coverage factor of 2 provides a 95% confidence level in the collected data [38]. The expanded combined uncertainty for pressure measurement using a normal distribution is 0.306 MPa and 0.402 MPa, respectively. The combined uncertainty calculations are outlined in the following sub section.

3.1.2.3 - Rectangular combined uncertainty measurement calculation:

Let:

- a(y) = accuracy of the instrument
- mu(y) = uncertainty of the instrument
- mu_c(y) = combined uncertainty
- mu_x(y) = expanded combined uncertainty
- y = 1 be the DAQ module
- y = 2 be the pressure transducer
- k = coverage factor

The uncertainty of each instrument is calculated by Eq. (3-1) [38]:

$$mu(y) = \frac{a(y)}{\sqrt{3}} \qquad (3-1)$$

Then the combined uncertainty of system is then found through Eq. (3-2) [38],

$$mu_c(1,2) = \sqrt{\left(\frac{a(1)}{\sqrt{3}}\right)^2 + \left(\frac{a(2)}{\sqrt{3}}\right)^2} \qquad (3-2)$$

The expanded uncertainty is then calculated by Eq. (3-3) [38]:

$$mu_x(1,2) = kmu_c(1,2) \qquad (3-3)$$

As mentioned above, these calculations were performed for the combination of pressure transducers and DAQ modules to obtain combined expanded uncertainties. The expanded uncertainty is combined with the standard deviation of the final pressure of each cascade in Section 3.3 to provide a valid range when validating the numerical model outputs against the experimental data.

3.1.3 – Experimental Process & Data Measurement

3.1.3.1 – 165 L Hydrogen Gas Cycle Experiment – Pressure Evaluation

Fig. 22 and Fig. 23 show a sample of the data captured during testing of the 165 L FCEV. In Fig. 22, the vehicle pressure is compared to the storage pressure of each cascade during the refueling cycle and demonstrates how cascade refueling is carried out. The vehicle pressure starts with an initial pressure of less than 2 MPa, and all the storage banks are filled to their respective initial pressures. The first cascade storage bank is opened, and hydrogen gas is allowed to flow into the FCEV. The first cascade remains open until the first cascade nearly equalizes with the FCEV. Once the difference in pressure between the storage bank and the FCEV is less than the pre-determined pressure delta, the first cascade storage bank is closed, the second storage bank is opened, and refueling continues. The pre-determined pressure deltas were set to 5 MPa, 9 MPa, 9 MPa, 3 MPa, 3 MPa, and 3 MPa for each of the 6 cascades, respectively. By the end of the third cascade, the FCEV has reached a pressure of 63.5 MPa. Although the NWP of the cylinder has been nearly reached, cascades 4, 5 and 6 are required to bring the FCEV to a pressure greater than 87.5 MPa (1.25 times NWP). During this cycle the final pressure achieved was 88.1 MPa. It is clear that the first and fourth cascades have the most significant impact on increasing the FCEV pressure. This is because, as the vehicle pressure approaches the initial pressure of the storage bank, there is less pressure gradient to flow from storage to the vehicle. The result is that less volume is necessary in the later cascades of the same pressure. Note that, as the fourth cascade was opened there is a sharp increase in pressure. This sharp increase is due to a sudden change of the inlet pressure in the pressure control valve. At the end of the second cascade and during

the third cascade, the pressure control valve is nearly fully opened to maintain the APRR, 21.9 MPa/min, as there was not a great enough pressure delta between the storage and the vehicle, approximately 9 MPa, causing the fueling rate to decrease. When the fourth cascade is opened, hydrogen gas rushes through the PCV, causing a sharp increase in pressure, until the feedback loop is able to respond.

Once all 150 cycles were completed, the data was processed. The initial and final pressure of each cascade, and the final pressure of the FCEV after each cascade, were extracted. This data will be compiled and compared to the model results, in section 3.3.1 of this chapter.

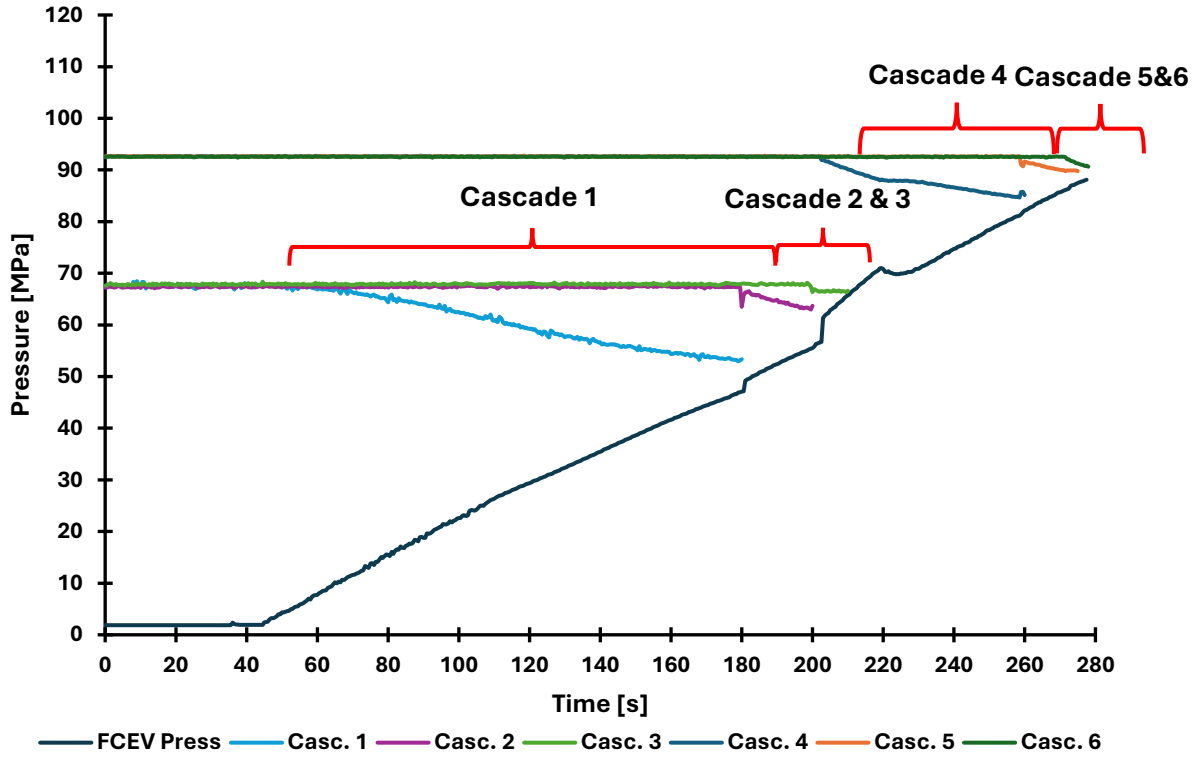

Fig. 22. Experimental refueling cycle comparing cascade pressure and FCEV pressure - 165 L.

3.1.3.2 – 165 L Hydrogen Gas Cycle Experiment – Temperature Evaluation

In Fig. 23, the internal tank temperature of the vehicle is compared to the fuel delivery temperature throughout the refueling cycle. At 45 seconds it is observed that the internal tank temperature begins to increase, and the fuel delivery begins to decrease, representing the start of the refueling cycle. The fuel delivery temperature meets a temperature below -40°C in 22 seconds and maintains an average of -42.6°C throughout the rest of the cycle. Maximum internal tank temperature of 58°C is experienced, and an average temperature of 47°C is observed after the first 30 seconds of the refueling cycle. As will be discussed in the assumptions, there is a sharp increase in the vehicle temperature at the start of the cycle, as the initial gas that enters the tank is close to ambient temperature. However, once the fuel delivery temperature reaches -40°C, the rate of temperature increase in the FCEV significantly slows, as expected from the results found in research [38, 39]. The reason for the internal tank temperature starting at approximately -30°C is that each refueling cycle in the experiments started immediately following the defuel of the previous cycle. This represents a possible extreme condition that may be experienced when the FCEV arrives at an HRS with an empty tank.

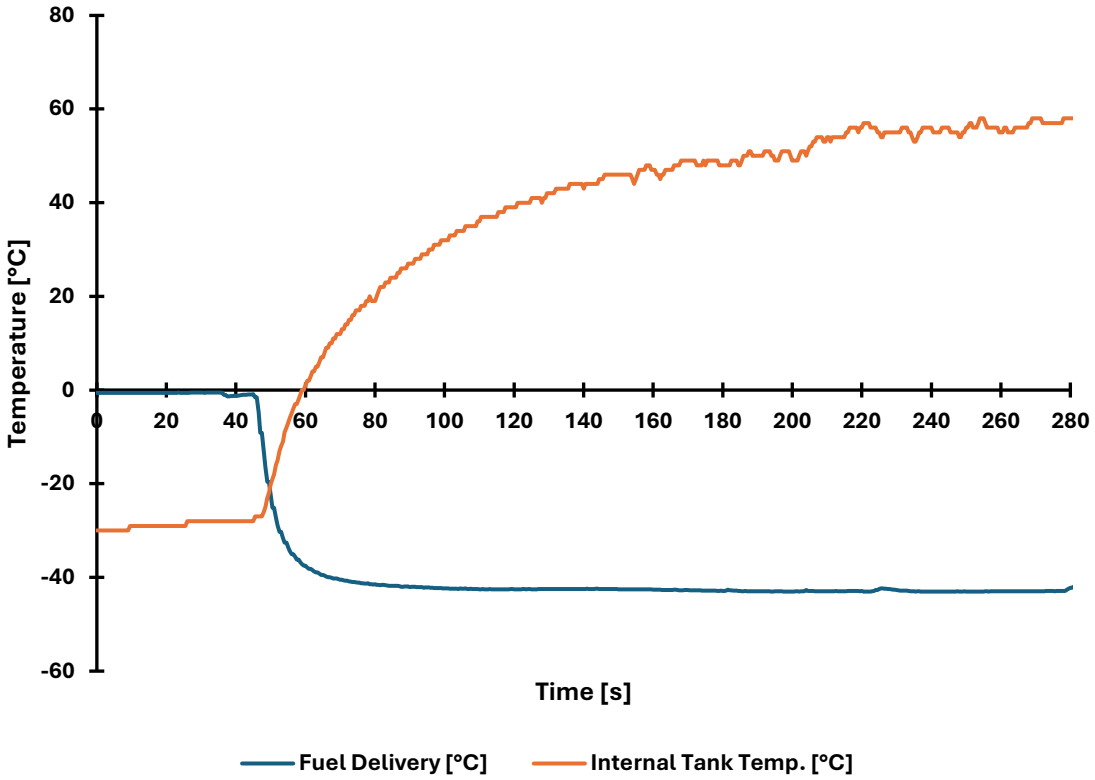

Fig. 23. Experimental comparison of Fuel Delivery temperature & Internal FCEV temperature - 165L.

3.1.3.3 – 350 L Hydrogen Gas Cycle Experiment – Pressure Evaluation

Fig. 24 shows a simplified schematic for the gas cycle facility used to perform the 350 L experiment. Note that, by changing to a target SOC, the final pressure of each cycle will be closer to 80.5 MPa, which is less than 87.5 MPa, the target pressure of the original release of the standard. This is because the internal tank temperature is expected to reach 50°C to 60°C, which means that the final FCEV pressure will only need to reach 80.5 MPa for 100% SOC to be achieved; a final pressure of 87.5 MPa is equivalent to 106% SOC at 55°C. Despite this reduction in the target pressure, 875 L of 70 MPa hydrogen storage was added to the first cascade of this test so that the target SOC could be reached.

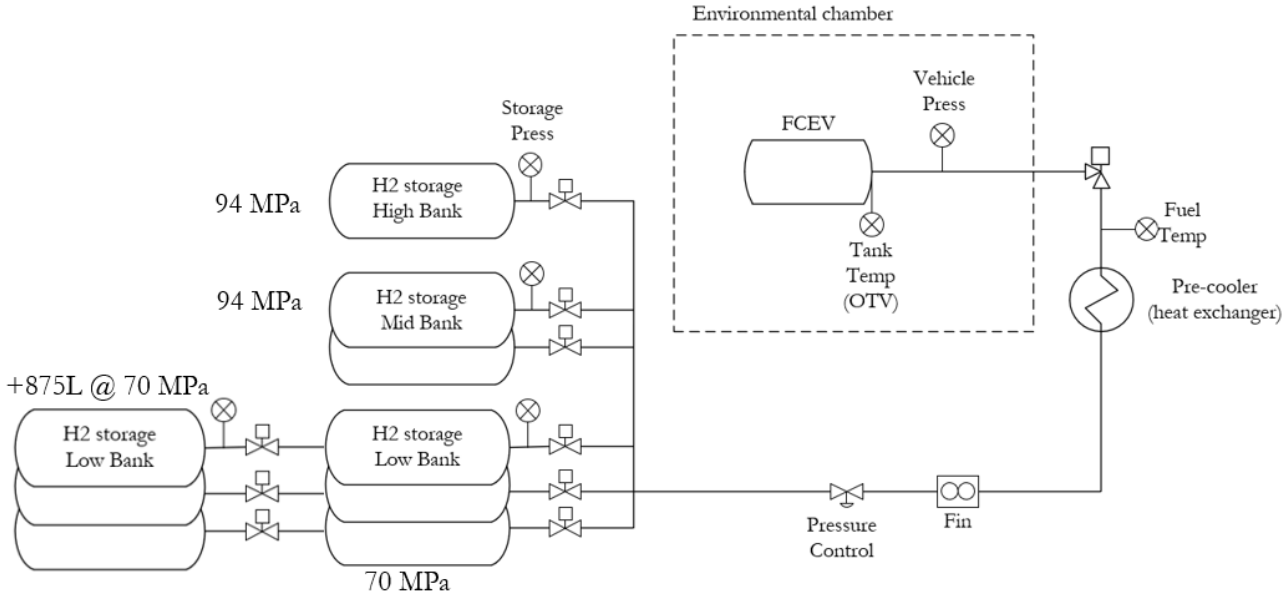

Fig. 24. Test Schematic for 350 L experiment.

Fig. 25 and Fig. 26 show the data collected during the 350 L FCEV experiment. The pressure profiles, shown in Fig. 25 for the 350 L experiment, show very similar results when compared to the 165 L experiment. In this experiment, the pressure deltas between the storage and vehicle were increased so that the APRR, 14.5 MPa/min, was maintained throughout the refueling cycle. The first and fourth cascades have the biggest impact on increasing the pressure in the vehicle. However, when compared to the 165 L experiment, much more gas is depleted from the later cascades, approximately 4.2 kg of a total of 14 kg for the 350 L refueling experiment, compared to approximately 1.4 kg of a total 6.6 kg for the 165L refueling experiment. This is likely due to the volume ratio of each cascade being significantly smaller in the case of the 350 L experiment. The SOC data is non-linear due to SOC being a function of pressure and temperature, as shown later in the methodology section. However, as the end of the refueling cycle is approached, the

trend becomes more linear as the internal tank temperature approaches a more constant value. The final pressure during this refueling cycle was 81.1 MPa.

Once all 150 cycles were completed, the data was processed, and the initial and final pressure of each cascade, and the final pressure in the FCEV after each cascade, were extracted. The results are shown in section 3.3.2 of this chapter.

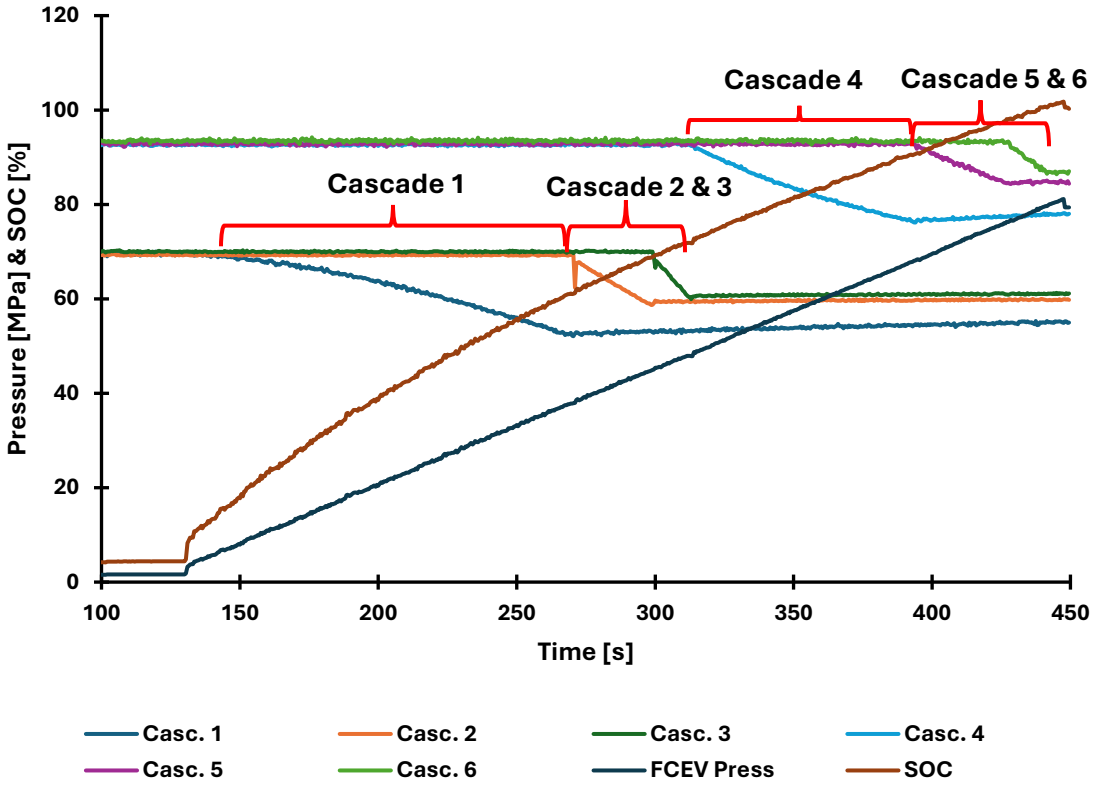

Fig. 25. Experimental refueling cycle comparing cascade pressure and FCEV pressure & SOC - 350 L.

3.1.3.4 – 350 L Hydrogen Gas Cycle Experiment – Temperature Evaluation

In Fig. 26, the internal tank temperature of the vehicle is compared to the fuel delivery temperature throughout the refueling cycle for the 350 L experiment. In this experiment, the fuel delivery temperature was set to achieve the fuel delivery temperature corridor of -33°C to -40°C

within 30 seconds of the start of the fill, required by the latest release of the standard. A fuel delivery temperature corridor is the temperature range the fuel delivery temperature must stay within throughout the fill; otherwise, the fill is aborted. In the 350 L experiment, a difference of approximately 6°C was observed in the fuel delivery temperature, when compared to the 165L experiment. The initial temperature was -37°C, which was about 10°C less than that of the 165L, and the final temperature was 50°C which was approximately 5°C less than in the 165 L experiment. The difference in final temperature could be associated with the differences in initial temperature, fuel delivery temperature, and the APPR. However, despite the differences, the results show the general trend that is expected from research referenced in the 165 L experiment. The effect of initial and final vehicle pressure is presented in Section 4.1.

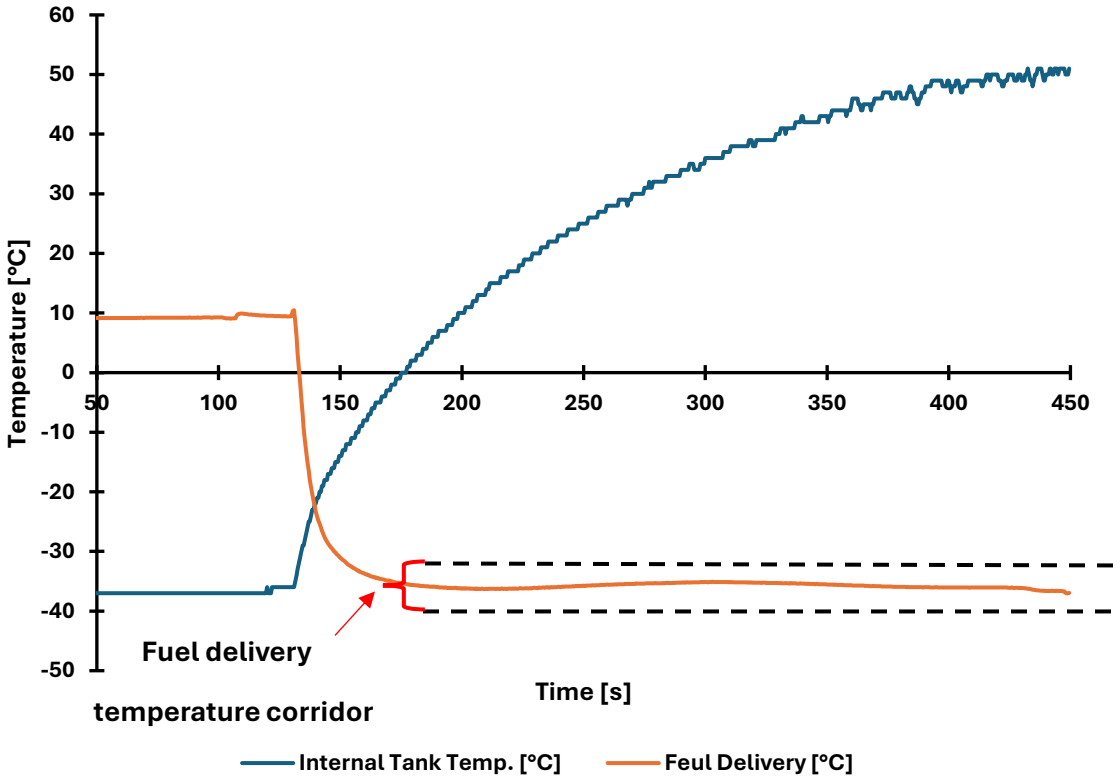

Fig. 26. Experimental Comparison of Fuel Delivery temperature & Internal FCEV temperature - 350 L.

There are very few laboratories with hydrogen infrastructure capable of performing the experiments in this section. Fortunately for the author of this study, access to a hydrogen test lab was provided by Powertech Labs Inc., a research, development, and testing subsidiary of BC Hydro located in Surrey, BC. The testing facility and the data obtained throughout testing were permitted to be presented in this study.

3.2 - Numerical Modelling:

Hydrogen infrastructure, specifically HRSs, is a cornerstone of the widespread adoption of FCEVs in the HD transportation sector. Research has shown that as the hydrogen industry expands into the HD transportation sector, there is a gap in understanding refueling strategies for fueling HD hydrogen vehicles. In this section, a unique numerical model, using equations of state and GRG nonlinear programming techniques, is developed for estimating the high-pressure hydrogen storage required for refueling HD vehicles. A problem definition is presented, and the initial and stopping conditions of the numerical model are defined. The overall methodology is presented, and the model assumptions are outlined.

3.2.1 - Problem Definition

The goal of this study is to develop and validate a numerical model to estimate the high-pressure hydrogen storage required to refuel heavy-duty hydrogen vehicles with a nominal working pressure of 70 MPa and on-board storage of 60 kg of compressed hydrogen gas.

The 165 L experiment will be used to validate the model for light-duty vehicles, whereas the 350 L experiment will be used to validate the model for heavy-duty vehicles. By validating the model against both the 165 L and 350 L experiments, the numerical model can be said to be valid for both light-duty and heavy-duty vehicles which are equivalent to passenger vehicles and small trucks. Increasing the valid range of the numerical model to 60 kg means that long-haul trucking, marine, and aviation applications can be studied using the numerical model.

3.2.2 - Initial Conditions

The following parameters were used to initialize the starting conditions of each storage tank:

- Initial Storage Pressure, $P_{sn,i}$ is 35 MPa to 95 MPa
- Storage tank water volume, V_{sn} is 250 L to 4,500 L
- Cascades, n is 3 to 8
- Initial Vehicle Pressure, P_{vi} is 2 MPa
- Initial temperature, T_{vi} is 15°C

3.2.3 - Stopping Conditions

The model will consider a fill to be complete if one of two stopping conditions are met.

1. The vehicle state of charge is greater than 100 %, SOC > 100 %
2. The mass of the final cascade has been depleted, thus there are no other storage tanks to attempt to fill the FCEV.

SOC will be calculated after each cascade of the fueling strategy being evaluated in the model. SOC will be evaluated according to Eq. (3-4) below:

$$SOC\ [\%] = \frac{\rho_{P,T}}{\rho_{NWP,15°C}} * 100 \qquad (3-4)$$

3.2.4 – Methodology

As discussed previously, a major goal of this study is to develop a numerical model to predict the hydrogen storage required to refuel HD FCEVs. Consequently, the goal is to simplify an HRS down to a model that focuses on storage banks and on-board vehicle storage. Fig. 27

shows a simplified schematic of the components and equipment used in an HRS, from the storage banks to the vehicle.

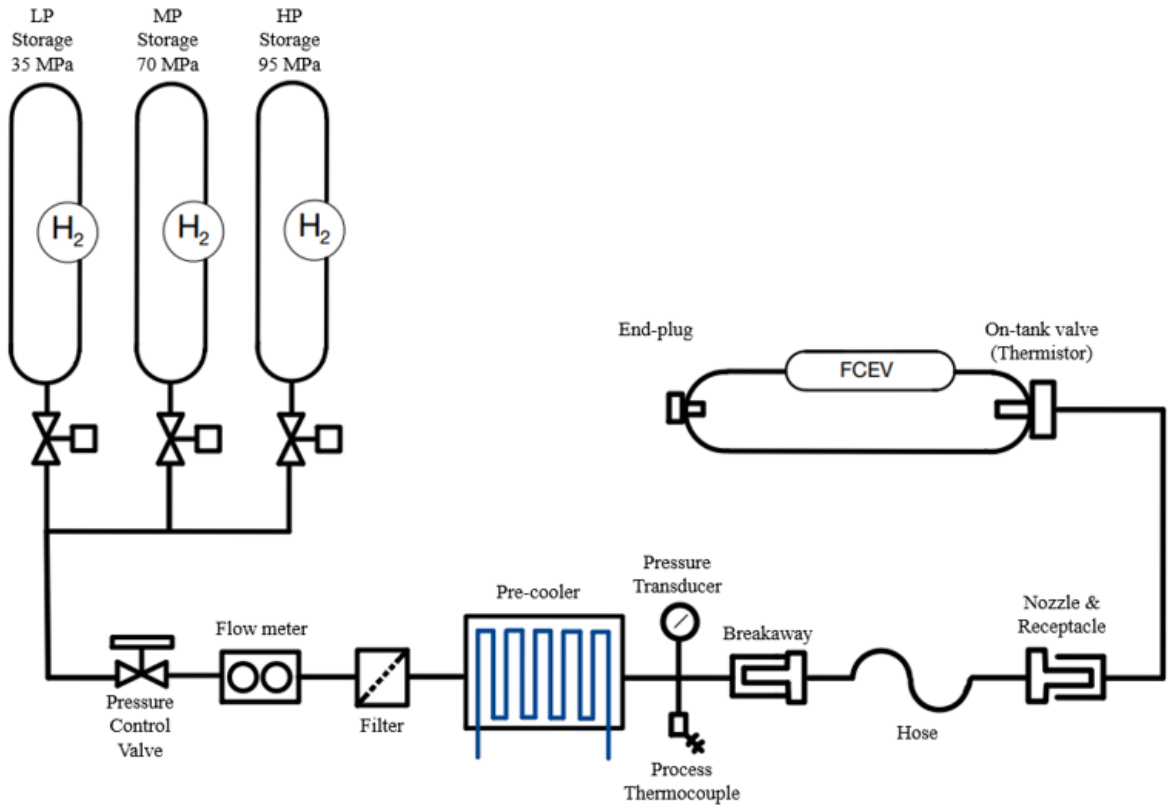

Fig. 27. Simplified Schematic of key components used in HRS from Storage banks to FCEV.

Note that the schematic example used shows the storage banks split into three pressure zones, similar to those presented in the literature review portion of this report [18, 23-30]. This schematic can be simplified further, as shown in Fig. 28, where the pressure control valve, flow meter, heat exchanger (commonly referred to as a pre-cooler), process instrumentation, breakaway, hose, nozzle, and receptacle are removed.

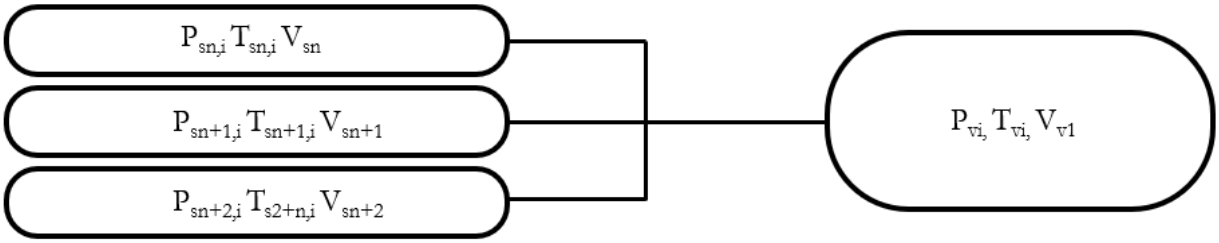

Fig. 28. Simplified HRS for Numerical Modeling.

Where:

- P_s is the storage pressure
- P_v is the vehicle pressure
- T_s is the storage temperature
- T_v is the vehicle temperature
- V_s is the storage bank volume
- V_V is the vehicle volume
- i is the initial value
- n is the number of banks (cascades)

To describe the thermo-properties of both the storage banks and the vehicle, the equation of state (EoS) developed by Lemmon et al. is employed as follows in Eq. (3-5a) [34]:

$$Z(P,T) = \frac{P}{\rho RT} = 1 + \sum_{i=1}^{9} a_i \left(\frac{100\ K}{T}\right)^{b^i} \left(\frac{P}{1\ MPa}\right)^{c^i} \qquad (3-5a)$$

The constants associated with the equation above are described in Table 6. Pressure, 'P', is given in MPa, and temperature, 'T', is given in K. The universal gas constant, 'R', was taken to be 8.314472 J/(mol.K), and the molar mass of diatomic hydrogen, 'M' = 2.01588 g/mol.

Table 6. Constants associated with the Lemmon et al. density equation for hydrogen [34].

i	a_i	b_i	c_i
1	0.05888460	1.325	1.0
2	-0.06136111	1.87	1.0
3	-0.002650473	2.5	2.0
4	0.002731125	2.8	2.0
5	0.001802374	2.938	2.42
6	-0.001150707	3.14	2.63
7	0.9588528 x 10E-4	3.37	3.0
8	-0.1109040 x 10E-6	3.75	4.0
9	0.1264403 x 10E-9	4.0	5.0

The mass in each tank, at any given pressure and temperature, is calculated by first calculating the Z factor, then solving the density by manipulating the Lemmon et al. EoS as shown in Eq. (3-5b), then multiplying the density by the water volume of the cylinder shown in Eq. (3-6).

$$\rho = \frac{P}{Z\frac{R}{M}T} = \frac{(0.101325\ MPa + P)}{Z * \frac{8.314472\frac{J}{mol\ K}}{\frac{2.01588g}{mol}} * (273.15 + T)K} * \frac{1000\ L}{m^3} \qquad (3-5b)$$

$$m = \rho V \qquad (3-6)$$

Calculating the mass is important because the model compares the mass depleted from each storage bank to the mass filled into the vehicle, in accordance with the continuity equation, also known as the conservation of mass, Eq. (3-7).

$$m_{depleted} - m_{filled} = 0 \qquad (3-7)$$

The nonlinear programming technique, known as the Generalized Reduction Gradient (GRG) method for nonlinear programming, requires a minimum of two components: a decision variable and an objective function.

The GRG method for nonlinear programming was developed for computer programming by Ladson et al. [39] and was implemented as one of the solver functions in Excel. GRG is a modification of the gradient descent method, which was introduced to solve nonlinear problems and to accommodate both linear and nonlinear, equality or inequality, constraints for optimization applications [39]. Ultimately, gradient descent techniques take an initial guess, chosen within a feasible range, and then look for the steepest path, or greatest change from the initial guess, in search of a minimum value of a given function. The procedure is repeated until a local minimum is found. This method can also be used to find a local maximum value or solve for a specific value, as is considered in this study. In GRG nonlinear programming, the objective function is calculated based on the initial guess, then small variations of the decision variable are made until the objective function is improved towards the goal. The difference is that in standard gradient descent, the step size toward in the direction of the steepest path is fixed, whereas in GRG, the step size is variable, which results in more efficient convergence towards the goal.

The non-linear problem to be solved is assumed to have the following form:

$$f(x) = m_{filled} - m_{depleted}$$

$$solve\ f(x) = 0\,, \qquad P_{sf} = x$$

Subject to:

$$0 \leq x \leq 95$$

Where Eq. (3-8) describes the mass being filled in the vehicle,

$$m_{filled} = \frac{V_v * \left(P_{vf} + P_{atm}\right)}{\frac{R}{M} * Z_{vf} * T_{vf}} - \frac{V_v * (P_{vi} + P_{atm})}{\frac{R}{M} * Z_{vi} * T_{vi}} \qquad (3-8)$$

And Eq. (3-9) describes the mass depleted from each storage bank,

$$m_{depleted} = \frac{V_s * (P_{si} + P_{atm})}{\frac{R}{M} * Z_{si} * T_{si}} - \frac{V_s * (x + P_{atm})}{\frac{R}{M} * Z_{sf} * T_{sf}} \qquad (3-9)$$

Eq. (3-10) defines that the final vehicle pressure is equal to the difference between final storage pressure and the pressure delta:

$$P_{vf} = x - \Delta P \qquad (3-10)$$

In this study, the decision variable is considered to be the final storage bank pressure, $P_{sf,}$ and the objective function is the continuity equation. The function starts by initializing the decision variable. Then the objective function is evaluated, and a convergence check is performed. If convergence is achieved, the program ends; if not, a search direction is determined, and a step size is chosen. The decision variable is updated using Newton's method, and Newton's convergence is checked. If convergence is not achieved, then the step size reduced, and the steps repeat. If convergence is achieved, a check to ensure that the result is in a feasible range is

performed. If the result is not within the feasible range, the step size is increased, and a new search direction is determined. If the result is in the feasible range, then the function returns to 'A' and the routine is repeated until convergence is met, and the program ends. How to apply GRG nonlinear programming is shown in Fig. 29.

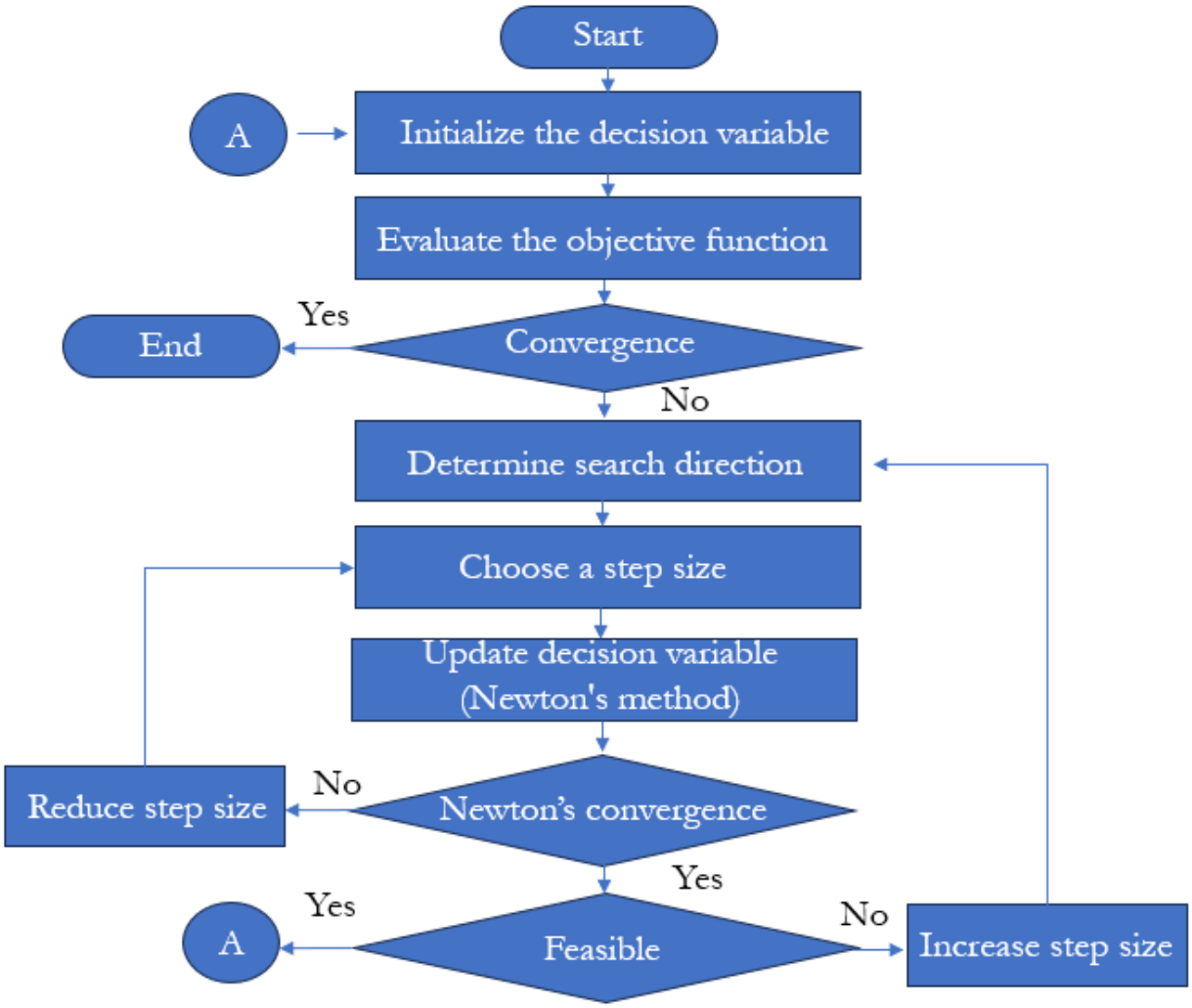

Fig. 29. GRG non-linear solver flow chart.

Rather than solving for a minimum value, the GRG method is set to search for a specific value. As the conservation of mass is the equation being evaluated, the GRG algorithm must continue to update the decision variable until the objective function is 0, signifying that the mass depleted from the active storage bank is equal to the mass filled into the vehicle. Since this is a numerical method, an exact solution is unattainable, so a convergence threshold is required. In this study, a threshold of less than 0.0001 kg was established. A maximum difference in the final storage pressure was found to be 0.038% and 0.0027%, when compared to thresholds of 0.001 kg and 0.00001 kg, respectively.

With the GRG nonlinear solver established, an updated simplified model, which considers the utilization of GRG nonlinear programming, is shown in Fig. 30.

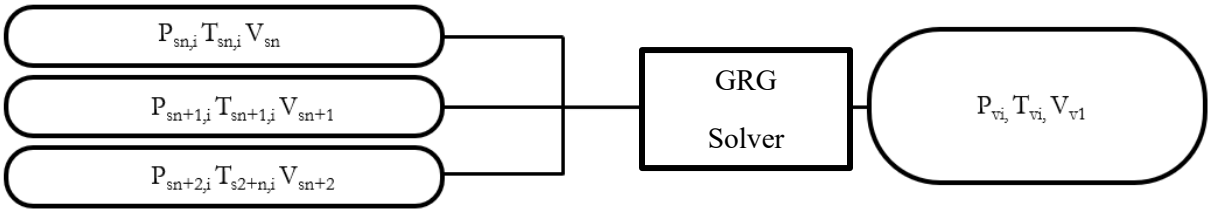

Fig. 30. Simplified HRS for Numerical Model with GRG non-linear programming implemented.

The GRG method is repeated for each of the storage banks initialized in a specified refueling strategy, effectively making the GRG method a sub-routine of a larger calculation, as shown in Fig. 31, below. Although in this study the number of cascades is limited to 8 cascades, this process could be performed for any number of cascades.

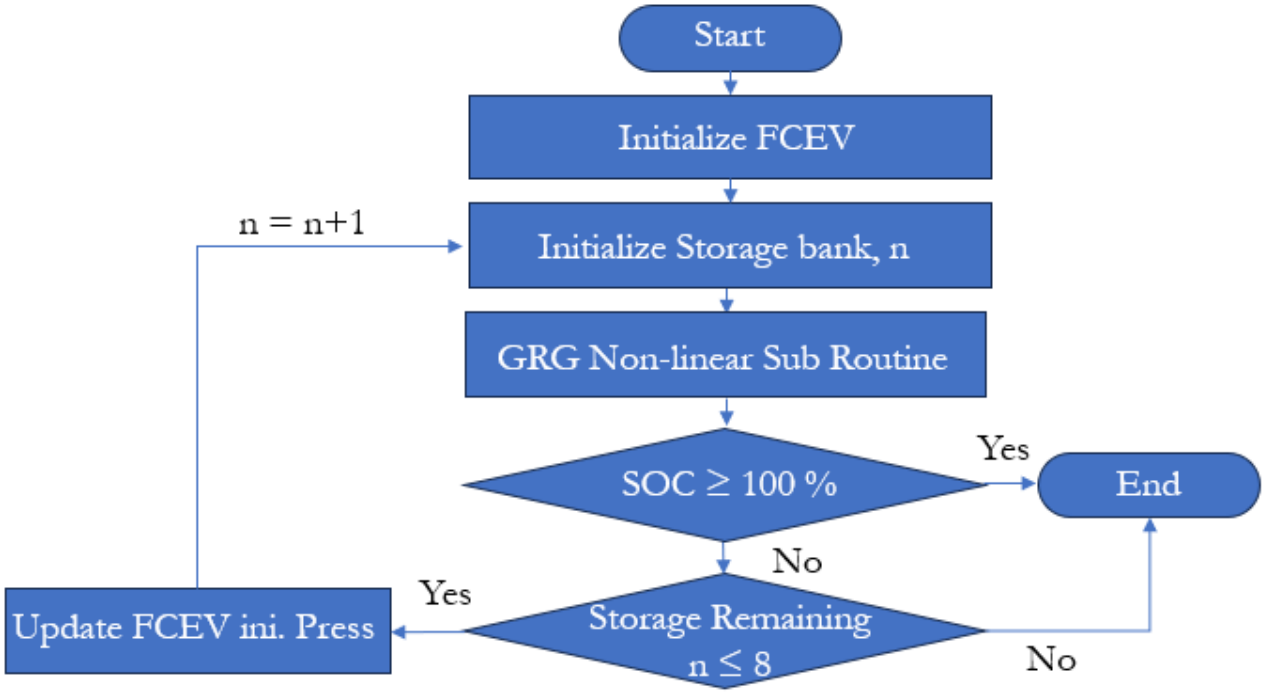

Fig. 31. Flow chart for the numerical model to estimate the high-pressure hydrogen storage for HD FCEV refueling.

To evaluate the change in energy, or rather the energy consumed per cascade, another equation of state is used to find the specific internal energy, 'u' measured in kJ/kg, before and after each cascade. The equation is presented in SAE J2601 [14], and is said to be accurate between 0.5% and 1%. The specific internal energy equation is shown below where, 'P' is absolute pressure in MPa, and 'T' is absolute temperature in Kelvin:

$$u = 496.1 * [(-2.51102 * 10^{-7} * P^2 + 3.270544 * 10^{-5} * P) * T + (1.10237178 * 10^{-4} * P^2 - 1.4948338423 * 10^{-2} * P - 0.706955972653)] \quad (3 - 11)$$

With the change of specific internal energy obtained, the energy consumption of each cascade can be found by multiplying the specific internal energy by the mass depleted from the respective cascade storage bank, in kJ.

3.2.5 - Model assumptions

3.2.5.1 - There are no phase changes during refueling

For hydrogen refueling applications, the purity of hydrogen gas must comply with fuel cell grade hydrogen, so that the impurities in the hydrogen gas do not cause deterioration of the vehicle fuel cell [40]. Fuel cell grade hydrogen is defined to have a purity of 99.97% by mole fraction [41]. In this study, it is assumed that the impurities are negligible, and thus, pure diatomic hydrogen gas is assumed to be used throughout the refueling process. The critical temperature (Tc) and critical pressure (P_c) for hydrogen gas are 33.145 K and 1.2964 MPa, respectively. Using the data provided by NIST it is found that, in the pressure and temperature ranges of this study, hydrogen gas is only in the supercritical phase [36]. Therefore, it can be assumed that only one phase is present. Additionally, as the operable range of this study is significantly far from the critical point of hydrogen gas, we can assume that small fluctuations of pressure and temperature will not result in sharp changes in the properties of the supercritical hydrogen.

3.2.5.2 - There are no external or internal leakages.

In hydrogen the smallest molecule in the known universe, which means it is easily passes through damaged valve seats and stems, resulting in internal and external leakages. External leakages are a loss of hydrogen to the environment during refueling, which results in the reduction in the final pressure in the FCEV. Internal leakages during refueling can reduce the effectiveness of the cascading strategy. External leaks mean that hydrogen gas is being lost to the environment and not being used to refuel the vehicle. Internal leaks mean that the hydrogen gas

may be flowing in and out of an inactive storage tank, resulting in some of the hydrogen gas flowing to a lower pressure storage bank and not into the vehicle. In both cases, leakages result in a reduction of hydrogen being used to fill the vehicle.

Internal and external leakages are often the results of wear of internal components after numerous on-off cycles. Additionally, hydrogen embrittlement can have severe effect on the many material properties of stainless steels, such as reduced fatigue life, increased crack propagation and hardening rate, as shown by Bouledroua et al. [42]. To ensure material compatibility, it is important that the process valves chosen for use in an HRS have undergone hydrogen embrittlement testing via test methods such as those conducted by Bromley [43] and Fukunaga [44]. In this study it is assumed that the HRS has new valves, rated for hydrogen use, with an NWP of 105 MPa, and have been installed correctly, such that there are no internal or external leakages.

It is also assumed that the refueling sequence is programmed in such a way that no hydrogen is allowed to flow from one storage bank into another.

3.2.5.3 - The change in storage internal tank temperature is small

Although there is a significant change in the pressure and temperature in the vehicle, as has been discussed, it is assumed that if the storage volume is large, then the change in pressure during fueling will be small, resulting in a proportionally small change in internal tank temperature. This is illustrated by Rothuizen et al. [25], where a small change in temperature is experienced at the outlet of the storage tank as mass is depleted.

3.2.5.4 - Final temperature in the FCEV after each cascade is approximately 55°C.

It is assumed, in this study, that all refueling cycles are done in accordance with the fueling standards such as SAE J2601 and ECE R134. Consequently, this assumption means that T40 gas conditioning, -33°C to -40°C, is applied, and the APRR is appropriately applied per the water volume of the FCEV. Therefore, it is assumed that the final temperature in the FCEV is approximately 55°C after each cascade. During refueling, the temperature in the FCEV increases sharply at the start of the refueling cycle. This is because the pre-cooling of the gas lags the increase in pressure, as shown by Reddi et al. [45]. However, once the pre-cooling threshold is met, the increase in internal tank temperature can be observed to increase at a significantly slower rate as shown by Luo et al. [46]. Taking an average of the temperatures of the refueling cycles observed experimentally, and the results presented in the aforementioned research papers, an estimated final FCEV internal tank temperature of 55°C is assumed after each cascade.

3.2.5.5 - Pressure drops across the tubing is captured in a pressure switch difference value

It is estimated that there will be some pressure loss across the tubing and process valves used as hydrogen flows from the storage banks, through the dispenser, and into the FCEV. Hanada et al. showed that this pressure loss across the dispenser can often result in the final SOC of a vehicle to being several percent less than what was observed by the HRS [47]. In this study, the pressure loss is captured in the pressure switch difference value (PSDV). As discussed previously, the PSDV is the difference between the storage pressure and the FCEV and the value at which the active cascade is closed, and the next cascade begins. During refueling, it is important to maintain a sufficient pressure gradient to maintain the flow of gas. As the difference in pressure between

the storage banks approaches pressure in the FCEV, the cascade becomes less useful. The threshold at which the cascade is no longer useful is approximately when the pressure loss is equal to the pressure difference between the storage bank and the vehicle, at the target flow rate. This suggests that selecting a pressure delta should be selected in accordance with the pressure loss estimated at any point during the refueling cycle.

Based on the results from the NREL presentation, for heavy-duty refueling, a pressure delta of 3 to 4 MPa is sufficient, assuming that the outside diameter of the tubing is at least ¾" and 9/16" air operated valves are used.

3.2.5.6 – Adiabatic decompression is assumed

To be able to use the energy consumption per cascade as described above, it is necessary to assume that the fast-refueling process is considered to be adiabatic decompression from the point of view of the storage banks, meaning that as the hydrogen gas expands, and the storage cylinders cool, there is no heat exchange with the environment around the cylinders.

3.3 – Data Analysis & Numerical Model Validation

The following section describes how the data collected from both 165 L and 350 L experiments were analyzed. The numerical model is validated against the analyzed experimental data.

Once all the data had been collected from each of the experiments, the initial and final cascade pressures, P_{si} and P_{sv}, were extracted. Then the average value of both variables was calculated from all 150 cycles. The internal tank temperature of the FCEV, T_{vf}, was extracted at the end of each cascade. The average value for the initial cascade pressure, P_{si}, and the FCEV internal tank temperature, T_{vf}, were used as inputs in the numerical model. The final cascade pressure output from the numerical model, P_{sf}, was compared to the experimental results to validate the numerical model.

The standard deviation of the experimental final cascade pressure was determined and was applied as error bars as shown in Fig. 32 and Fig. 34, for each cascade. If the model results fall within the error bars, it can be said that the model can predict the final cascade pressure for each of the vehicles within statistical uncertainty. However, it is also important to consider the combined expanded measurement uncertainty.

An expanded combined measurement uncertainty was used to obtain a 95% confidence level [38]. A 95% confidence level ensures that the experimental results obtained are accurate and can be used to validate the numerical results obtained from the model presented in this study. The error bars presented in Fig. 32 and Fig. 34 consider both the statistical uncertainty and

the expanded uncertainty of the instrumentation used. The valid range calculation is shown below, where σ represents the standard deviation [38].

$$Valid\ range = P_{sf,avg.} \pm [\sigma - \ mu_x(y)] \qquad (3-12)$$

3.3.1 – Model Validation for Light-Duty Vehicles Using the 165 L FCEV Experiment [~6.6kg]

The results of the 165 L experiment are shown in Fig. 32. When comparing the model results to the experimental results, the small change in storage temperature assumption was used. It can be seen that the numerical model output results show a similar trend to the experimental results and are nearly within statistical uncertainty for all cascades. The largest difference is found at the first cascade with a difference of 6.01% from the experimental data; the final pressures of the last three cascades are within 2% of the experimental results. The inaccuracy of the first two cascades is likely a result of the small change in temperature assumption. Reviewing the data from both the model and the experiment, it is observed that there is a significant reduction in the storage pressure of the first two cascades, resulting in a change of pressure of 17.3 MPa and 6.5 MPa, respectively.

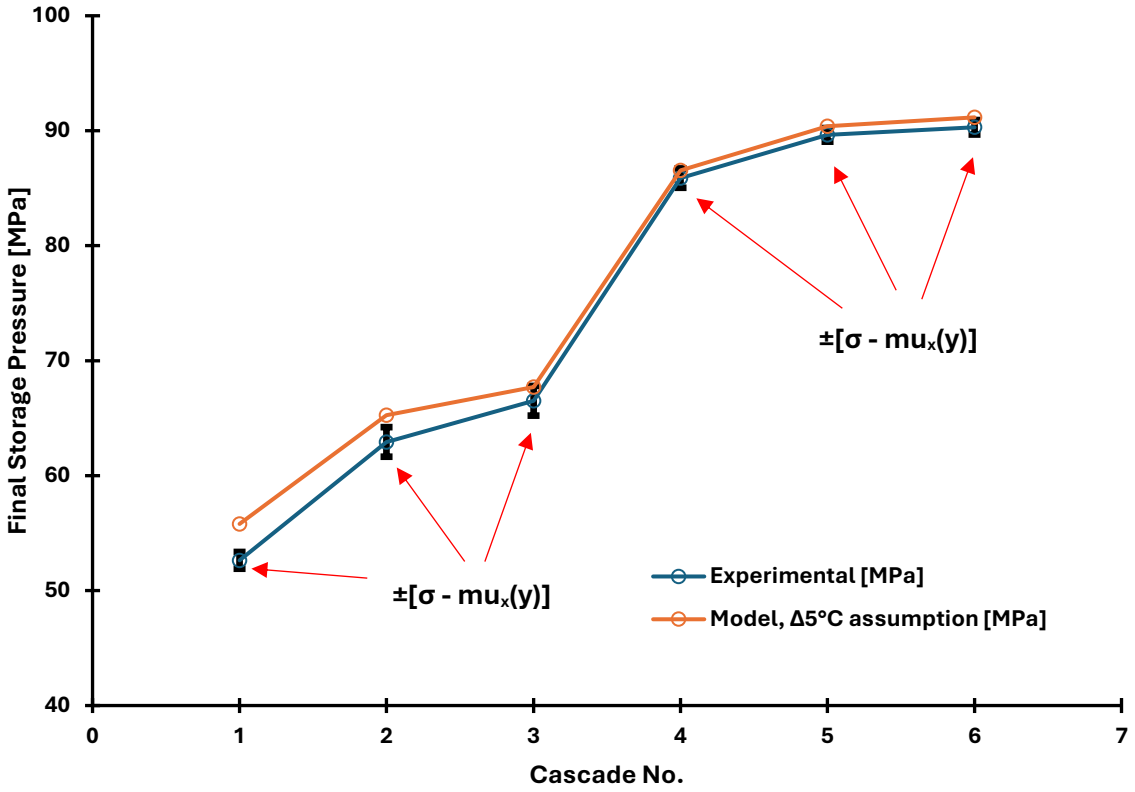

Fig. 32. Comparison of Experimental & Numerical Final Cascade Pressure, P_{sf}, Results, Δ5°C assumption 165L.

Through a trial-and-error final temperature study, reducing the final temperature of the first and second cascade in 5°C increments, the numerical model was adjusted to obtain results for all cascades within statistical uncertainty of the experimental results, shown in Fig. 33. This suggests that, with the proper temperature adjustments, that the numerical model can be used with confidence to produce results that are accurate for vehicles up to 165 L.

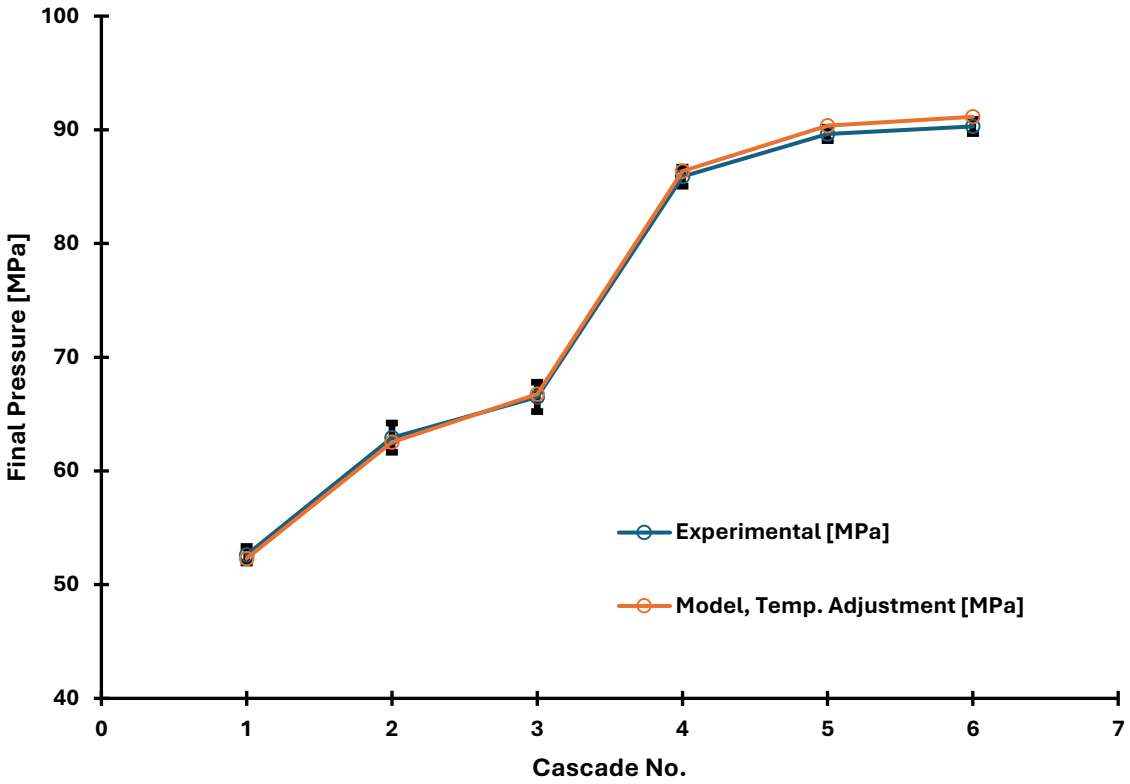

Fig. 33. Comparison of Experimental & Numerical Final Cascade Pressure, P_{sf}, Results, Adjusted Final Temperature, T_{sf} - 165L.

Notably, the difference in numerical results of the final 3 cascades is less than 0.5%, when comparing the small temperature change assumption to the adjusted temperature results.

3.3.2 – Model Validation for Heavy-Duty Vehicles Using 350 L FCEV Experiment [~14 kg]

When performing the comparison for the 350 L FCEV, considering the same small change in temperature assumption, it can be observed that the numerical model provides results that are much less accurate than those from the 165 L experiment, as shown in Fig. 34. On average, the error between numerical model and experiment was found to be approximately 7.5%.

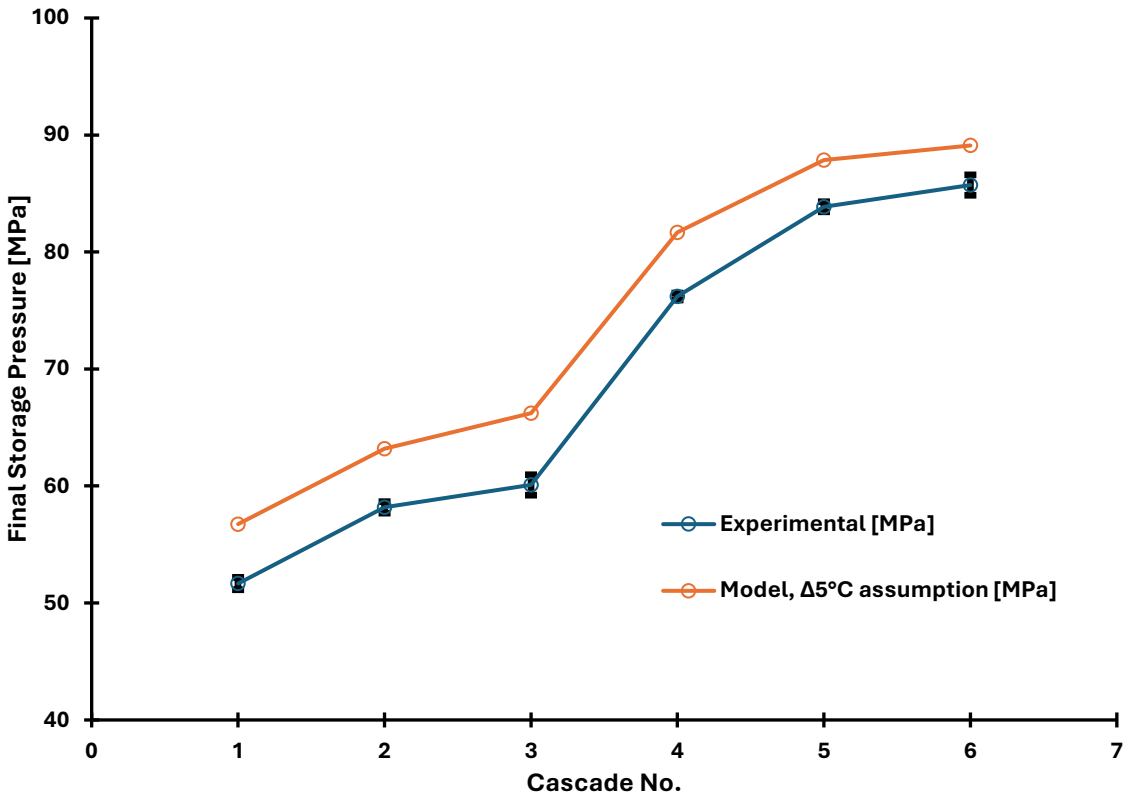

Fig. 34. Comparison of Experimental & Numerical Final Cascade Pressure, P_{sf}, Results, Δ5°C assumption - 350 L.

The final storage temperature in the numerical model can be adjusted through trial and error to achieve results that fall within the statistical uncertainty of the experimental data, as illustrated in Fig. 35. This shows, for cylinders up to 350 L, the model can be considered validated if the following temperature adjustments are applied:

- $\Delta P_s \leq 5$ MPa, $\Delta T_s = 5°C$
- 5 MPa $< \Delta P_s < 10$ MPa, $\Delta T_s = 15°C$
- $\Delta P_s \geq 10$ MPa, $\Delta T_s = 25°C$

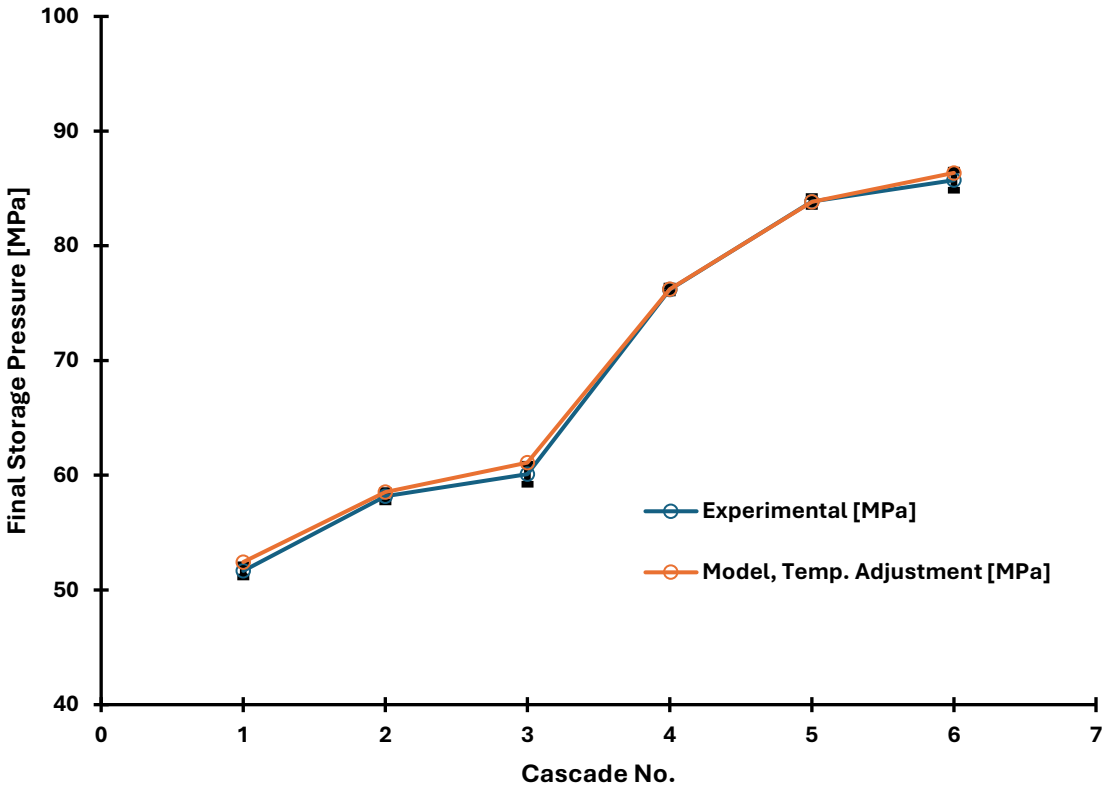

Fig. 35. Comparison of Experimental & Numerical Final Cascade Pressure, P_{sf}, Results, Adjusted Final Temperature, T_{sf} - 350 L.

3.3.3 – Model Validation for Heavy-Duty Vehicles Using NREL HD Fast Flow Testing [~82.3 kg]

To validate the model for H70 HD vehicles with more than 60 kg, the model is compared with the approximate data extracted from the NREL test presented in the literature review of this report. The initial and final pressures and temperatures were estimated from the data presented in Fig. 17 and Fig. 18. Table 7 shows the estimated initial and final storage pressures and temperatures.

Table 7. Initial and final pressure and temperature estimates taken from NREL HD fast flow tests [37].

Cascade	Initial Pressure [MPa]	Final Pressure [MPa]	Initial Temperature[°C]	Final Temperature[°C]
1	41.4	24	18	-10
2	93	48	16	-28
3	93	48	18	-28
4	93	52	20	-20
5	93	55	25	-17
6	93	59	24	-13
7	93	72	15	-8
8	93	72	17	-4
9	93	72	15	-5
10	93	78	18	2
11	93	79	15	2
12	93	84	17	5
13	93	86	20	10
14	93	86	20	10

The water volume and cascading strategy were estimated using the information provided within the slides presented by Onorato and Kuroki [37]. It was estimated that the total CHSS volume was approximately 1,900 L. The initial pressure in the CHSS was 1.52 MPa and the final storage pressure was 83.4 MPa. Fig. 36 shows a comparison of the estimated NREL results and the developed model output. The results show agreement between the estimates made from the NREL HD fast flow tests and the developed model output, with a maximum difference of 3.7%. As the actual data is not available, it is difficult to say definitively that the model is accurate for H70 vehicles. However, based on the estimates taken from the NREL data, the comparison suggests that the model is valid within a range of ± 3.7%, as shown in Fig. 36. Because the temperature of the storage banks was measured and presented in the NREL fast flow testing [37], the initial and final storage temperatures can be input directly into the numerical model. This is beneficial for validating the numerical model final pressure results and shows that by accurately describing the

storage temperature, accurate final storage pressures can be achieved. The relatively high accuracy of the numerical output model when using estimated measured temperature results, demonstrates the importance of accurately estimating the final storage temperature when using the numerical model. The effect of the final storage temperature is discussed in more detail in the Results & Discussion section of this report.

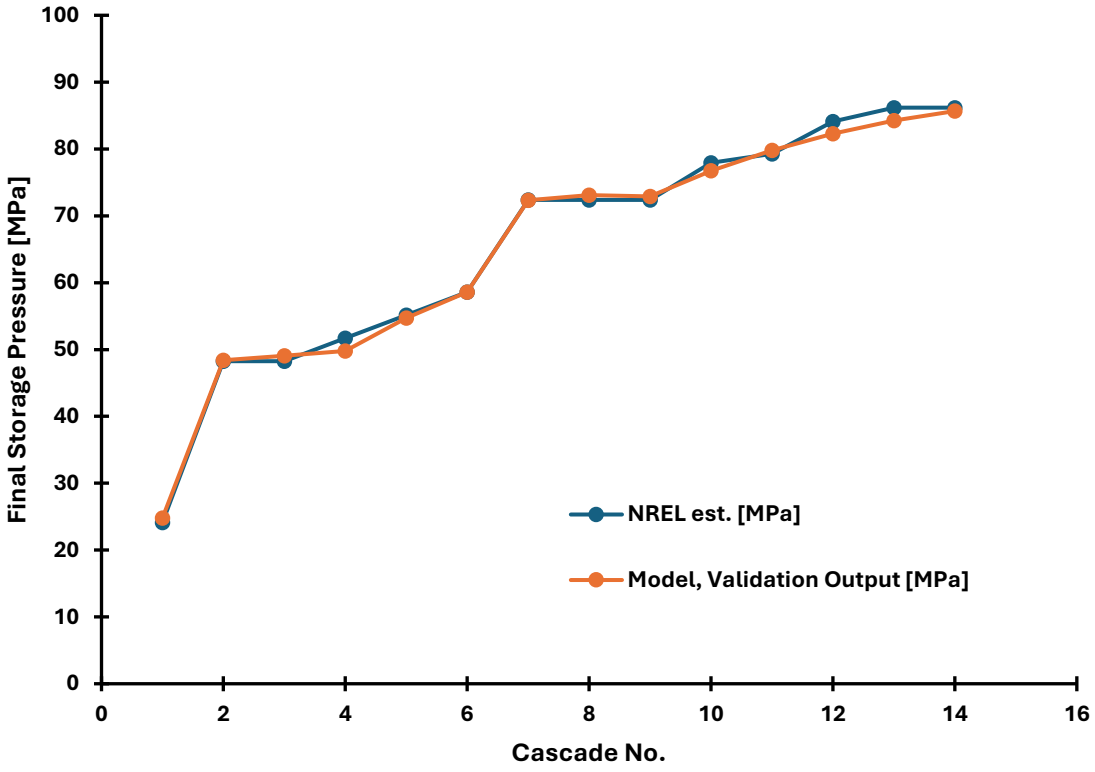

Fig. 36. Comparison of NREL final pressure estimates to the model final pressure output - 1900 L.

3.3.4 - Deviations:

Below is a summary of possible deviations that could result in differences between the experimental data and the results from the numerical model.

- It is known that thermistors react more slowly than pressure transducers during refueling experiments, which makes it difficult to estimate the exact temperature and pressure in the vehicle at any given moment.
- Pre-cooled gas flows past the thermistor and has been shown to influence the thermistor measurement during refueling.
- Pressure is measured at the inlet of the OTV of the cylinder, as a result the pressure in the vehicle cylinder is likely to be less than the pressure being measured during refueling due to the pressure drop across the OTV.
- The instrumentation signal from the storage pressure transducers requires some filtering which could contribute to a deviation from the true result
- Pneumatic valves take time to open and close which can contribute to gas leaking from one bank into another

Chapter 4 – Results & Discussion

In this section, parametric studies exploring the effects of changing the storage and vehicle pressure, and the effect of using different compressibility equations, are performed. The numerical model is used to investigate the effect that storage volume, pressure and number of cascades have on achieving 100% SOC during refueling for a 1,500 L hydrogen vehicle. The energy consumed, the volume ratio (VR) and the final pressure are investigated as the key parameters for cascading strategies. Finally, a case study focusing on refueling a 1,500 L FCEV, with an NWP of 70 MPa, using the available hydrogen storage at Powertech Labs Inc., is performed. The energy consumption is used as the key parameter to suggest the ideal cascading strategy for the test laboratory.

4.1 – Parametric Studies

4.1.1 - Effect of Storage temperature

It is clear from the model validation section of this study that the final storage temperature has a significant impact on the model results. This is because of the relationship between pressure and temperature for pneumatic systems. As can be derived from the Lemmon et al. EoS, Eq.(3-5a), when pressure decreases there is a proportional decrease in temperature. Therefore, a large reduction in pressure should correspond to a large decrease in temperature, as shown by the data from the HD fast flow testing performed by NREL [37]. Both the data recorded during the NREL test and the model validation demonstrated that the small change in pressure assumption is not a valid assumption across all cascades, especially for the early cascades. Therefore, it is important

to develop a new approach to determining the appropriate final cascade temperature. Using the trial-and-error method, new assumptions for each cascade can be approximated as follows:

- For a $\Delta P \leq 5$ MPa, assume $\Delta T = 5°C$
- For $5 < \Delta P < 10$ MPa, assume $\Delta T = 15°C$
- For $\Delta P \geq 10$ MPa, assume $\Delta T = 25°C$

However, the change in temperature and pressure data, estimated by taking the maximum and minimum temperature and pressure points of each cascade from the NREL test, can be extracted and plotted, as shown in Fig. 37, to determine a relationship between the change in temperature and the change in pressure. The least squares method can be used to calculate the slope and y-intercept for a linear equation relating change in temperature and change and pressure can be determined. The relationship between change in storage pressure and change in storage temperature can be applied to the numerical model to obtain a unique final storage temperature per change in pressure, when starting from 95 MPa, rather than applying a common estimate across a range of pressure changes. The value of determining the relationship between change in pressure and change in temperature lies in increasing the accuracy of the model.

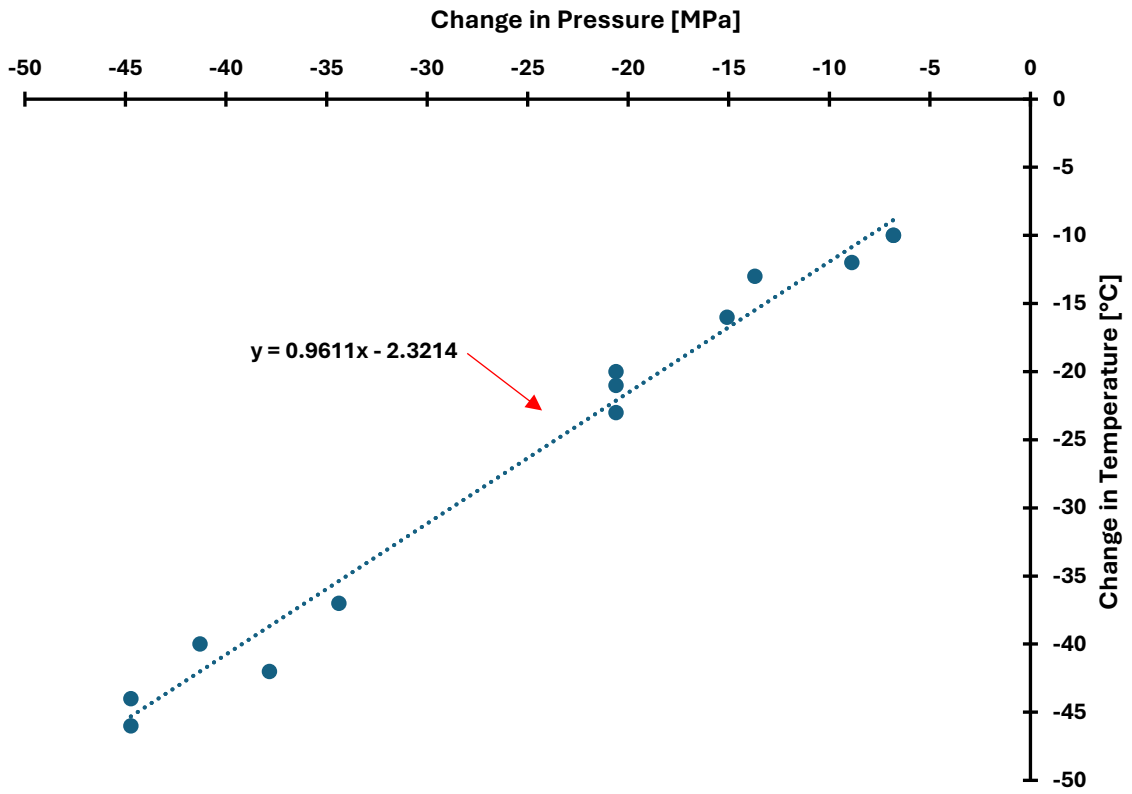

Fig. 37. Linear relationship between storage ΔP & ΔT for 95 MPa hydrogen storage, estimated from the data provided in the NREL test [37].

Fig. 38 shows the results of the model when applying this equation across all cascades for the 165 L FCEV. It can be observed that the model is better at approximating the final storage pressure compared to the original small change in temperature assumption. However, there are still some results outside the range of statistical uncertainty. Alternatively, if the trial-and-error assumptions are used for the 70 MPa cascades and the linear relationship is used for the 95 MPa cascades, it can be observed that all the model results are within statistical uncertainty in the case of the 165 L vehicle.

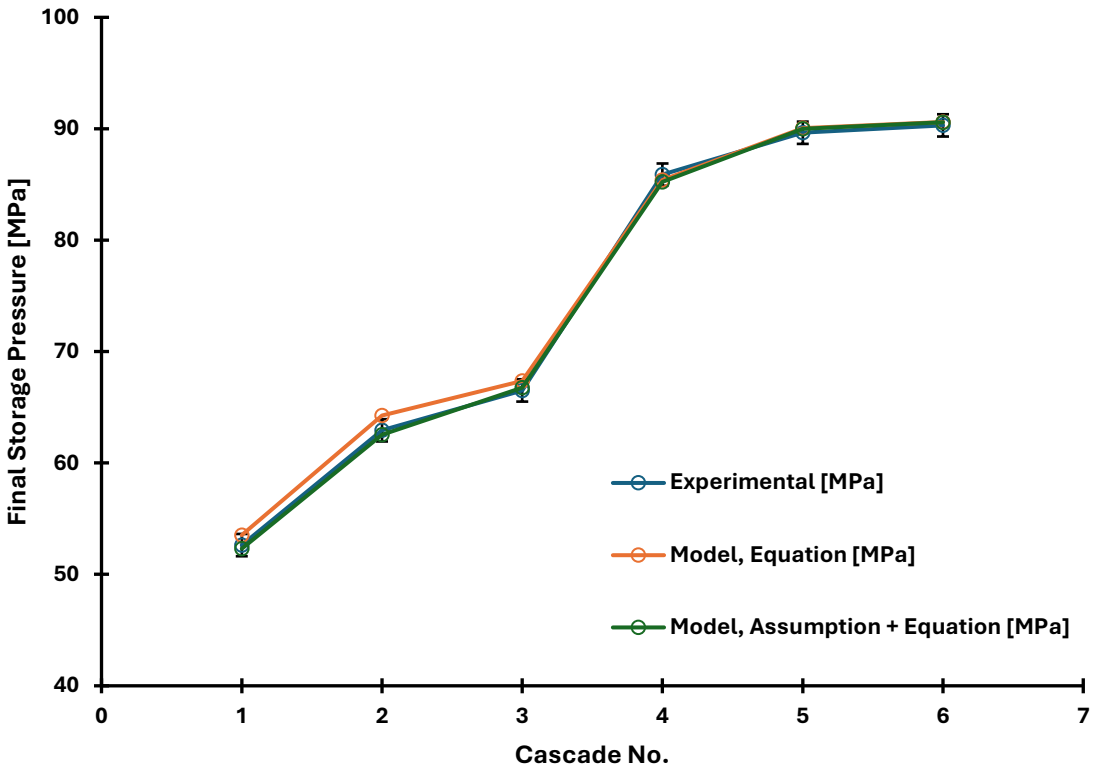

Fig. 38. Final storage pressure, P_{sf}, comparison between experimental data and final temperature, T_{sf}, estimate techniques - 165 L.

When the best-fit relationship is applied to the 350 L FCEV, shown in Fig. 39, it is observed that the final storage pressure is overestimated and outside of the statistical uncertainty for all cascades. However, by applying the trial-and-error temperature estimates for the first three cascades, the cascades starting from 70 MPa, and then applying the best-fit relationship for cascades 4 to 6 results in pressure estimates that are within statistical uncertainty for all cascades. This shows that the best-fit relationship should only be applied to cascades starting from 95 MPa. Using the trial-and-error estimates for all cascades starting from 35 MPa and 70 MPa and then applying the best-fit relationship for cascades starting from 95 MPa has been shown to provide accurate final pressure estimates when compared to experimental data.

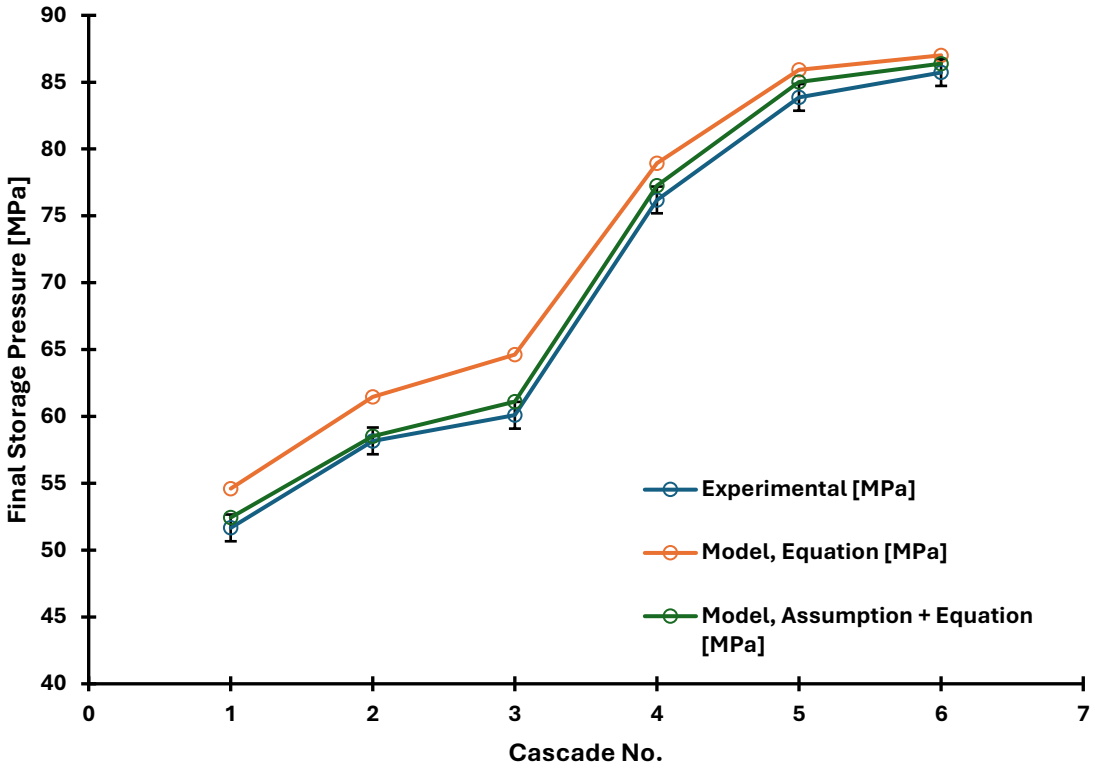

Fig. 39. Final storage pressure, P_{sf}, comparison between experimental data and final temperature, T_{sf}, estimate techniques - 350 L.

Using the trial-and-error estimates for the first cascade and the equation for all subsequent cascades, then comparing the results to the estimates from the NREL data, a maximum difference of 4.15 % is found. When considering the trial-and-error temperature estimates, a maximum difference of 5.3% is found. Both cases show a significant improvement, compared to the original small temperature assumption, where a maximum difference of 11.7% was found. Fig. 40 shows the comparison of the model results using different temperature approximations to the NREL data [37].

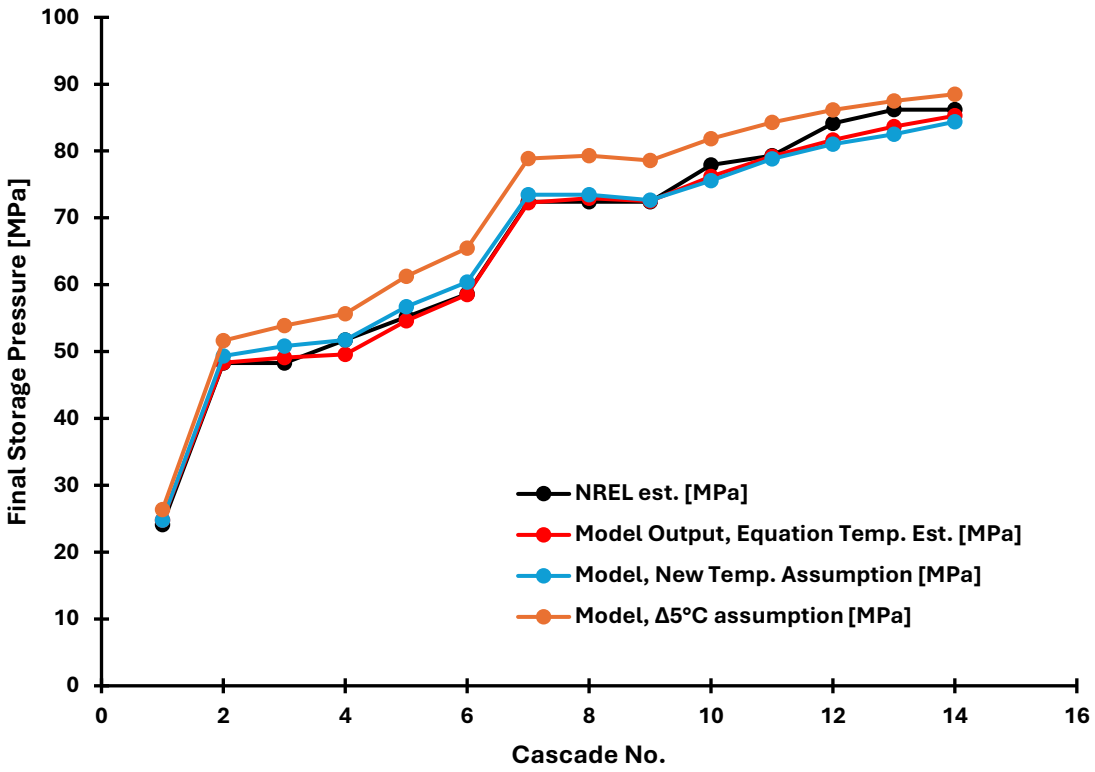

Fig. 40. Final storage pressure, P_{sf}, comparison between experimental data and final temperature, T_{sf}, estimate techniques - 1900L.

When considering a 1,900 L CHSS, the results show that the best-fit relationship between change in pressure and change in temperature provides accurate final pressure estimates, within the scope of this project, when the initial storage pressure is approximately 93 MPa to 95 MPa.

When applying the model, it is crucial to accurately approximate the final storage temperature. Otherwise, as shown from the 350 L comparison, the model may output results that overestimate the storage and cascade strategy capacity for refueling a vehicle. The overestimation of storage pressure is directly related to the underestimation of the change in storage temperature. By underestimating the change in storage temperature, the numerical model calculates the storage pressure to be higher which means that more mass can be

transferred from the storage bank to the vehicle. If the results are improperly interpreted, and the station is designed accordingly, the HRS may not be able to refuel vehicles to 100% SOC.

4.1.2 - Effect of Vehicle Temperature

As was shown in section 4.1.1, temperature clearly plays a key role from the perspective of storage; large changes in pressure result in proportional changes in temperature, and if not accounted for, this results in overestimation of the final storage pressure. It stands to reason that if the effect of storage temperature is significant, then it would be beneficial to investigate the effects of differing vehicle temperature conditions. An important parameter to investigate is the starting temperature of the FCEV. The initial vehicle temperature will depend on many different factors. Variations include, but are not limited to, the outdoor environmental conditions, differences between highway or city driving, the driving style of the operator, or the distance from parking location to refueling station. To investigate the effect the initial temperature has on the model results, two scenarios were tested for both the 165L and 350L FCEVs. In each case, the first scenario considered an initial temperature of -40°C, while the second scenario considered an initial temperature of 50°C. Both temperatures were selected based on the UN GTR No.13 standard, which requires 5 refueling cycles to start with the fuel system soaked to -40°C and 5 cycles starting from 50°C. In both cases the results were compared to the experimental results. The model considered the new temperature assumption for the 70 MPa cascades and the linear equation for the 95 MPa cascades.

As can be observed in Fig. 41, focusing on the 165 L fuel system, there is a negligible difference between the two extremes of the initial starting temperature. This is an unexpected result as the influence of temperature on the final storage pressure was so significant.

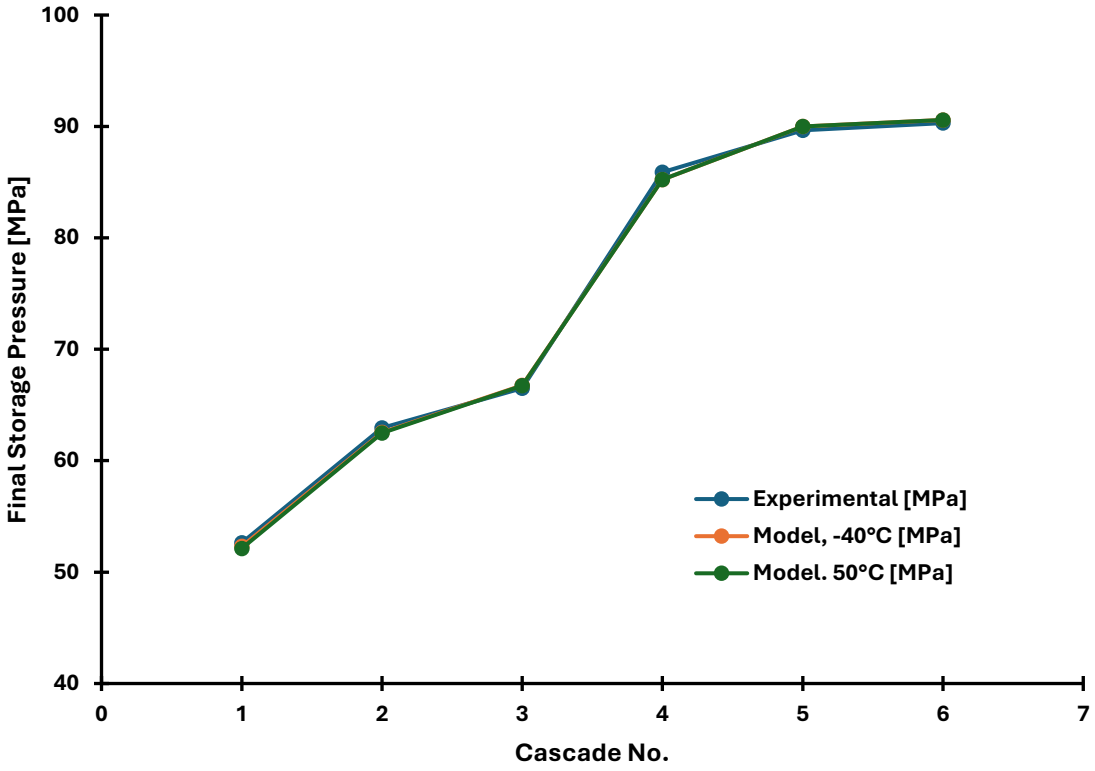

Fig. 41. Final storage pressure, P_{sf}, comparison of experimental data and initial FCEV temperature - 165 L.

A similar result is observed in the case of the 350 L fuel system, shown in Fig. 42.

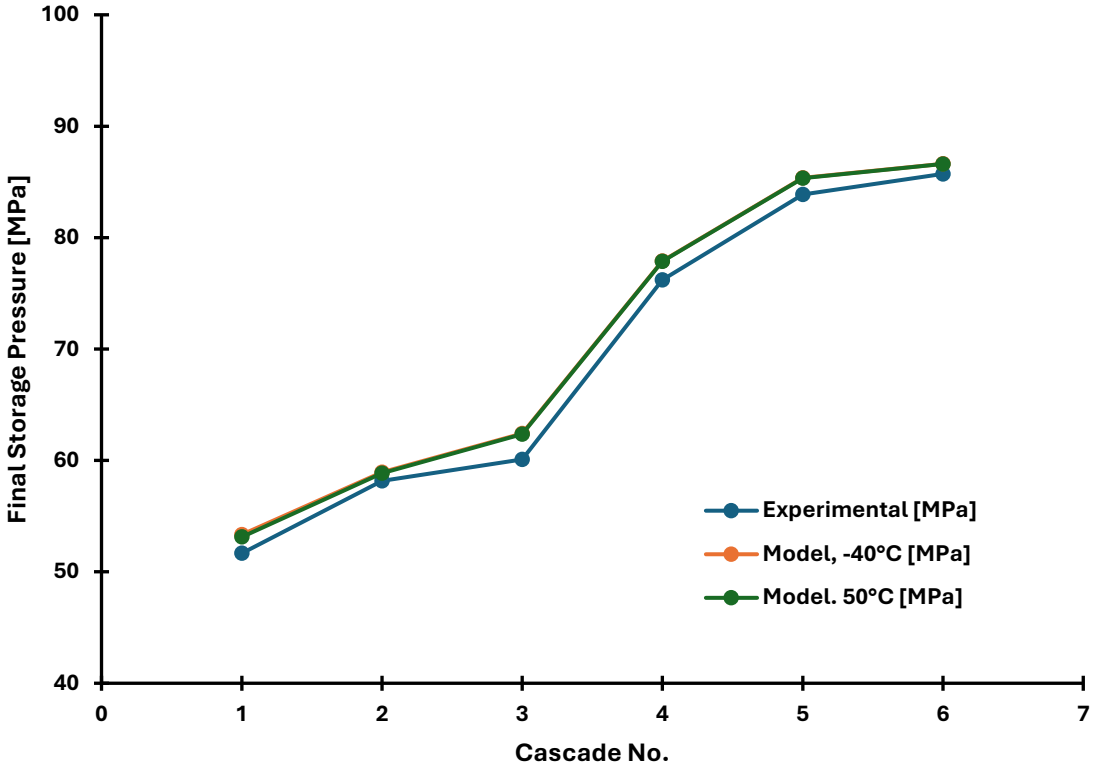

Fig. 42. Final storage pressure, P_{sf}, comparison of experimental data and initial FCEV temperature - 350 L.

The difference is that the change in temperature of a system during a single refueling event has a large impact on the final pressure, whereas a difference in starting temperature results in a very small change in the starting density. As explained by Hanada et al. [47], the change in density is only about -0.28% per °C at 50 MPa when considering an initial temperature of -40°C compared to 0°C. Assuming the same initial pressure, the difference in initial mass is approximately 0.1 kg and 0.2 kg for the 165 L and 350 L FCEVs, respectively. In both cases, the difference is approximately 1.5% of the total mass of the vehicles. This suggests that the initial FCEV temperature is negligible when applying the model to predict the high-pressure storage

requirements of refueling a vehicle. A good approximation when applying the model would be to choose the average outdoor temperature at the HRS as the initial vehicle temperature.

This is not to say that the initial vehicle temperature can be completely ignored. An important factor to consider is that in cases where the vehicle temperature is high, approximately 50°C, a station must be able to adjust the APRR and ensure proper pre-cooling is maintained so that the FCEV does not develop an internal tank temperature greater than 85°C. As briefly mentioned in the literature review, temperatures beyond 85°C begin to approach the glass transition temperature of the thermoplastic liner, resulting in the liner becoming softer and increasing the risk of liner failure.

To complete the understanding of the model from the perspective of vehicle temperature, it is also important to understand how the final vehicle temperature affects the model's results. The model is run considering final vehicle temperatures starting from 25°C to 85°C in 30°C increments, and the results are compared for both the 165 L and 350 L systems. In both cases the difference in final storage pressure after each cascade is somewhat significant for the first cascade. Fig. 43 and Fig. 44 show the results considering the 165 L and 350 L fuel systems, respectively.

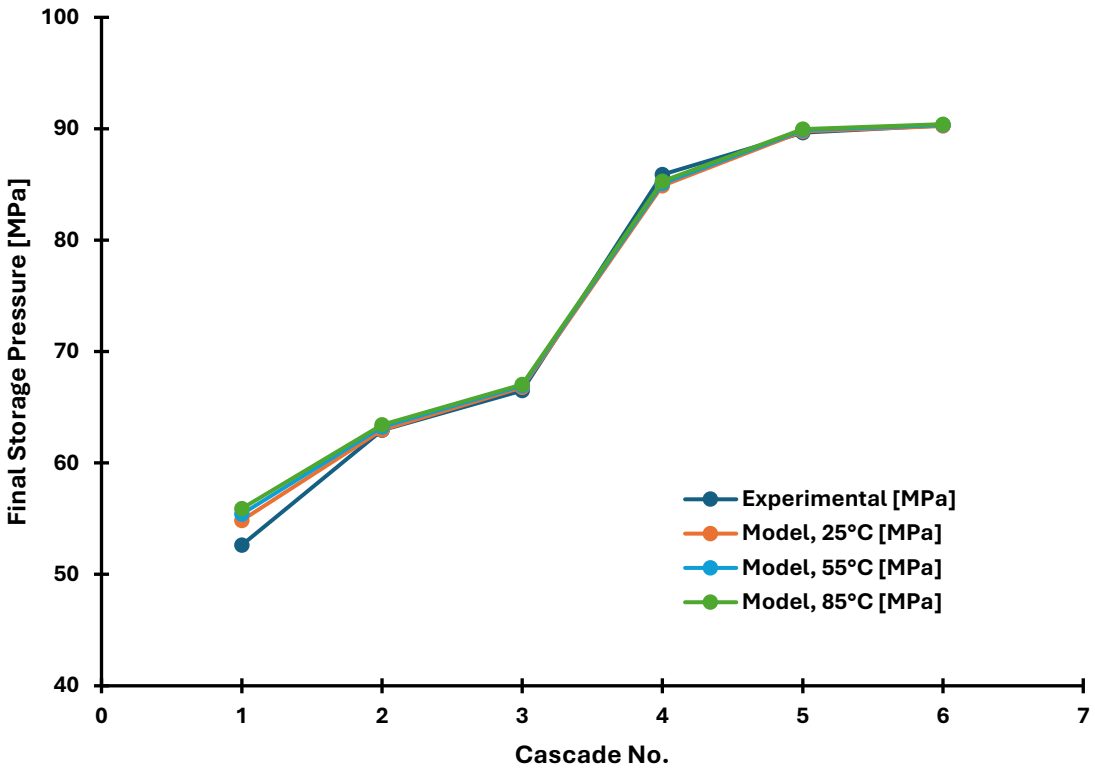

Fig. 43. Final storage pressure, P_{sf}, comparison of experimental data and Final FCEV temperature - 165 L.

The maximum difference found for the first cascade is 6.2% and 5.0 % for the 85°C final FCEV temperature in the 164 L and 350 L FCEVs. Despite the large difference for the first cascade, by the final cascade, a difference of 1.5%, or less, is observed. Although the overall difference in pressure is relatively small, it is important to evaluate the change in SOC of the FCEV at the end of the refueling cycle. In the case of the 165 L FCEV, the final SOC of the 25°C trial is equal to 114.6% if allowed to take gas from all 6 cascades. This result is a difference of 13% when compared to the 85°C trial. Both trials indicate that the HRS would be able to complete a fill to 100%.

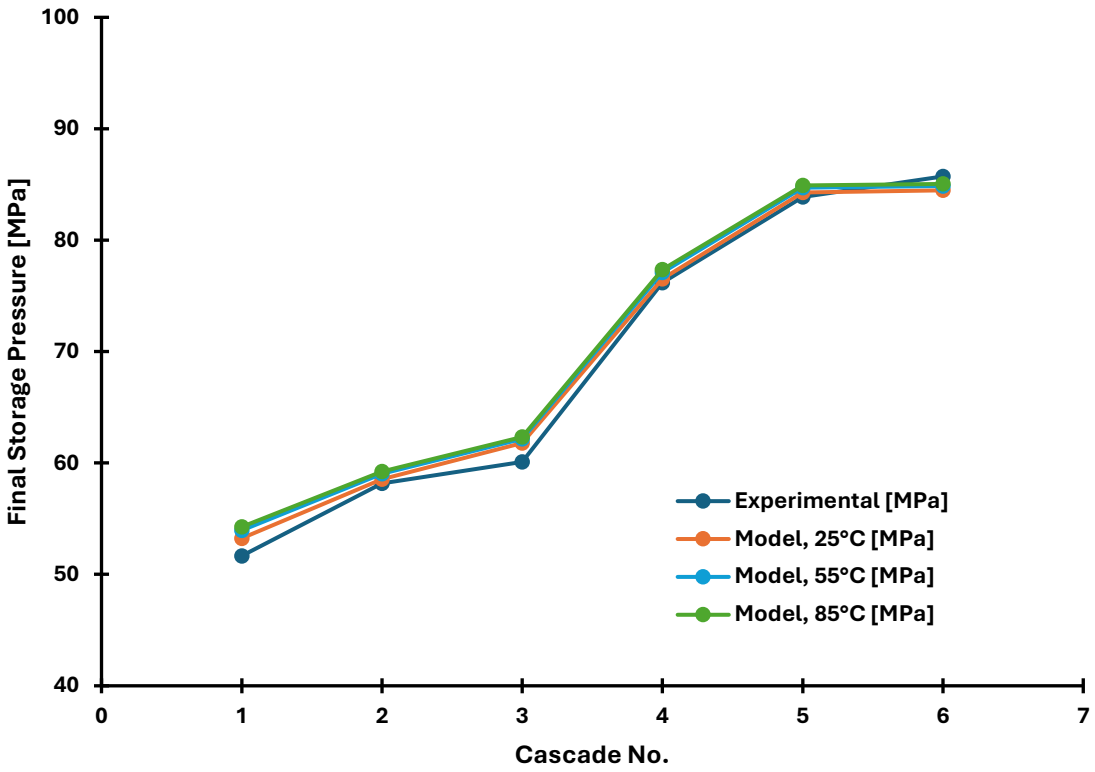

Fig. 44. Final storage pressure, P_{sf}, comparison of experimental data and Final FCEV temperature - 350 L.

In the 350 L FCEV case, the trials reveal a final SOC of 107.2%, 100.8% and 95.1%, respectively. This indicates that if the temperature is allowed to increase to the maximum allowable limit, the HRS will almost be unable to complete a fill for a 350 L FCEV per SAE J2601, which considers 95% SOC a full vehicle. For a vehicle to achieve high internal tank temperatures, either the gas conditioning is not being maintained, or the APRR is too high. The results from this section highlight the importance of maintaining the correct fueling protocols, either table-based fueling or MC method, so that the development of the in-tank temperature is kept within a moderate range.

When applying the model without experimental or real-world data, it is suggested to use a final vehicle temperature of 55°C. As seen in the data from the experiments performed in this study, and the NREL fast flow testing results [37], an average temperature of 55°C is common during refueling when the proper pre-cooling and fueling protocols are applied.

4.1.3 - Effect of Z Compressibility Factor

As mentioned earlier, the *Revised Standardized Equation for Hydrogen Gas Densities for Fuel Consumption Applications*, developed by Lemmon et al. [34], is used in this study, however, there are other equations that can be found in research which can be used in place of the Lemmon equation. As presented in the literature review, the EoS presented by Chen et al. [33], offers greater simplicity, having much fewer terms than the Lemmon EoS. Fig. 45 shows that there is a negligible difference between the model output when comparing the Lemmon et al. and Chen et al. equations to the experimental data for a 165L vehicle.

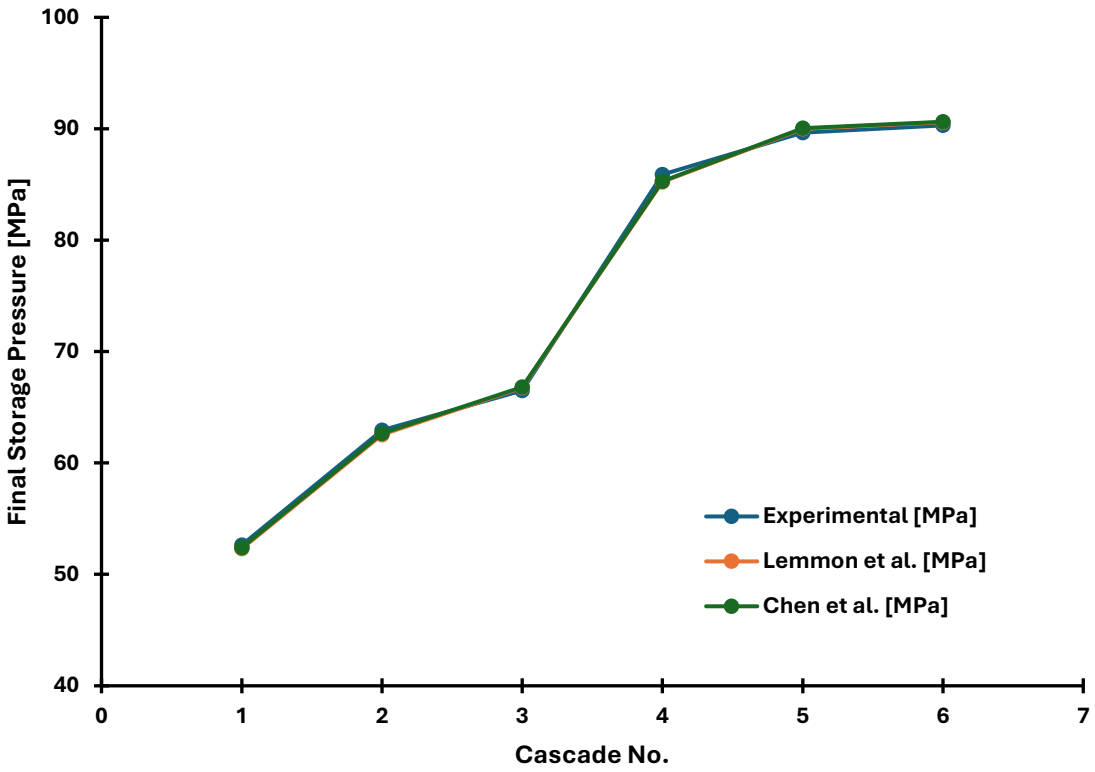

Fig. 45. Final storage pressure, P_{sf}, comparison of experimental data and Z Compressibility EoS - 165 L.

It is observed that the Chen EoS outputs a higher final storage pressure in all cascades, when considering the 350 L vehicle, with a maximum difference of 4.2% when compared to the experimental results, shown in Fig. 46. One possible explanation is the difference in accuracy, when compared to NIST data, for the pressure and temperature ranges experienced in the experiment. When compared to the NIST data, the accuracy of each EoS is 0.04% and 1.1% for Lemmon and Chen EoS, respectively. If this were true, we would expect to see a similar difference when applying the Chen EoS to the NREL results.

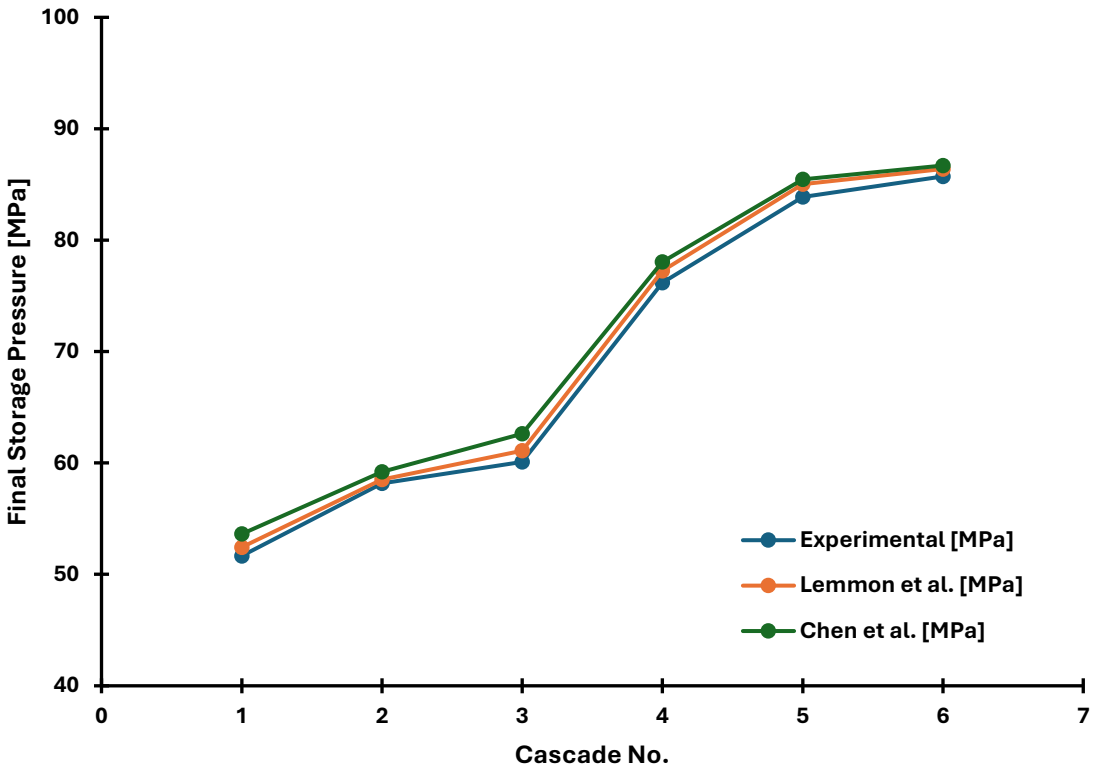

Fig. 46. Final storage pressure, P_{sf}, comparison of experimental data and Z Compressibility EoS - 350 L.

However, as shown in Fig. 47, there is once again a negligible difference in the model outputs when considering both equations. Another possible explanation for the difference observed in the 350 L FCEV case could be due to sensitivity of temperature inaccuracies in the Chen EoS. Meaning that when the temperature assumption is more inaccurate, the Chen equation tends to deviate further from the experimental results than the Lemmon equation. This suggests that, although the second term in both the Lemmon and Chen equations is the largest term, the higher order terms result in the Lemmon equation being more robust to temperature inaccuracies and variations than the less complex Chen equation.

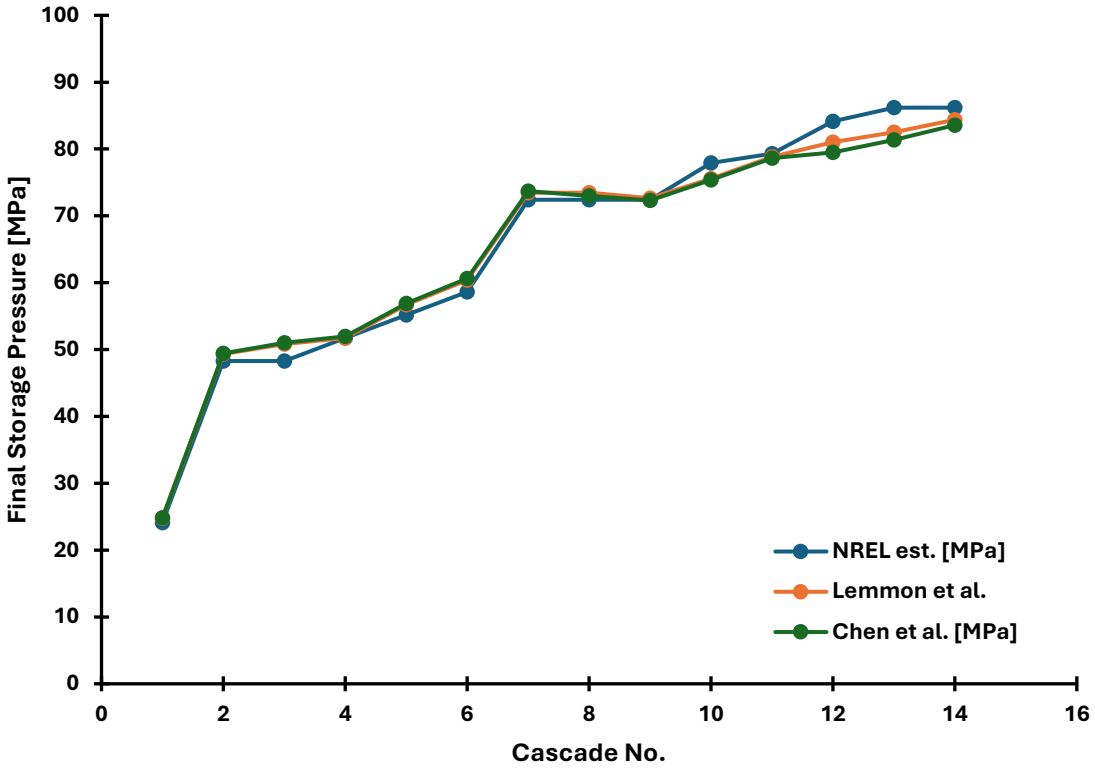

Fig. 47. Final storage pressure, P_{sf}, comparison of experimental data and Z Compressibility EoS - 1900 L.

Using virial equations can represent the behavior of a gas over a wider range of pressure and temperatures by including a sufficient number of terms, compared to less complex equations [48]. For this reason, when applying the model, it is best to use the equation by Lemmon et al. For hand calculations or simplicity, the Chen EoS is also acceptable.

4.2 – Investigating the effects of storage volume, pressure & cascades

In this section, the numerical model is used to investigate the effect of storage volume, storage pressure, and the number of cascades. The model is compared to the optimized strategies presented in literature for LD refueling and assesses the validity of these strategies for HD refueling. Volume ratio (VR) and the energy consumed in refueling are used as key performance indicators of various strategies.

The model will be applied based on what was learned in Chapters 3 and 4. A 1,500 L H70 vehicle is used to evaluate the effect of increasing storage volume, pressure and number of cascades. The initial conditions presented in Section 3.2.2 are used. The new temperature assumptions, combined with the trendline equation, from Section 4.1.1, are used to estimate the final storage temperature. The final vehicle temperature is assumed to be 55°C after each cascade. The pressure delta is set to 3 MPa.

4.2.1 - Increasing Storage Volume

In this section, the model is used to understand the effect of increasing the hydrogen storage volume when considering refueling a 1,500 L H70 fuel system, which holds 60 kg of hydrogen gas at 100% SOC. For simplicity, 3 cascades are considered in this study, each pressurized to 35 MPa, 70 MPa, and 95 MPa, respectively. The volume of each cascade will start at 1500 L and will be incrementally increased by 250 L.

4.2.1.1 - Increasing 35 MPa storage volume

To investigate the effect of increasing the 35 MPa storage volume on filling a 1,500L FCEV, 13 iterations were performed, increasing the low-pressure storage by 250L for each iteration. The change in final pressure for the LP, MP and HP storage banks when increasing the low-pressure storage is shown in Fig. 48. The change in specific internal energy of each bank is shown in Fig. 49.

It can be observed that the pressure results resemble a square root function, showing that increasing the LP storage results in a diminishing increase in final pressure after each cascade. When the 35 MPa storage is doubled, to 3,000 L, the final pressure after the first cascade increased from 18.48 MPa to 22.87 MPa, resulting in a 23.8% increase in the first cascade pressure. However, the second and third cascades only yielded an increase of 7.1% and 3.1% increase in the final pressure, respectively. When further increasing the pressure to by an additional 1,500L, for a total of 4,500L of 35MPa storage, there is only an increase of 10.5% in the final pressure of the LP storage, which results in an increase of 3.4% and 1.5% in final pressure of the MP and HP storage, respectively. The results of these trials suggest that increasing the LP storage volume can have an impact on increasing the final pressure of the vehicle; however, only increasing the LP storage volume alone is not sufficient to complete a fill of a 1,500L FCEV, as even with an LP volume of 4,500 L, at 35 MPa, the cascade refueling strategy would only achieve an SOC of 80.7%.

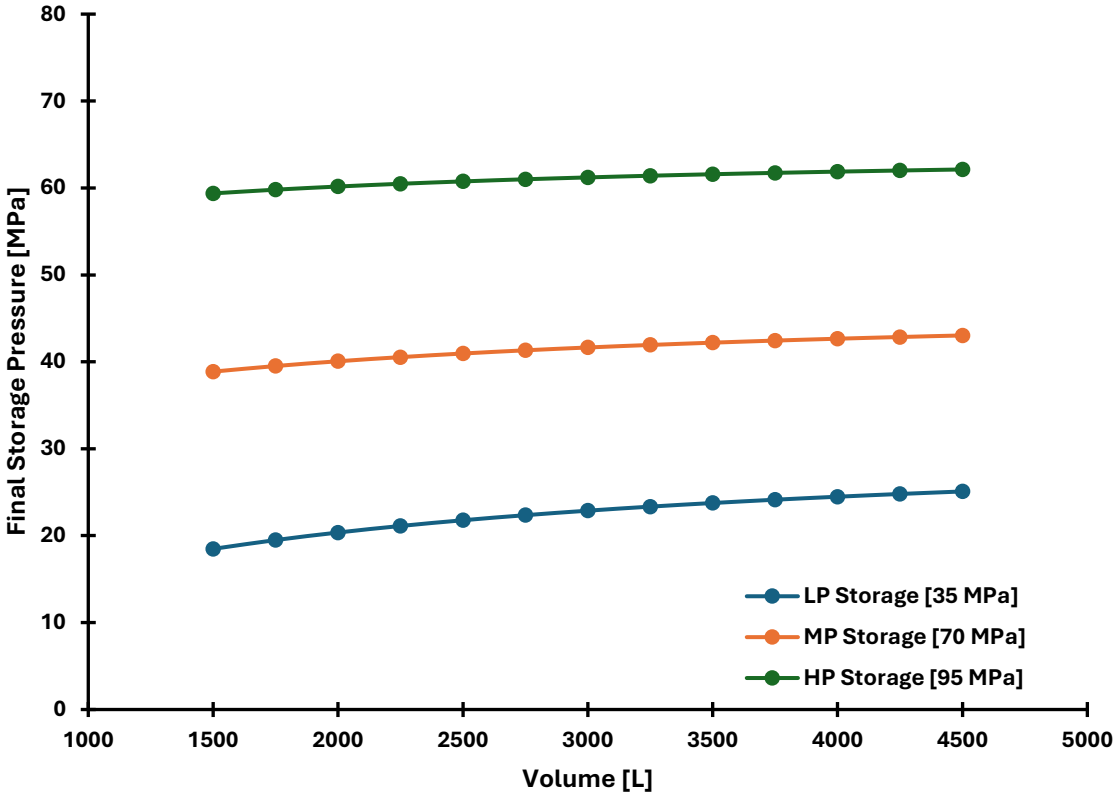

Fig. 48. The effect of increasing LP storage volume - Pressure analysis.

Although the increase in pressure is not significant, the model results for the change in internal energy, shown in Fig. 49, reveal that by increasing the volume of the LP storage, the change in energy of the MP and HP storage is reduced. Furthermore, the total change in energy is decreased as the LP storage volume is increased. This is because the LP storage can achieve a higher final storage pressure and dispense more mass into the FCEV, resulting in a smaller change in pressure and temperature of the MP and HP storage, effectively reducing the change in specific internal energy. Additionally, less mass is dispensed from the MP and HP storage banks. With the change in internal energy being the product of the change in mass and the change in specific internal energy, as the LP storage's change in energy increases, there is an overall reduction in the change in energy as less energy is required from the MP and HP storage.

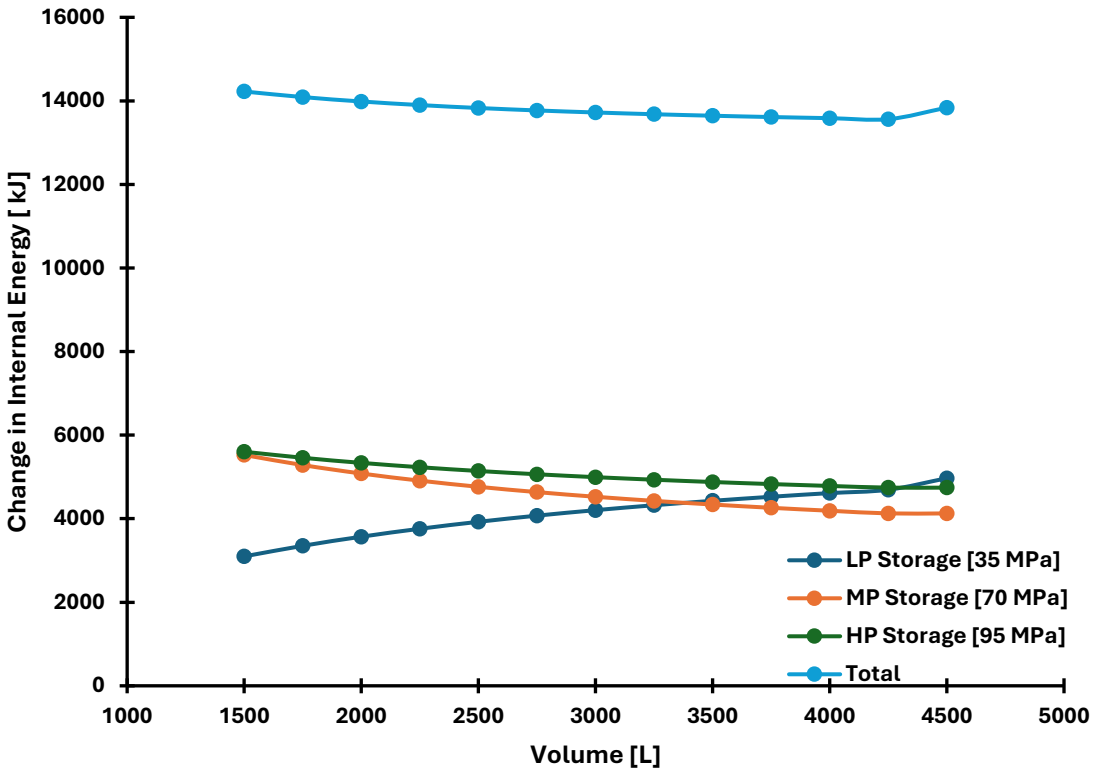

Fig. 49. The effect of increasing LP storage volume - Internal energy analysis.

The energy savings come at the cost of increasing the HRS storage volume. As Blazquez-Diez noted [27], the storage banks represent the most significant initial investment costs when designing HRSs, therefore it stands to reason that it would be valuable to reduce the volume required to meet the fueling requirements. Meanwhile, the energy consumed during refueling cycles can represent a significant cost over the life cycle of HRSs. This highlights 2 major considerations: total volume versus energy consumption, for manufacturers and integrators of refueling stations.

4.2.1.2 - Increasing 70 MPa storage volume

Repeating the above investigation with the MP storage banks reveals similar square root functions for both MP and HP storage pressure; however, no change is observed in the low-pressure storage. Of course, no change in final pressure is expected as there is no change in the starting pressure of the FCEV nor is there a change in volume for the LP storage volume. Fig. 50 and Fig. 51 show the data for pressure and internal energy. In this case doubling the volume of the MP storage results in a 23.8% and 10.3% increase in the final storage pressure of the MP and HP storage banks, respectively. Furthermore, when compared to increasing the LP storage to 3,000 L, the MP and HP the FCEV pressure is increased by 5.5 MPa and 3.6 MPa, respectively. This result is expected because the pressure, mass and energy stored in the MP banks are much higher than that of the LP storage banks. This shows that assigning additional volume to MP storage is more useful than assigning it to LP, as there is more useful pressure and energy in the doubling the MP storage volume than in doubling the LP storage bank.

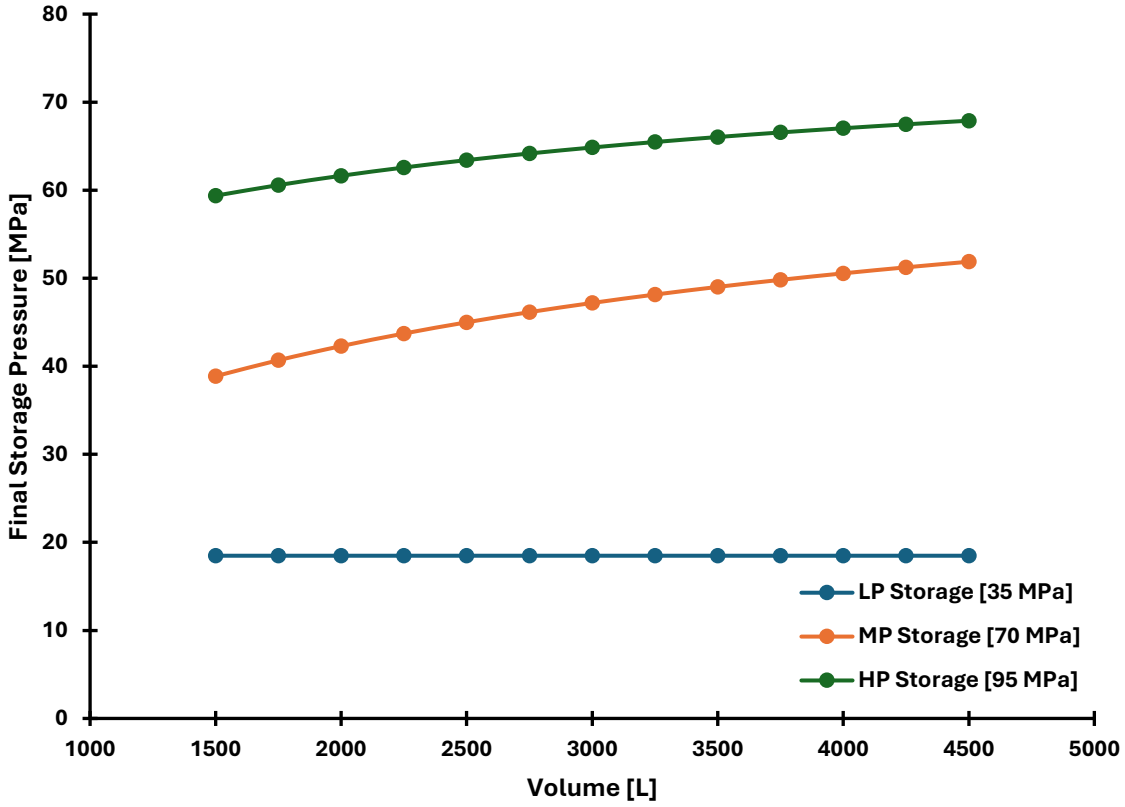

Fig. 50. The effect of increasing MP storage volume - Internal energy analysis.

Moreover, from the perspective of energy consumption, increasing the MP storage volume has a greater impact on reducing the total change in energy than increasing the LP storage volume. Although the MP energy consumption is increased by 3%, the HP energy consumption is reduced by 33.2%. This result may be significantly impacted by the temperature assumptions made in this study. However, as the pressure change is reduced in the MP and HP storage, there is a significant reduction in the change in temperature, further reducing the energy needed from the HP storage banks and having a significant impact on the total energy consumption with an equivalent total system storage volume. Note that by increasing the MP storage volume to 4,500 L, the HP storage energy consumption reducing nearly equally to the consumption of LP storage.

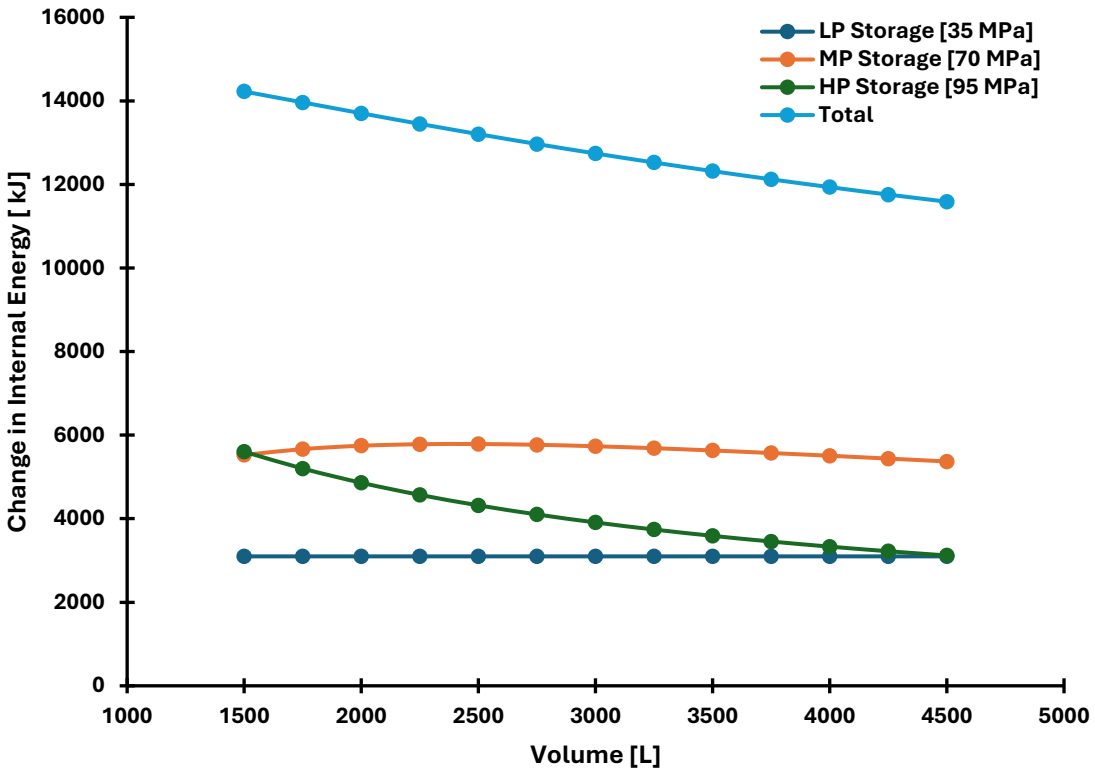

Fig. 51. The effect of increasing MP storage volume - Internal energy analysis.

4.2.1.3 - Increasing 95 MPa storage volume

Repeating the study for a third iteration, focusing on the HP storage banks, it is observed that increasing the volume of the HP storage banks results in the most significant increase in the final pressure achieved by the cascading strategy. The function of the HP final storage pressure is still in the shape of a square root function, suggesting a nearly asymptotic relationship between increasing the storage volume and the final storage pressure, shown in Fig. 52. Comparing the final pressure results of the LP, MP, and HP storage banks, increasing the HP storage volume to 4,500 L results in an 11.5 MPa increase and a 5.7 MPa increase compared to increasing the LP and MP storage to 4,500 L, respectively. This shows that from the perspective of volume ratio,

increasing the storage of the highest-pressure banks has the most value for increasing the achievable pressure of a cascade refueling strategy.

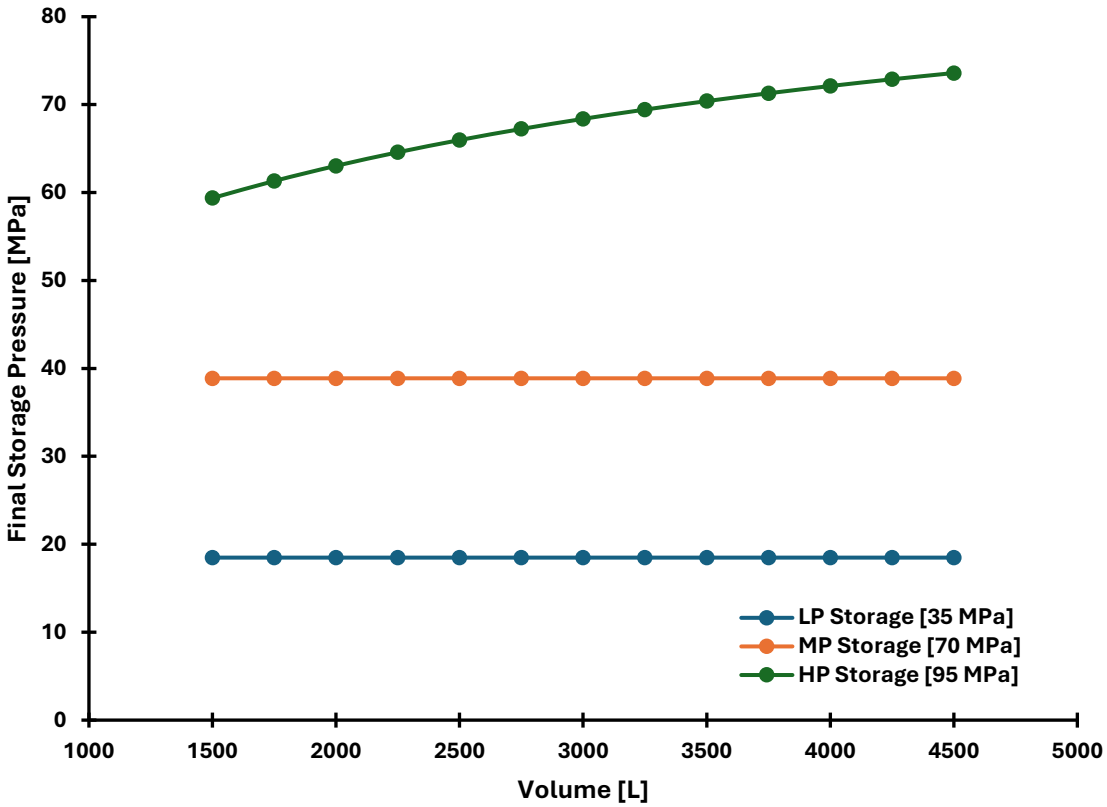

Fig. 52 The effect of increasing the HP storage volume – Pressure analysis.

The cost of this result comes from the energy consumption of the cascading strategy as the volume is increased. As illustrated in Fig. 53, the initial energy consumption increases, rather than decreases in the case of then LP and MP studies. This makes intuitive sense as the final starting pressure does not change, but the final pressure is increased, meaning that more mass is being depleted from the bank and a larger change in specific internal energy is calculated. However, the energy appears to reach a maximum as the HP storage volume is increased between 2,500 L and 2,750 L. This result is somewhat unintuitive, as the expectation is that energy will continue to increase the more the HP storage is able to fill the vehicle. In the case of filling a 1,500

L FCEV, what is observed is that the change in specific internal energy is decreasing as the volume increases, because there is a small change in pressure and temperature from the perspective of the storage tank. Additionally, the mass depleted is increasing at a decreasing rate, as the HP storage is increased. The result is that the total energy consumption begins to decrease beyond HP storage volumes of 2,750 L. This decrease in energy will continue as the HP storage increases. However, an asymptote will be encountered at very large volumes, which are not likely feasible, nor worth the initial investment to save on energy costs over long-term refueling cycles.

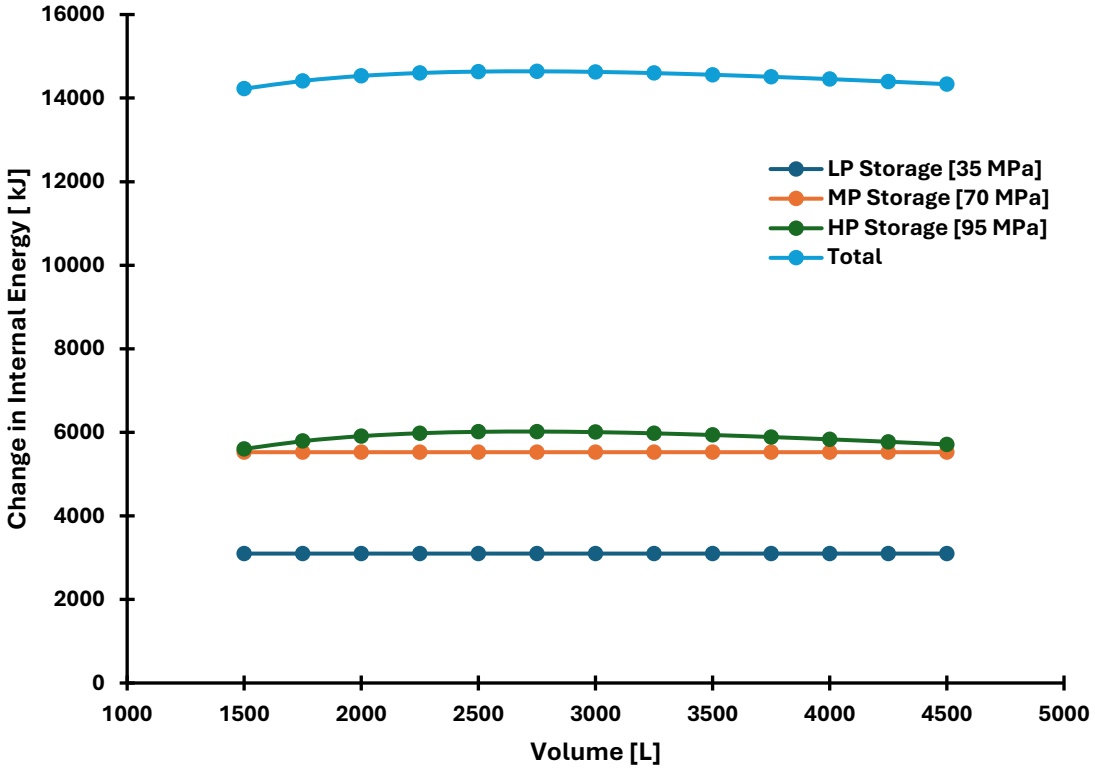

Fig. 53 The effect of increasing the HP storage volume - Internal energy analysis.

It is important to note, however, that none of the cascade strategies were able to achieve a 100% state of charge for a 1,500 L vehicle. Even by increasing the volume of all cascades to 4,500 L, the numerical model only outputs a final SOC of 97.3%.

Alternatively, applying cascade strategies suggested in existing research, which was discussed in the literature review of this report, cascade configurations that achieve 100% SOC can be analyzed. For example, Yu et al. [32], suggested two cascade strategies with a volume ratio of 4:3:3 and 1:5:4, depending on the available ground storage at a test facility. By applying the same cascade strategies to the 1,500L vehicle, considered in this study, it is found that both cascades are able to meet the 100% SOC and consume less energy than each of the cases presented in this section, 8,133 kJ and 8,984 kJ, respectively. The results from the Yu et al. suggestions highlight the tradeoff between energy consumption and volume ratio; as the volume ratio is increased, energy consumption can be reduced. However, the perspective of energy savings is important, as shown by Talpacci et al. [26], who suggested a cascade strategy with all storage banks pressurized to 87.5 MPa and a volume ratio of 3:3:25. Talpacci et al. approached minimizing energy consumption from the perspective of cooling capacity at a hydrogen refueling station; however, from the perspective of energy consumption due to compression, the energy consumed would be 17,002 kJ per refueling cycle. Notably, by adjusting the LP, MP, and HP storage to 35 MPa, 70 MPa, and 95 MPa, and applying a volume ratio of 3:3:25, the energy consumption from compression is 7,094 kJ per cycle, which highlights the value of appropriately distributing the initial pressure of each cascade, which is discussed in more detail in the following section. Additionally, the effect of distributing the volume over a greater number of cascades is also discussed in the following section.

4.2.2 - The effect of Storage Pressure and Cascades

In this section, the model is used to understand the effect of varying the hydrogen storage pressure and the number of cascade when considering refueling a 1,500 L H70 fuel system. Suggested light-duty cascading strategies from literature are evaluated based on energy consumption and the volume ratio. A three-cascade strategy with LP, MP, and HP storage, pressurized to 35 MPa, 70 MPa, and 95 MPa, respectively, will be considered the baseline case.

4.2.2.1 – Storage Pressure

To investigate the effect that the initial storage pressure has on the energy consumed by a cascade system, the baseline cascade strategy is compared to four variations, considering differing initial pressures of the first two cascades, and equivalent storage volume. Fig. 54 shows the baseline cascade with the initial pressure distributed across 35 MPa, 70 MPa, and 95 MPa, each with a volume of 10,000 L. The total volume ratio is 20:1 for the whole system of 6.67:1 per cascade. The energy consumed for refueling a 1,500L FCEV is shown as the area under the energy consumption curve and is equivalent to 5,089 kJ/cycle.

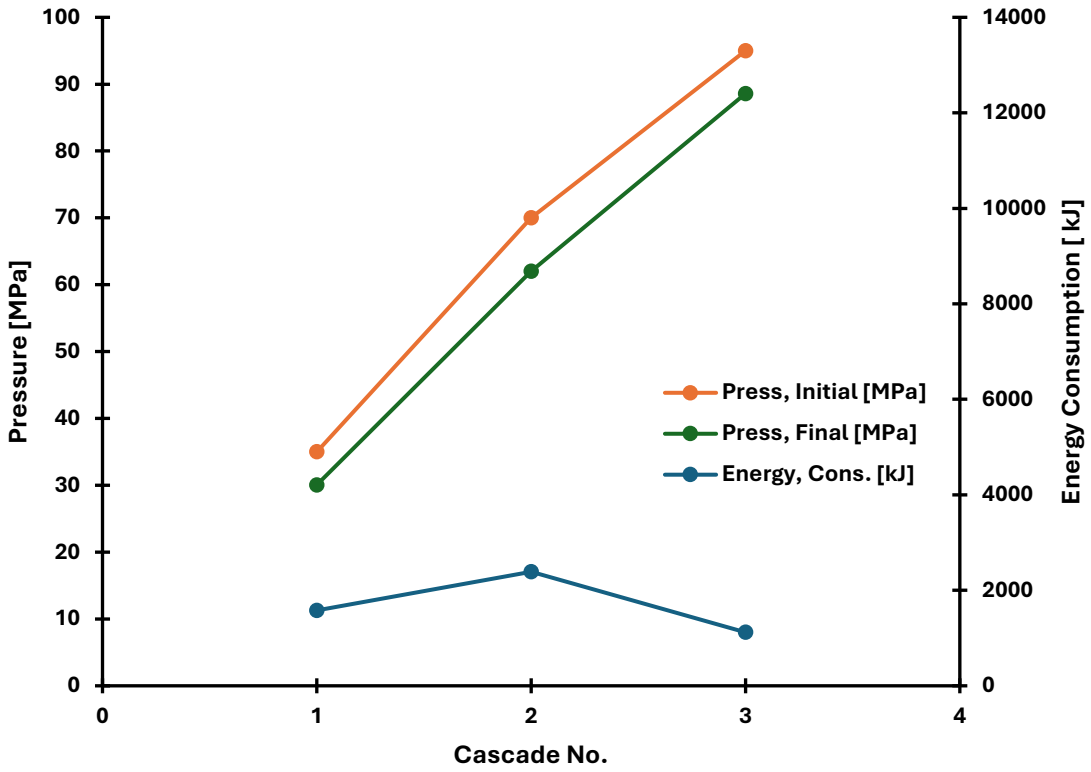

Fig. 54. Initial & final storage pressure and energy consumption for a 3-cascade strategy - 35 MPa-70 MPa-95 MPa.

The four variations of this cascade are shown in Fig. 55a through Fig. 55d. It is observed that all four variations of the baseline cascade result in higher energy consumption when compared to the baseline. In all of the variations the energy consumption from at least one of the cascades has both: a large change in internal specific energy, which is directly related to a large change in pressure and temperature, and a large change in mass. This is seen in the third cascade of Fig. 55a, the first cascade of Fig. 55b, the first and second cascade of Fig. 55c, but is most obvious in the case of the 95 MPa - 95 MPa - 95 MPa strategy, shown in Fig. 55d. With an initial pressure of 95 MPa for the first cascade, the vehicle is filled to NWP, nearly achieving a complete refuel using a single cascade, resulting in a very high energy consumption for the first cascade and very little energy consumed in the subsequent cascades. The same is seen in Fig. 55a and Fig. 55b, where the first cascade provides

the most significant pressure change in the vehicle from 35 MPa and 70 MPa, respectively, which is the result of an uneven distribution of mass transfer per cascade.

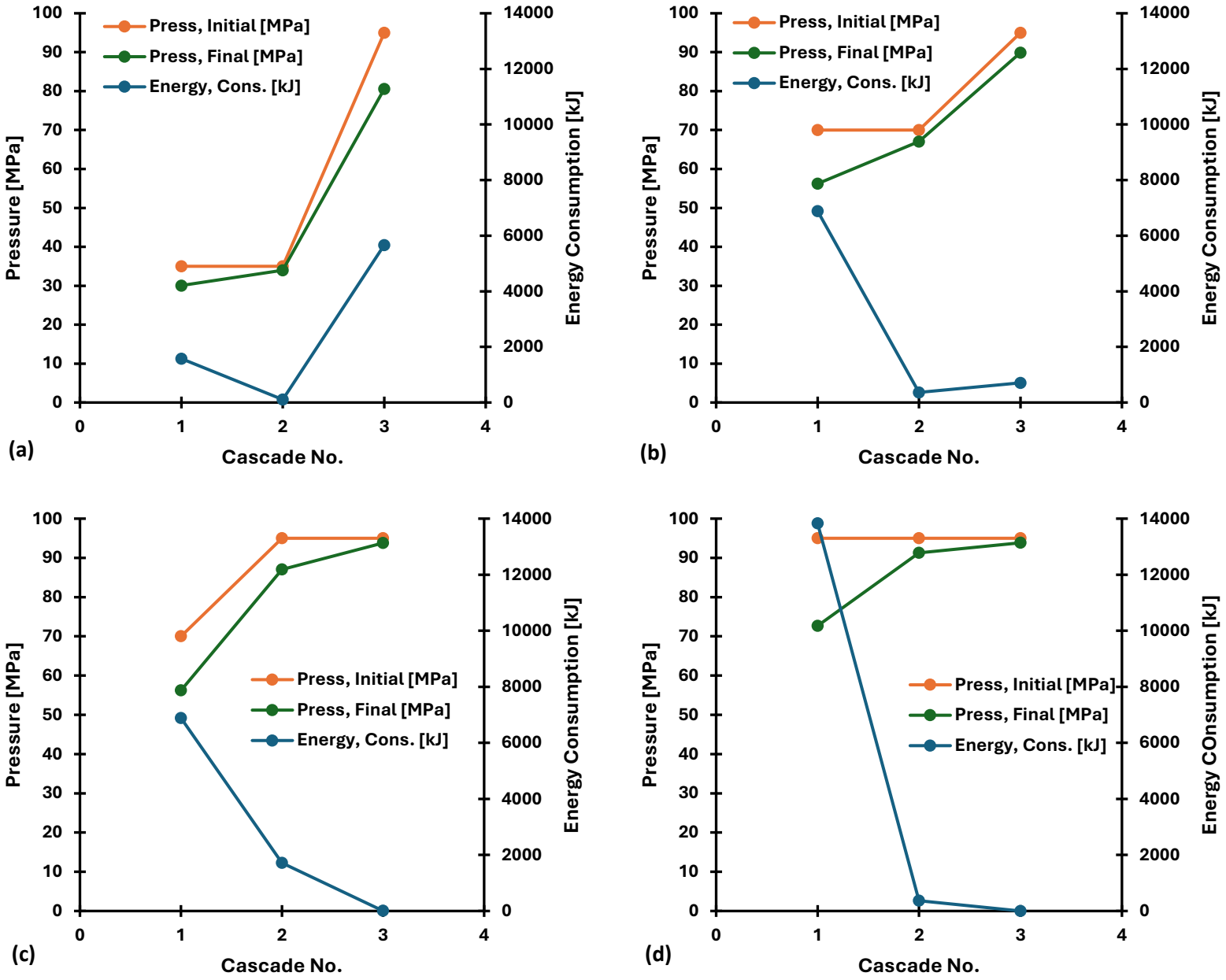

Fig. 55 Comparison of variations in cascading fueling strategies assuming 3-cascades and initial pressure of 35 MPa, 70 MPa and 95 MPa, (a) 35 MPa–35 MPa–95 MPa, (b) 70 MPa-70 MPa–95 MPa, (c) 70 MPa–95 MPa-95 MPa, (d) 95 MPa-95 MPa-95 MPa

The results indicate that cascade strategies that distribute the initial pressure of each cascade between low-pressure and high-pressure storage banks can benefit from significant energy savings, which agrees with the findings of Rothuizen et al. [20]. In the baseline case and all the variations shown in Fig. 55, the volume ratio was set at approximately 6.5:6.5:6.5. Rothuizen et al. suggested for the same volume ratio the optimal initial storage pressure should be 35 MPa, 65 MPa, and 87.5 MPa resulting in energy consumption of 4,804 kJ per refueling cycle, again showing that the proper distribution of pressure across the cascading strategy plays a significant role in energy savings.

4.2.2.2 – Increasing the number of cascades

So far, all strategies considered in this report have been variations of three cascade configurations. However, there is a limitation on the energy savings of a three-cascade strategy, specifically because there is a limitation on how to distribute the pressure and volume across only three cascades. Alternatively, increasing the number of cascades to achieve 100% SOC can have a significant impact on reducing energy consumption. To show the effect of increasing the number of cascades, the numerical model was used to evaluate the energy consumed for refueling configurations consisting of one to eight cascades, with pressures evenly distributed between 40 MPa and 95 MPa. The results of the investigation are illustrated in Fig. 56, clearly showing that as the number of cascades increase, energy consumption is reduced, so long as the initial pressures are evenly distributed. These results show a very similar trend to Fig. 14, which shows an equivalent study performed by Rothuizen et al. [20].

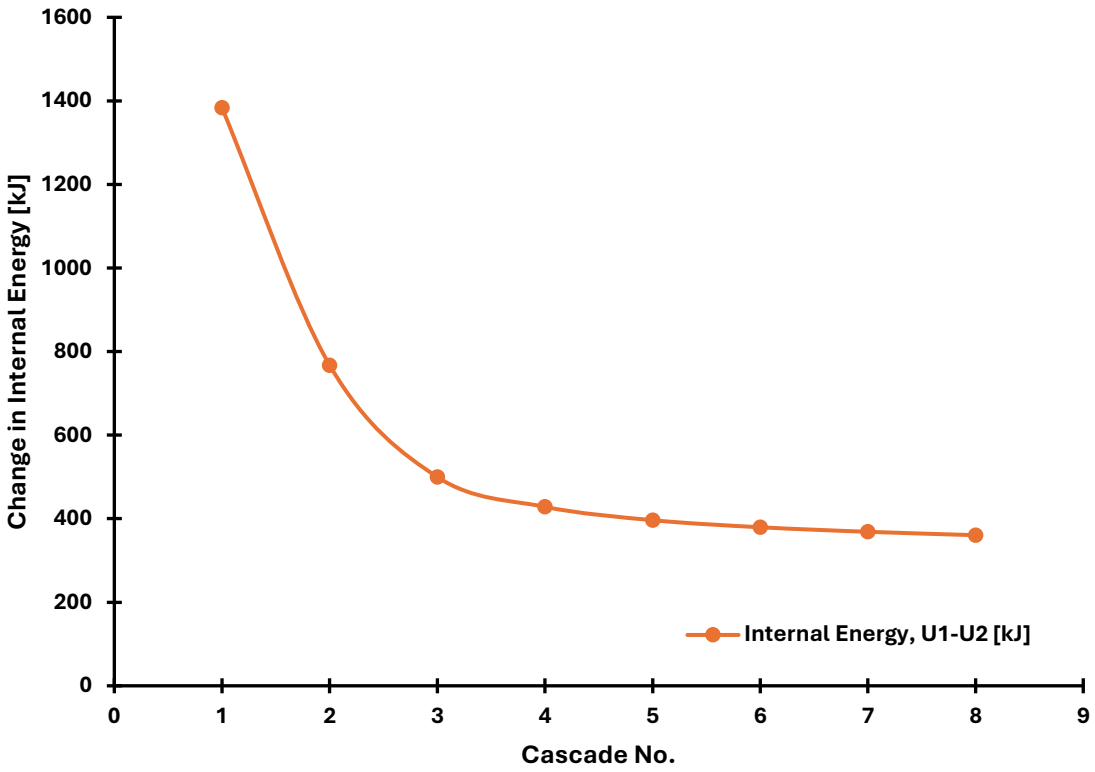

Fig. 56. Energy consumption as a function of the number storage tanks in a cascade strategy.

As expected, the energy consumption comes at a cost of volume, however, an additional cost for complexity of the hydrogen refueling station control system should also be considered. This cost comes in the form of additional valves, tubing, pressure relief devices and a more sophisticated control system. Additionally, the risk of valve failure and the costs associated with down-time and maintenance should be considered. For these reasons Rothuizen et al. concluded that a three to four cascade strategy is optimal for light-duty refueling. The same appears to be true in the case of heavy-duty refueling.

4.3 - Case Study

As briefly touched on in the introduction, one of the major advantages of numerical models is the ability to predict the behavior of systems that have yet to be built. Additionally, numerical models, like the one developed in this study, are much more cost effective and time-efficient than performing physical experimentation, as long as the numerical model is validated. Given that the numerical model in this study has been validated, it can be used to conduct a case study based on the available hydrogen storage at a hydrogen test lab. The test facility has five gas cycle test frames that are used to perform hydrogen refueling cycles for hydrogen vehicles with up to 600 L of on-board storage, which is equivalent to 24 kg of hydrogen pressurized to 70 MPa. The hydrogen storage is divided into three pressure storage zones kept at 35 MPa, 70 MPa, and 95 MPa. The facility was initially developed to perform light-duty hydrogen gas cycling per the pneumatic sequential tests, ECE R134 (ECE/TRANS/WP.29/2014/ 78), Section 5.3 [16]. The goal of the case study is to evaluate possible heavy-duty cascade refueling strategies considering the existing hydrogen storage at a test facility located in Surrey, BC. The strategies are evaluated based on energy consumption and total volume. The hydrogen vehicle to be filled in this case study has a stored on-board mass of 60 kg at 100% SOC, which has an equivalent volume of 1,500 L and an NWP of 70 MPa. The vehicle description and initial conditions are provided in Table 8.

Table 8. Heavy-duty vehicle description and initial conditions.

Water Volume [L]	NWP [MPa]	Target SOC [%]	Mass, 100% SOC [kg]	Initial Pressure [MPa]	Initial temperature [°C]
1,500	70	≥ 100	60	2	15

The available hydrogen storage is described in Table 9. Additional minimum pressure constraints must be considered for this case study based on the operational range of the compressors used at the test facility. Breaching the minimum pressures could damage the compressors resulting in additional maintenance costs. A maximum of eight cascades were considered for this case study. A pressure delta of 3 MPa is assumed to be sufficient based on the results provided in the NREL presentation [37], which assumes that the tubing at the test facility has ¾" diameter tubing rated to 20,000 psi, and that the control valves used are sized to at least 9/16".

Table 9. Available hydrogen storage available at the hydrogen test facility.

Bank	Cascades	Cylinders per Cascade	Volume per Cylinder [L]	Max Press. [MPa]	Min Press. [MPa]
1	1	1	2250	34	21
2	1	1	2250	34	21
3	3	6	250	70	40
		4			
		2			
4	3	8	175	70	40
		5			
		3			
5	1	5	175	70	40
6	3	3	255	93	40
		2			
		1			
7	3	3	255	93	40
		2			
		1			
8	1	8	255	93	40

Using the available hydrogen storage at the test facility yields many possible cascading strategies. Three strategies were chosen to be evaluated: two strategies that used all the available storage and one strategy that used approximately 80% of the available storage. The first strategy consisted of eight cascades, used in the order as presented in Table 9. The numerical results of this strategy are illustrated in Fig. 57, showing three distinct energy consumption peaks throughout the refueling cycle found at cascades 1, 3, and 6. Each of these peaks corresponds to the first cascade of each pressure level, 35 MPa, 70 MPa, and 93 MPa, respectively. The peaks are the result of a large change in pressure, relative to each of the other cascades during fueling. The

overall energy consumed per cycle based on this eight cascade strategy is found to be 9,055 kJ per cycle.

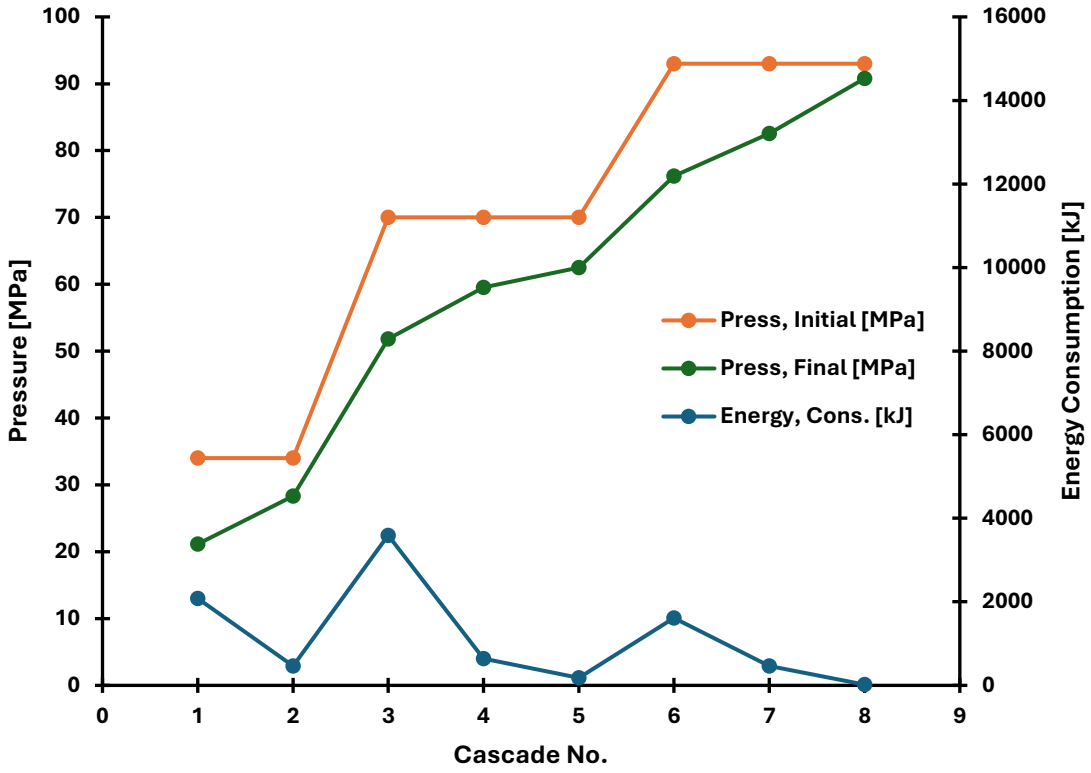

Fig. 57. Evaluation of an 8-cascade fueling strategy using the available hydrogen storage.

An alternative approach, described in Table 10, combines the LP and MP storage in two storage banks, then distributes the HP storage across three cascades, resulting in a five-cascade fueling strategy. As shown in Fig. 58, only one major energy consumption peak is observed for the second cascade. The energy consumption is found to be 8,731 kJ per cycle, resulting in a reduction of 3.5% when compared to the eight-cascade strategy shown in Fig. 57. This is counterintuitive, as the expectation is that energy consumption should decrease as the number of cascades increases, as previously discussed. The difference is due to the poor distribution of pressure across the eight-cascade strategy, resulting in underutilization of the majority of the storage banks

and higher energy consumption. Both approaches use all the available storage, however, the five-cascade strategy would be the better option based on overall energy consumption. Still, it is observed that the latter cascades are somewhat underutilized.

Table 10. Description of a 5-cascade fueling strategy using available storage at the hydrogen test facility.

Cascade	Volume per Cascade [L]	Initial Press. [MPa]	Pressure Delta [MPa]
1	4500	34	3
2	5475	70	3
3	2040	93	3
4	1530	93	3
5	1530	93	3

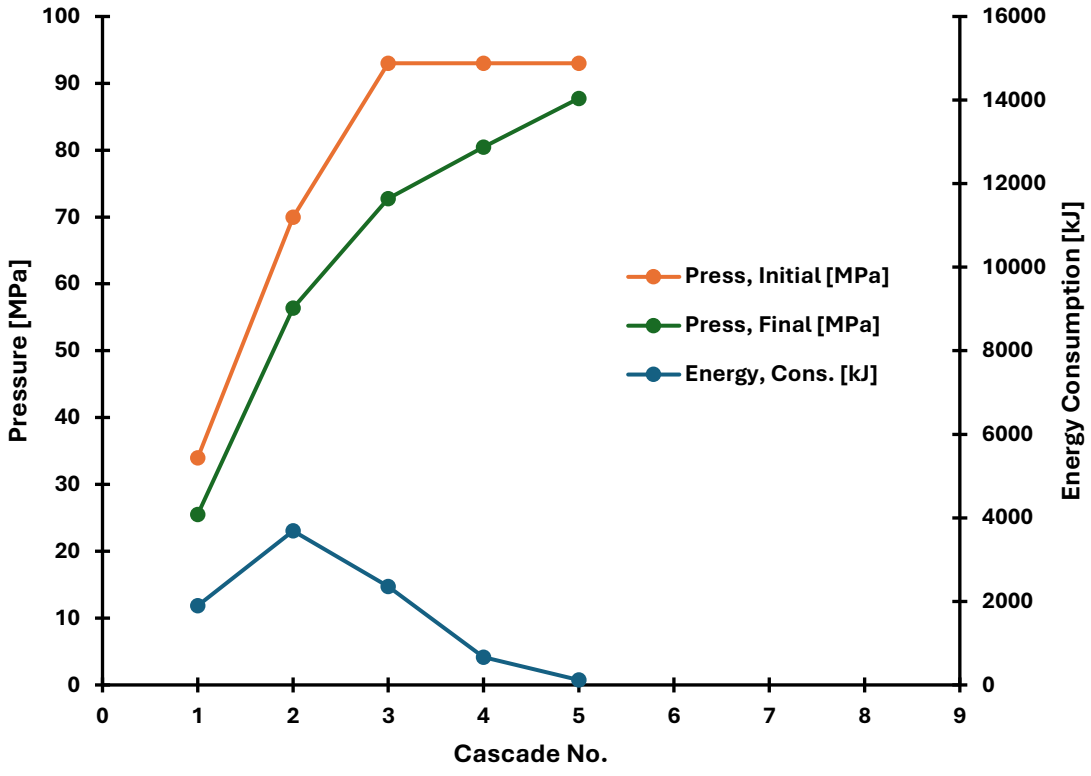

Fig. 58. Evaluation of a 5-cascade fueling strategy using the available hydrogen storage.

Rather than using all the available storage, a six-cascade strategy which considered approximately 83.5% of the available storage, described in Table 11, was evaluated. The overall energy consumption was 10,837 kJ per cycle, which is higher than both the eight-cascade and five-cascade strategies presented. This is an expected result as decreasing the volume increases the energy consumption due to greater utilization of each storage bank, as previously discussed. Fig. 59 shows the numerical results, which somewhat mimic the results of the 8-cascade strategy, though only showing two major peaks. The reduction in volume results in a 24% increase in energy consumption.

Table 11. Description of a 6-cascade fueling strategy using available storage at the hydrogen test facility.

Cascade	Volume per Cascade [L]	Initial Press. [MPa]	Pressure Delta [MPa]
1	4500	34	3
2	1500	70	3
3	1500	70	3
4	2040	93	3
5	1530	93	3
6	1530	93	3

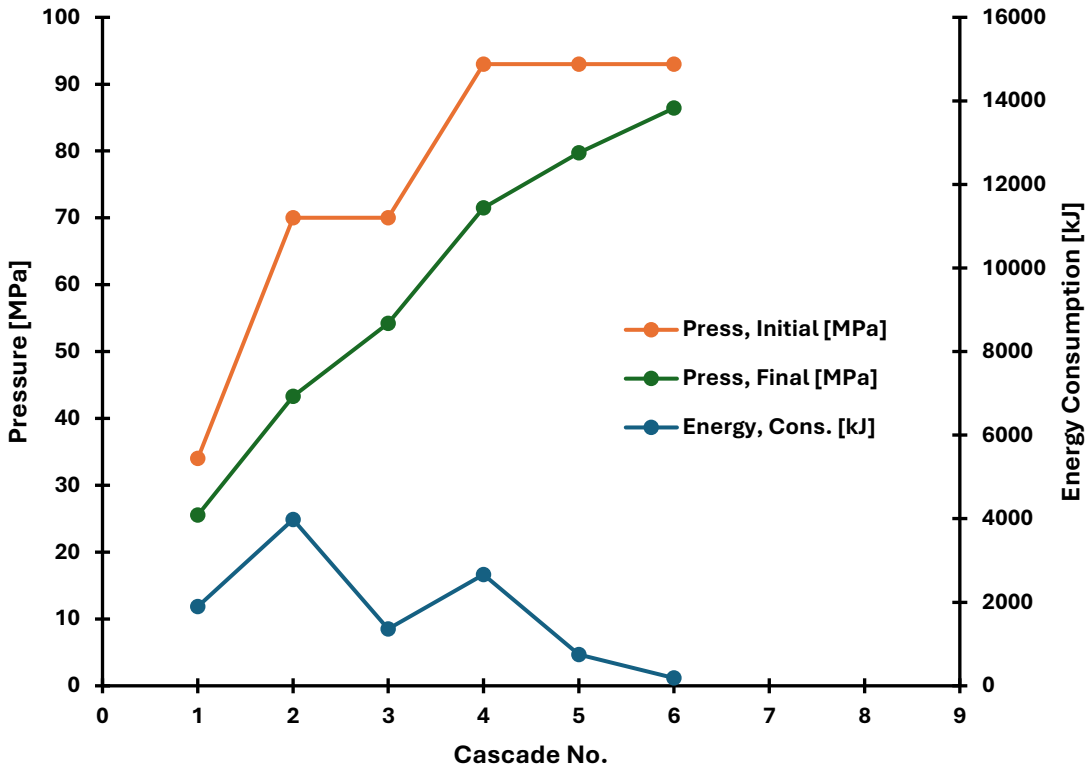

Fig. 59. Evaluation of a 6-cascade fueling strategy using the available hydrogen storage.

From the three cases studied, it appears that the five-cascade strategy would be the best solution for the test lab to shift to for HD refueling cycles, from the perspective of energy consumption, which is likely to have a greater long-term impact on cost when compared to reducing volume, as the test lab has already spent the initial investment. However, as noted above, in both the eight-cascade and six-cascade cases, there are several underused storage banks. This suggests that there is an opportunity to reconfigure each strategy to distribute energy consumption across all storage banks. One method to do so would be to adjust the initial pressure, as shown by the optimization performed by Rothuizen et al. [20]. This would increase complexity at the test lab, which has already established a control narrative and process control across the on-campus hydrogen infrastructure. Alternatively, the pressure delta of each storage

bank could be adjusted to utilize all storage banks and reduce the energy consumption peaks across the fueling cycles. As is shown Fig. 60, which illustrates the effect of adjusting the pressure deltas to reduce the overall energy consumption of the six-cascade strategy. In this case both the second and fourth cascades had the pressure deltas adjusted from 3 MPa to 16 MPa and 8 MPa, respectively, effectively increasing the utilization of the other cascades and reducing the overall energy consumption by 6.4%. This may be considered a small amount of energy savings across a single fueling cycle, however over the course of an entire pneumatic sequence, which consists of 500 cycles, this is a reduction in energy consumption of approximately 347 MJ.

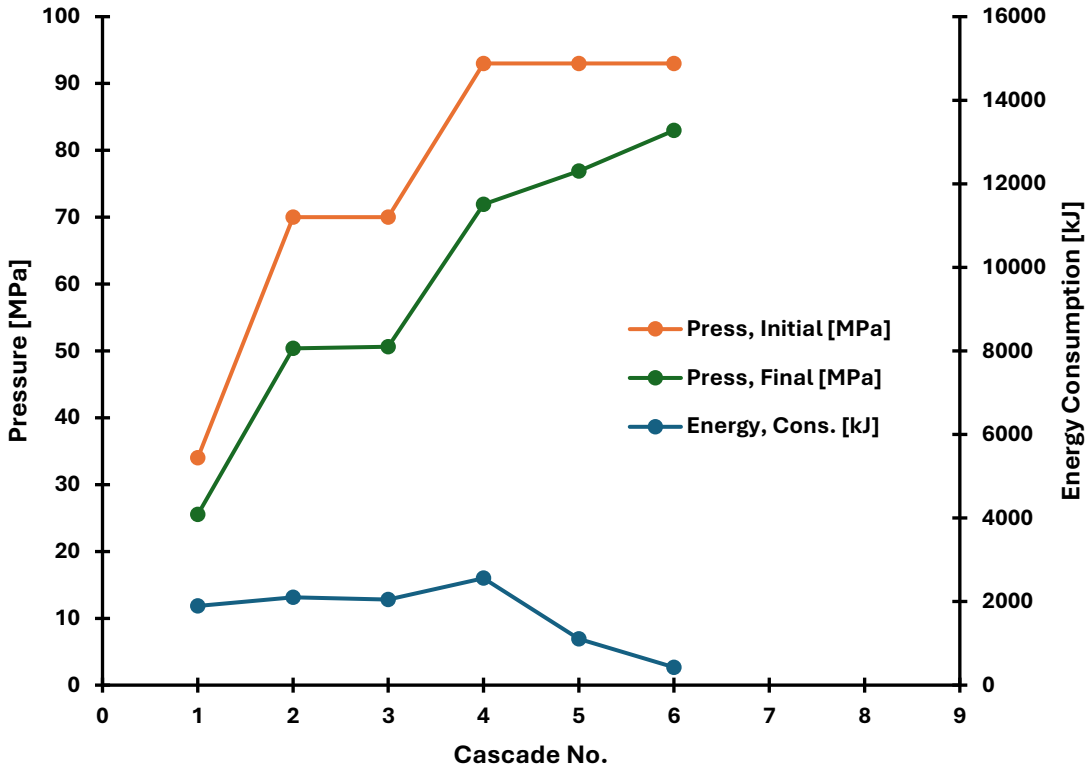

Fig. 60. Modified 6-cascade fueling strategy using the available hydrogen storage.

This same effect is also experienced when modifying the eight-cascade fueling strategy, adjusting the first, third, fourth, and sixth cascade pressure delta from 3 MPa to 12 MPa, 20 MPa,

10 MPa, and 14 MPa, respectively. Fig. 61 shows that the energy consumption peaks are greatly reduced, compared to the original evaluation, resulting in an overall reduction of 9.6% compared to the original evaluation and 5.7% compared to the 5-cascade strategy.

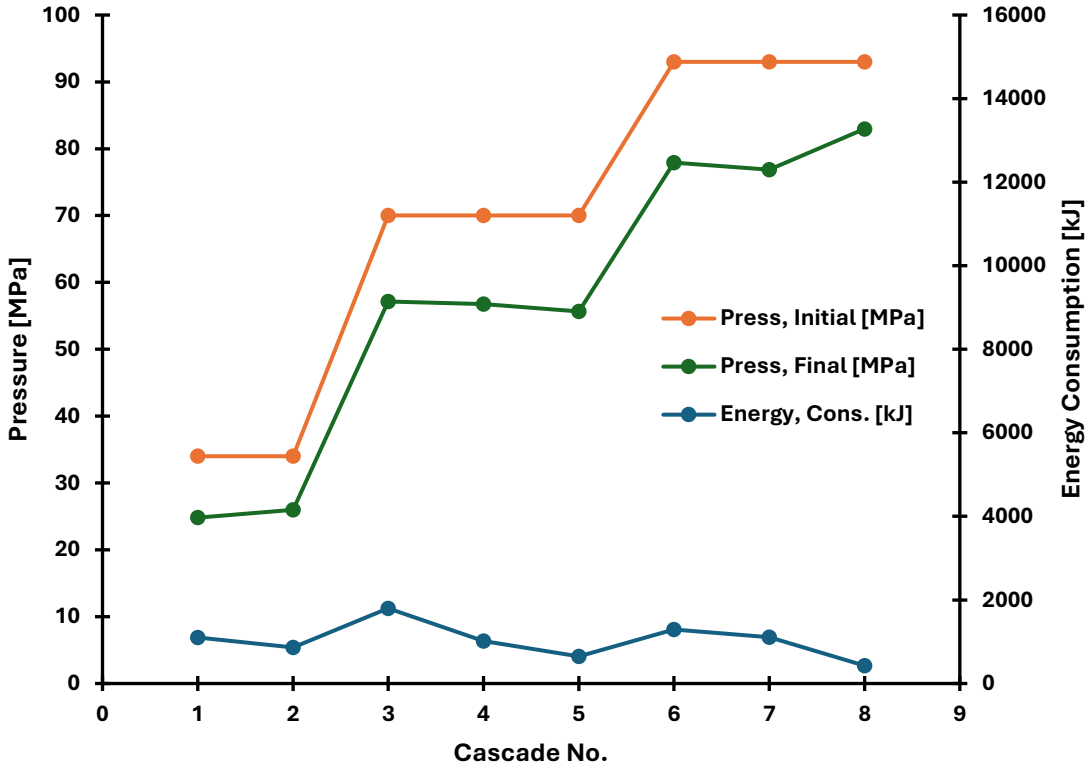

Fig. 61. Modified 8-cascade fueling strategy using the available hydrogen storage.

Based on the cases studied, the ideal approach for refueling a 60 kg HD hydrogen vehicle with a nominal working pressure of 70 MPa is to refuel the vehicle using the modified eight-cascade refueling strategy. The modified eight-cascade strategy yields the least energy consumed per fueling cycle which results in very large energy savings over long term cycling.

Chapter 5 – Conclusions & Future Works

5.1 – Conclusions

This thesis developed a numerical model to estimate the high-pressure hydrogen storage required to refuel heavy-duty hydrogen vehicles. Rather than using traditional thermodynamic equations to develop the numerical model, this thesis combined equations of state and GRG non-linear programming to solve the continuity equation.

The physical experimentation was performed on 165 L and 350 L hydrogen fuel systems, representing light-duty and heavy-duty vehicles, respectively. Each hydrogen fuel system performed 150 gas cycles in accordance with the ambient temperature cycles described ECE R134 (ECE/TRANS/WP.29/2014/ 78), Section 5.3. The data from the gas cycles were analyzed. The output of the numerical model was compared to the experimental data and was found to be accurate within statistical uncertainty for both hydrogen fuel systems. Additionally, the numerical model was compared against results from an 83.4 kg refueling cycle performed by NREL and was found to be accurate to within 3.7%. Therefore, the model is considered to be validated for heavy-duty hydrogen vehicles with a nominal working pressure of 70 MPa and an on-board storage of approximately 80 kg.

A parametric study was conducted to understand the effects of storage and vehicle temperature on the numerical model outputs. A linear relationship between the change in storage pressure and the change in storage temperature for storage banks with and initial pressure of 95 MPa was estimated and integrated into the model to estimate the final storage

temperature after each cascade. Additionally, a study was performed to understand the effect of the Z compressibility factor with respect to the model outputs.

The numerical model was used to investigate the effect of increasing the storage volume, storage pressure and the number of cascades for refueling HD hydrogen vehicles. Then a case study, focusing on refueling a 1,500 L hydrogen vehicle with an NWP of 70 MPa using the available hydrogen storage at a test facility in Surrey, BC, was performed. The energy consumption and total volume were key parameters used to evaluate and compare different cascade strategies.

The results of the investigations show that energy savings come at the come the cost of storage volume, agreeing with existing research studies focused on light-duty hydrogen refueling. Cascading strategies with the initial pressure evenly distributed throughout refueling showed the largest reduction in energy consumption.

Finally, based on the results of the case study, it was recommended that an eight-cascade refueling strategy, modified to distribute energy consumption across all storage banks, would be the best approach based on overall energy consumption for refueling a 1,500 L hydrogen vehicle. The storage was deemed to be a negligible factor, in the case study, as the hydrogen storage considered had already been purchased when the test lab was originally designed for light-duty hydrogen gas cycling.

5.2 – Future Works

Future research could focus on exploring the relationships between temperature and pressure when starting from lower pressures, aiming to develop equations that relate changes in pressure to changes in temperature. This could lead to more accurate results from the numerical model. One potential approach would be to conduct refueling experiments that measure the pressure and temperature of storage cylinders starting from pressures of 35 MPa, 50 MPa, and 70 MPa. To enhance the accuracy of storage temperature estimates, new methods should be explored and incorporated into the numerical model. Experimental testing should concentrate on measuring the internal storage temperature and should be carried out to validate the final temperature estimates used in the model.

This thesis does not address the cost of the storage tank. However, incorporating a cost per kilogram of hydrogen storage into the numerical model would improve the model, particularly for designing hydrogen refueling stations. Once the cost of hydrogen storage is included in the model, optimization techniques should be explored and applied to identify the most efficient hydrogen cascade configurations, with a focus on refueling heavy-duty hydrogen vehicles that have on-board storage exceeding 80 kg.

References

[1] M. Filonchyk, M. P. Peterson, L. Zhang, V. Hurynovich and Y. He, "Greenhouse gases emissions and global climate change: Examining the influence of CO2, CH4, and N2O," *Science of The Total Environment,* vol. 935, p. 173359, 2024.

[2] cleanBC, "2020 Climate Change Accountability Report," Province of British Columbia, 2020.

[3] Q. Zhang and T. Ihara, "Comparative cost analysis of FCVs, BEVs, and ICVs: A consumer perspective in Japan," *Applied Energy,* vol. 382, p. 125231, 2025.

[4] J. L. Breuer, R. C. Samsun, D. Stolten and R. Peters, "How to reduce the greenhouse gas emissions and air pollution caused by light and heavy duty vehicles with battery-electric, fuel cell-electric and catenary trucks," *Environment International,* vol. 152, p. 106474, 2021.

[5] S. Vengatesan, A. Jayakumar and K. K. Sadasivuni, "FCEV vs. BEV — A short overview on identifying the key contributors to affordable & clean energy (SDG-7)," *Energy Strategy Reviews,* vol. 53, p. 101380, 2024.

[6] cleanBC, "B.C. Hydrogen Strategy," Province of British Columbia, 2021.

[7] Zen Xlean Energy Solutions, "British Columbia Hydrogen Study," BCBN Publications, 2019.

[8] Y. Zhou, B. Han, Y. Liu, W. Shi, B. Li, L. Chen and P. Liu, "Comparative analysis of impact damage and residual burst pressure of type III and type IV hydrogen storage cylinders," *International Journal of Hydrogen Energy,* vol. 98, pp. 370-383, 2025.

[9] J. Li, T. Wang, Q. Yang, P. Song and H. Su, "Towards fast and safe hydrogen filling for the fuel vehicle: A variable mass flow filling strategy based on a real-time thermodynamic model," *International Journal of Hydrogen Energy,* vol. 53, pp. 20406-20418, 2023.

[10] United Nations, "Addendum 13: Global technical regulations No. 13," *Global Registry,* 2013.

[11] CSA Group, "Compressed hydrogen gas vehicle fuel containers," *CSA/ANSI HGV2:23*.

[12] M. McDougall, "SAE J2579 VAlidations Testing Program - Powertech Final Report," National Renewable Energy Laboratory, 2010.

[13] Environment Canada, "Historical Climate Data," 1971 - 2000. [Online]. Available: https://climate.weather.gc.ca/historical_data/search_historic_data_stations_e.html?searchType=stnProv&timeframe=1&lstProvince=&optLimit=yearRange&StartYear=1971&EndYear=2000&Year=2025&Month=4&Day=15&selRowPerPage=25. [Accessed 12 02 2024].

[14] SAE International, "Fueling Protocols for Light Duty Gasesous Hydrogen Surface Vehicles," *SAE J2601,* 2020.

[15] SAE International, "High-Flow Prescriptive Fueling Protocols for Gaseous Hydrogen Powered Medium and Heavy-Duty Vehicles," *SAE J2601-5,* 2025.

[16] United Nations, "Proposal for 02 series of amendments to UN Regulation No. 134 (Hydrogen and Fuel Cells Vehicles)," *Economic Comission for Europe,* 2023.

[17] International Energy Agency, "The Future of Hydrogen," June 2019. [Online]. Available: https://www.iea.org/reports/the-future-of-hydrogen. [Accessed 12 December 2022].

[18] N. Wolf, R. Neuber, A. Madlow and M. Hock, "Techno-economic analysis of green hydrogen supply for a hydrogen refueling station in Germany," *International Journal of Hydrogen Energy,* vol. 106, pp. 318-333, 2025.

[19] R. Caponi, A. M. Ferrario, L. Del Zotto and E. Bocci, "Hydrogen refueling stations and fuel cell buses four year operational analysis under real-world conditions," *International Journal of Hydrogen Energy,* vol. 48, no. 54, pp. 20957-20970, 2023.

[20] E. Rothuizan and M. Rokni, "Optimization of the overall energy consumption in cascade fueling stations for hydrogen vehicles," *International Journal of Hydrogen Energy,* vol. 39, no. 1, pp. 582-592, 2014.

[21] T. Kuroki, K. Nagasawa, M. Peters, D. Leighton, J. Kurtz, N. Sakoda, M. Monde and Y. Takata, "Thermodynamic modeling of hydrogen fueling process from high-pressure storage tank to vehicle tank," *International Journal of Hydrogen Energy,* vol. 46, no. 42, pp. 22004-22017, 2021.

[22] A. G. Galeev, "Review of engineering solutions applicable in tests of liquid rocket engines and propulsion systems employing hydrogen as a fuel and relevant safety assurance aspects," *International Journal of Hydrogen Energy,* vol. 42, no. 39, pp. 25037-25047, 2017.

[23] R. R. Ratnakar, N. Gupta, K. Zhang, C. van Doorne, J. Fesmire, B. Dindoruk and V. Balakotaiah, "Hydrogen supply chain and challenges in large-scale LH2 storage and transportation," *International Journal of Hydrogen Energy,* vol. 46, no. 47, pp. 24149-24168, 2021.

[24] J. C. Moreno-Blanco, F. Elizalde-Blancas, A. Gallegos-Muñoz and S. M. Aceves, "The potential for avoiding hydrogen release from cryogenic pressure vessels after vacuum insulation failure," *International Journal of Hydrogen Energy,* vol. 43, no. 16, pp. 8170-8178, 2018.

[25] E. Rothuizen, W. Merida, M. Rokni and M. Wistoft-Ibsen, "Optimization of hydrogen vehicle refueling via dynamic simulation," *International Journal of Hydrogen Energy,* vol. 38, no. 11, pp. 4221-4231, 2013.

[26] E. Talpacci, M. Reuβ, T. Grube, P. Cilibrizzi, R. Gunnella, M. Robinius and D. Stolten, "Effect of cascade storage system topology on the cooling energy consumption in fueling stations for hydrogen vehicles," *International Journal of Hydrogen Energy,* vol. 43, no. 12, pp. 6256-6265, 2018.

[27] C. Blazquez-Diaz, "Techno-economic modelling and analysis of hydrogen fuelling stations," *International Journal of Hydrogen Energy,* vol. 44, no. 2, pp. 495-510, 2019.

[28] M. Farzaneh-Gord, M. Saadat-Targhi and J. Khadem, "Selecting optimal volume ratio of reservoir tanks in CNG refueling station with multi-line storage system," *International Journal of Hydrogen Energy,* vol. 41, no. 48, pp. 23109-23119, 2016.

[29] M. Farzaneh-Gord, M. Deymi-Dashtebayaz and H. R. Rahbari, "Studying effects of storage types on performance of CNG filling stations," *Journal of Natural Gas Science and Engineering,* vol. 3, no. 1, pp. 334-340, 2011.

[30] M. Farzaneh-Gord, M. Deymi-Dashtebayaz, H. R. Rahbari and H. Niazmand, "Effects of storage types and conditions on compressed hydrogen fuelling stations performance," *International Journal of Hydrogen Energy,* vol. 37, no. 4, pp. 3500-3509, 2012.

[31] M. Hosseini, I. Dincer, G. F. Naterer and M. A. Rosen, "Thermodynamic analysis of filling compressed gaseous hydrogen storage tanks," *International Journal of Hydrogen Energy,* vol. 37, no. 6, pp. 5063-5071, 2012.

[32] Y. Yu, C. Lu, S. Ye, Z. Hua and C. Gu, "Optimization on volume ratio of three-stage cascade storage system in hydrogen refueling stations," *International Journal of Hydrogen Energy,* vol. 47, no. 27, pp. 13430-13441, 2022.

[33] H. Chen, J. Zheng, P. Xu, L. Li, Y. Liu and H. Bie, "Study on real-gas equations of high pressure hydrogen," *International Journal of Hydrogen Energy,* vol. 35, no. 7, pp. 3100-3105, 2010.

[34] E. W. Lemmon, M. L. Huber and J. W. Leachman, "Revised Standardized Equation for Fuel Consumption Applications," *Journal of Research of the National Institute of Standards and Technology,* vol. 113, pp. 341-350, 2008.

[35] M. Bilgili and R. F. Yumşakdemir, "Effects of real gas equations on the fast-filling process of compressed hydrogen storage tank," *International Journal of Hydrogen Energy,* vol. 53, pp. 816-828, 2024.

[36] J. W. Leachman, R. T. Jacobsen, S. G. Penonocello and E. W. Lemmon, "Fundamental Equations of State for Parahydrogen, Normal Hydrogen, and Orthohydrogen," *Journal of Physical and Chemical Reference Data,* vol. 38, p. 721, 2009.

[37] S. Onorato and T. Kuroki, "High-Throughput Hydrogen Fueling R&D at NREL," National Renewable Energy Laboratory, 2022.

[38] B. N. Taylor and C. E. Kuyatt, "Guidelines for Evaluating and Expressing the Uncertainty of NIST Measurement Results," National Institute of Standards and Technology, 1944.

[39] L. S. Ladson, R. L. Fox and M. W. Ratner, "Nonlinear optimization using the generalized reduced gradient method," *RAIRO- Operations Research - Recherche Operationnelle,* vol. 3, no. 8, pp. 73-103, 1974.

[40] A. Murugan, M. de Huu, T. Bacquart, J. van Wijk, K. Arrhenius, I. te Ronde and D. Hemfry, "Measurement challenges for hydrogen vehicles," *International Journal of Hydrogen Energy,* vol. 44, no. 35, pp. 19326-19333, 2019.

[41] SAE International, "Hydrogen Fuel Quality for Fuel Cell Vehicles," *SAE J2719,* 2020.

[42] O. Bouledroua, Z. Hafsi, M. B. Djukic and S. Elaoud, "The synergistic effects of hydrogen embrittlement and transient gas flow conditions on integrity assessment of a precracked steel pipeline," *International Journal of Hydrogen Energy,* vol. 45, no. 35, pp. 18010-18020, 2020.

[43] D. M. Bromley, "Hydrogen embrittlement testing of austenitic stainless steels SUS 316 and 316L," University of British Columbia, Vancouver, 2008.

[44] A. Fukunaga, "Hydrogen embrittlement behaviors during SSRT tests in gaseous hydrogen for cold-worked type 316 austenitic stainless steel and iron-based superalloy A286 used in hydrogen refueling station," *Engineering Failure Analysis,* vol. 106, p. 108158, 2024.

[45] K. Reddi, A. Elgowainy, N. Rustagi and E. Gupta, "Impact of hydrogen SAE J2601 fueling methods on fueling time of light-duty fuel cell electric vehicles," *International Journal of Hydrogen Energy,* vol. 42, no. 26, pp. 16675-16685, 2017.

[46] H. Luo, J. Xiao, P. Benard, C. Yuan, L. Tong, R. Chahine, Y. Yuan, T. Yang and C. Yao, "Thermodynamic modeling and analysis of cascade hydrogen refuelling with three-stage pressure and temperature for heavy-duty fuel cell vehicles," *International Journal of Hydrogen Energy,* vol. 63, pp. 103-113, 2024.

[47] K. Hanada and S. Yamaguchi, "Development of Real-time Pressure Loss Compensation Method for Hydrogen Refueling Station to Increase Refueling Amounts," *International Journal of Automotive Engineering,* vol. 9, no. 4, pp. 310-315, 2018.

[48] Y. A. Cengel, M. A. Boles and M. Kanoglu, Thermodynamics: An Engineering Approach, Ninth Edition, McGraw Hill, 2019.

[49] H. Sahin, "Hydrogen refueling of a fuel cell electric vehicle," *International Journal of Hydrogen Energy,* vol. 75, pp. 604-612, 2024.